Title
Models and Mechanisms of Adult Lung Repair and Regeneration

Author
Donne, Matthew Louis

Publication Date
2016

Peer reviewed|Thesis/dissertation

Models and Mechanisms of Adult Lung Repair and Regeneration

by

Matthew Louis Donne

DISSERTATION

Submitted in partial satisfaction of the requirements for the degree of

DOCTOR OF PHILOSOPHY

in

Developmental and Stem Cell Biology

in the

GRADUATE DIVISION

of the

UNIVERSITY OF CALIFORNIA, SAN FRANCISCO

[redacted]

Acknowledgements

First, I would like to acknowledge individuals who helped me throughout my post-baccalaureate work and graduate school career including my parents and extended family, Dr. Susan Fisher, Dr. Olga Genbacev-Krtolica, Dr. Robert Judson, Dr. Emin Maltepe, Dr. Carmen Domingo, Dr. Rich Schneier, Demian Sainz, and Lisa Magargal. I would not be where I am today without your guidance throughout the past decade. I would also like to acknowledge the tireless support and engagement from my fellow Rock Lab members. First and foremost I must thank Dr. Jason Rock for being our fearless leader; always supportive of our work and future, even during difficult times. I must also thank Gorica Amidzic, Dr. Ian Driver, Andrew Lechner, David Pardo, and Dr. Cindy Kanegai for their comradery, scientific insight and personal support. Lastly, I must thank my thesis committee members Dr. Susan Fisher, Dr. Dean Sheppard, and Dr. Ophir Klein for their expertise and guidance during this process.

The introduction is an unpublished review written by Dr. Rock, Dr. Kanegai, and myself. Chapter Two has been submitted for review in the journal *Stem Cell Reports*; this paper includes authorship by Dr. Ian Driver, Andrew Lechner, and Dr. Jason Rock. Dr. Ian Driver and I co-authored Chapter Five, along with Dr. Jason Rock; a soon-to-be submitted work. Ian's expertise in single-cell sequencing, data analysis and insights contributed significantly to this chapter. In addition, Ian wrote the analysis software, **Scicast**, which is used to perform clustering, PCA and significance testing. **Scicast** is available for public use at https://github.com/iandriver/scicast.

I am excited to see what new opportunities present themselves in my scientific future. I will be forever grateful for the friendships and relationships I have built while at UCSF over these past 10 years. Thank you.

Abstract

Until recently, adult lung regeneration has been a poorly defined phenomena in mammals. Publications from the 1970s demonstrated in small mammals the ability for tissue to expand, through a process called alveologenesis, post-pneumonectomy. Only recently have the molecular processes involved in adult alveologenesis begun to be defined. Using methods of non-pathologic lung injury and lineage tracing analysis, we demonstrate that the alveolar epithelial type II cells (AECII) are the predominant, proliferative epithelial cell population that contribute to formation of new alveolar epithelium. We also show that pneumonectomy induces proliferation in AECIIs in-vitro and in-vivo, and that two separate molecular pathways, Notch and Wnt, are seemingly necessary for both the proliferation and differentiation phase of AECIIs into AECIs during adult alveologenesis. For the first time, we have strongly suggestive evidence that non-human primate lungs are capable of adult alveologenesis, and that the AECII cell is the predominant proliferative cell type as well. These findings further support the potential for adult alveologenesis in humans and define a cell type of interest to pursue. In a separate study, we looked to better define heterogeneity within an adult lipofibroblast progenitor cell population. Initially, we used a cell transplantation technique after bleomycin injury to show that the PDGFR-A+ lipofibroblast cell can integrate themselves into areas of fibrosis in the lung. We then performed single-cell sequencing to demonstrate cell heterogeneity within this lipofibroblast population. This analysis led us to the TCF21 gene, a gene which has been associated with lung branching morphogenesis and also the cell of origin for cardiac myofibroblasts. Again, using lineage tracing techniques, we demonstrated that TCF21 cells are capable of differentiating in to pulmonary myofibroblasts in the context of bleomycin injury.

Table of Contents

List of Tables

Chapter 1: Introduction

Chapter 5: Single cell sequencing reveals lung fibroblast heterogeneity.

List of Figures

Chapter 1: Introduction

Chapter 2: The role of the Notch signaling pathway in lung regeneration

Chapter 3: The role of the Wnt signaling pathway in lung regeneration

Chapter 4: Caloric restriction diet as a model of lung regeneration

Chapter 5: Single cell sequencing reveals lung fibroblast heterogeneity.

Chapter 1

Models and mechanisms of lung repair and regeneration

Introduction 1.1

Lung disease is a major cause of morbidity and mortality in infants, children, and adults in the US. Chronic lung disease in infants is principally due to Bronchopulmonary Dysplasia, whereas the pulmonary disease burden in children is primarily linked to asthma and cystic fibrosis[1,2]. In adults, there are a broad spectrum of disease states from chronic obstructive pulmonary disease (COPD) to fibrotic lung diseases such as idiopathic pulmonary fibrosis (IPF)[3]. There remain few strategies for the treatment of many lung diseases, such as IPF, where the median survival is less than 3 years and ultimate treatment involves lung transplantation[4,5]. Therefore, there is a great need for new therapeutic options to treat this diverse and complex collection of diseases.

The lung is capable of a robust reparative response to injury, such as sometimes seen clinically in acute respiratory distress syndrome (ARDS) and in numerous animal models[6,7,8,9]. A promising therapeutic option would be to harness this reparative potential of the lung to reverse pathologic remodeling and restore lung function in disease states. Experimental data, primarily from animal models, have shed light on the progenitor cell populations that mediate the repair and regeneration of lung tissue after a variety of stimuli. However, further work is needed to define the molecular regulation of these progenitor populations under normal, regenerative, and pathological conditions to develop new therapies for patients with lung disease.

The airways of normal adult lungs are lined with a pseudostratified or columnar epithelium comprised of epithelial cell types that filter, humidify and carry air to the alveoli. A number of non-epithelial cell types, including fibroblasts, cartilage, smooth muscle, and vasculature structurally and functionally support the conducting airways[10]. The very thin squamous epithelium of the alveoli facilitates the diffusion of gases with the surrounding network of capillaries. Other cell types in the distal lung include fibroblasts, vascular and lymphatic endothelial cells, pericytes and immune cells. Normal lung function is dependent on the maintenance of specific proportions of these cells in a complex 3D arrangement with intimate cell-to-cell communication. A loss (or excess) of specific cell populations, oftentimes the result of disrupted intercellular communication or altered tissue properties, is seen in many lung diseases and contributes to pulmonary compromise.

Structure and cellular composition of the lung

The lung develops from the ventral foregut endoderm that buds into the surrounding splanchnic mesenchyme at around embryonic day (E) 9.5 in the mouse (~ gestational week 4 in humans)[10,11]. The developmental processes involved in prenatal lung maturation have recently been reviewed in detail[12,13]. The genetically encoded program of branching morphogenesis generates a network of tubes connected to terminal sacs[14]. These sacs are subdivided after birth by the process of secondary alveolar septation to increase the surface area available for gas exchange.

The proximal airways in mice, including the trachea and mainstem bronchi, are lined with a pseudostratified epithelium composed of club cells (previously “Clara” cells)[15], ciliated cells, mucus-producing goblet cells, basal cells, and neuroendocrine cells (Table 1). The bronchi

and bronchioles are lined with a simple columnar epithelium made up of club cells, ciliated cells and goblet cells (Figures 1 and 2). In mice, the transition between the conducting airways and alveoli is called the bronchioalveoar duct junction (BADJ). Brochioalveolar stem cells (BASCs), expressing markers of both airway (Sgcb1a1) and alveolar (SPC) lineages, are found in this region[16]. It is important to note that, despite overall functional similarities, there are important structural differences between mouse and human lungs. For example, the lungs of humans are larger with more generations of airway branches. Unlike mice, the intralobar airways of humans are lined with a pseudostratified epithelium and surrounded by cartilage rings or plates. The smallest airways in humans, called respiratory and terminal bronchioles, are distinct from the BADJ in mice (Figures 1 and 2). Each of these respiratory bronchioles, lined with a cuboid to columnar epithelium, is connected to many alveolar ducts. Importantly, BASCs have not been reported in human lungs.

The thin epithelial lining of the alveoli in both rodents and humans is largely comprised of two cell types: type I and type II alveolar epithelial cells (AECI and AECII, respectively). AECI compose 93% of the alveolar surface area and have a thickness of only ~50nm[11]. These extremely thin cells share a basement membrane with the surrounding network of capillaries to further facilitate the diffusion of gases from the alveolar lumen to the pulmonary circulation. AECIIs produce surfactant-associated protein C (SPC) and, although they only comprise ~7% of the surface area of the alveoli, they are the most abundant epithelial cells of the alveolar epithelium[11]. SPC is a one protein component of pulmonary surfactant, a thin lining that reduces surface tension to prevent alveolar collapse[17] (Table 1).

Stromal cell types

As previously mentioned, healthy lungs contain a number of non-epithelial (also broadly referred to as mesenchymal or stromal) cell populations (Table 1 and Figure 1). These cells carry out various functions ranging from structural support to host defense. In addition, mounting evidence suggests these stromal cells provide a component of the "niche" for the epithelial stem/progenitor cells and contribute either directly or indirectly to a number of pathologic conditions when deregulated[18,19,20]. Despite their importance, relatively little is known about the lineage relationships of these cell types in development, homeostasis or disease. This is, in part, owing to a lack of precise molecular markers and the complex three-dimensional structure of the lung.

One mesenchymal cell type of relevance here is a subpopulation of fibroblasts called lipofibroblasts. Recent evidence suggests that these cells express the receptor tyrosine kinase PDGFRA at steady state[21]. Lipofibroblasts are intimately associated with AECII and are thought to support them through the production of lipids[22,23] (Figure 3). Other populations of PDGFRA expressing cells are associated with airways and vessels and within the alveolar interstitia. In the healthy adult lung, there are relatively few mature myofibroblasts that, by definition, express the contractile protein aSMA. Recently published data demonstrates a strong evidence supporting the hypothesis that lipofibroblasts in the lung are capable of differentiating in to myofibroblasts during after bleomycin injury [24]. Unpublished research performed in our lab, using single-cell sequencing technology, further supports the hypothesis for the lipofibroblast cell found in distal alveolar structures of being capable of giving rise to myofibroblasts lineages as well.

During the developmental process of branching morphogenesis, pdgfr-a+ fibroblasts localize to the mesenchyme near the elongating distal tips. Genetic loss-of-function experiments

in mice have shown that these cells are critical for alveolar septation. PDGFRA -/- mice fail to undergo secondary alveolar septation owing to a lack of maturation of myofibroblasts, derived from fibroblasts, at the growing septal tips[25] . Recent evidence from in vitro and in vivo mouse models suggest that PDGFRA expressing interstitial fibroblasts are important niche cells that support epithelial progenitor populations in adult lungs[20,22,23]. For example, an in vitro co-culture model showed that PDGFRA expressing fibroblasts are required for the survival, proliferation and differentiation of AECII cells into 3D organoids containing AEC1 and AEC2[21].

A vast capillary network surrounds the alveoli to facilitate gas exchange. During embryonic lung development, the vascular plexus sprouts concomitantly with the distal alveolar buds of the developing lung[14,26,27]. This vasculature is multifunctional: the capillaries provide nutrients to the cells of the alveoli and shuttle freshly oxygenated blood back out into the circulatory system.

Pericytes (also referred to as mural cells), support the vasculature, including the alveolar capillaries. Although their functions are not well known they are thought to regulate vascular tone and promote angiogenesis[28]. Pericytes are only definitively identified at the electron microscope level; however, they generally express NG2 and Pdgfrb[2930].

Airway smooth muscle plays critical roles in embryonic lung development. Parabronchial smooth muscle cells produce FGF10 that are required for multiple aspects of patterning of the fetal lung. There are also mounting data to suggest that contractions of the fetal airway smooth muscle promote branching morphogenesis in the fetal lung, perhaps through modulating intraluminal pressure or other structural characteristics of the developing lung[31,32,33]. Data from an adult lung injury/repair model that involves systemic administration of naphthalene suggest that airway smooth muscle reactivates the expression of FGF10 to promote epithelial repair[34]. In some pathological states, such as chronic asthma, smooth muscle cells can become hypertrophic,

hyperplastic and hyperresponsive[35]. The net effect of these changes is a decrease in airway lumen diameter that can complicate breathing. In healthy adult lungs, the functional significance of airway smooth muscle has been a matter of debate.

Diseases of the Distal Lung

Anatomically, the distal lung includes the small respiratory bronchioles, alveolar ducts and the functional sites of gas exchange, the alveoli. Diseases of the distal lung can impair gas exchange by reducing the alveolar surface area, by disrupting the thin interface between the alveolar epithelium and the underlying capillary surface, or by impairing the flow of gases into and out of the lung. Diseases of the distal lung are categorized by clinical syndrome and histopathology. Here, we discuss examples of developmental, obstructive and interstitial lung diseases, to help illustrate the broad utility of animal models and stem cell technology in lung disease.

Developmental Diseases

Bronchopulmonary dysplasia (BPD) is a common chronic respiratory disease of newborn infants and is defined by the requirement for supplemental oxygen or mechanical ventilation[36]. The disease is thought to result from a combination of infectious, mechanical and oxidative stresses in the immature lung, which leads to defects in the development of the pulmonary vasculature and alveoli. In addition to limiting lung function in infancy, evidence suggests that BPD can also lead to pulmonary complications later in life and life-long reduction in lung function[36,37,38].

Obstructive Lung Diseases

Chronic obstructive pulmonary disease (COPD) is currently the 3rd leading cause of death in the USA[3,39]. This disease predominantly involves the acinar unit (respiratory bronchiole to alveolus) and is characterized by chronic inflammation of the airways and destruction of elastic fibers leading to dilation or destruction of acinar units (i.e., emphysema)[40,41]. The development of COPD is most commonly associated with cigarette smoking, but emphysema can also develop from other exposures and genetic causes such as alpha-1 antitrypsin deficiency[40,41].

Interstitial Lung Diseases

Interstitial lung disease (ILD) is a large and diverse category of lung diseases that involve inflammation and/or fibrosis (i.e., excessive abundance of myofibroblasts and collagen-rich extracellular matrix) of the lung parenchyma[42]. Three large histopathologic categories of ILD are: nonspecific interstitial pneumonia (NSIP) which is classically seen in connective tissue related ILDs or hypersensitivity pneumonitis; usual interstitial pneumonia (UIP), as classically seen in IPF; and diffuse alveolar damage, as seen in acute interstitial pneumonia (AIP), an idiopathic form of acute respiratory distress syndrome (ARDS)[42].

The NSIP histologic pattern can be idiopathic, associated with connective tissue related ILDs, or secondary to exposures such as a drug or an inhaled organic agent [46]. Generally, this category of diseases can present with respiratory symptoms in childhood or adulthood and has a variable clinical course depending on the underlying etiology and degree of fibrosis[43]. Importantly, NSIP is considered steroid-responsive when it is in a primarily cellular rather than fibrotic stage[43]. Histologically, it is characterized by chronic interstitial inflammation with or without loose or dense fibrosis that lack the fibroblastic foci seen in UIP[44].

The usual interstitial pneumonia histologic pattern (UIP) is classically associated with Idiopathic pulmonary fibrosis. UIP is characterized by mild chronic inflammation with heterogeneous fibroblastic foci and dense fibrosis with a "honeycomb" appearance prominently in sub-pleural regions[44]. The disease is typically is progressive with median survival of less than 3 years[44]. The etiology is unknown although there is evidence supporting both genetic and environmental risk factors. In particular, there is still controversy around the cells that are responsible for the increased numbers of matrix-producing myofibroblasts. A greater understanding of these cells and their molecular regulation has the potential to yield novel therapeutic interventions for this fatal disease.

Diffuse alveolar damage is a pathologic finding commonly associated with acute respiratory distress syndrome (ARDS) or acute interstitial pneumonia (AIP), the idiopathic form. ARDS clinically presents as acute hypoxic respiratory failure leading to diffuse lung injury and carries a mortality rate of approximately 30%[45]. ARDS can result from a variety of systemic insults including sepsis, burns, pancreatitis and trauma, among others. Pathophysiologically, there is damage to endothelial and epithelial surfaces and disruption of the lung's ability to regulate interstitial fluid. Histologically, the lung parenchyma displays acute inflammation, interstitial edema and hyaline membranes that can resolve or progress to fibrosis[44].

A better understanding of the disease mechanisms and the endogenous capacity of adult human lungs for repair and regeneration have the potential to revolutionize therapies for each of the diseases described above. It is not feasible to perform carefully controlled, longitudinal and mechanistic studies of pathogenesis and lung injury and repair in humans. However, a great deal of information can be obtained through animal models of lung disease and regeneration.

Animal models of diseased distal lungs

To understand the cellular and molecular changes that lead to the pathologies observed in humans, it is convenient to use animal model systems that recapitulate some aspects of human disease. In addition, animal models have provided insights about the endogenous capacity of the lung for repair and regeneration following various stimuli. Here, we will discuss recent efforts at modeling human alveolar lung disease in animals with particular emphasis on studies that have identified endogenous stem and progenitor cells that might be therapeutically manipulated to reverse pathological remodeling in human disease.

Modeling of COPD, BPD and Emphysema

Prematurity, mechanical ventilation, and hyperoxic injury can lead to BPD in infants (sandhaus 2013). A similar histologic pattern can be seen in rodents exposed to high levels of oxygen immediately after birth[46]. In the neonatal mouse, hyperoxia increases the sensitivity of AECII cells to TGF-beta induced apoptosis and blocks the ability for septation in the developing alveoli, in turn blocking alveologenesis[47]. One potential therapy for this condition is administration of conditioned media from bone-marrow derived mesenchymal stromal cells, that has the capacity to reverse BPD phenotype in neonatal mice[48,49]. Similarly, in a rat model system, introduction of either supplemental nitric oxide or administration of sildenafil, a vasodilator and pro-angiogenic drug, can prevent or repair BPD damage[46,50].

One rodent model of emphysema is the installation of neutrophil elastase to the lung, resulting in degradation of the alveolar walls, mucous cell metaplasia, hemorrhage and destruction of the respiratory epithelium. One potential drawback of this model is that the inflammation is transient and resolves within a week of elastase administration[51,52]. COPD is also

marked by chronic inflammation, which is mediated by resident immune cells. A method to recreate the chronic immune response in a mouse model is use of lipopolysaccharide (LPS). It was discovered that when introduced into airways, it produces a strong neutrophilic inflammation response that peaks between 6–24 h post-administration[53]. Chronic administration of LPS has also been shown to lead to airway remodeling, emphysema and altered lung function in mice. This chronic exposure recapitulates the chronic lung inflammation caused by sustained immune cell infiltration suffered by COPD patients[54].

Because the loss of alveolar surface area is central to the pathogenesis of COPD and other emphysematous alveolar diseases, identifying stem or progenitor cells that are capable of regenerating alveoli has potential to yield new cell and molecular therapies for lung disease. One alveolar stem cell population is the type 2 alveolar epithelial cell (AECII). Studies performed as early as the 1970s using tritiated thymidine incorporation in rats suggested that AECII both self-renew and give rise to type 1 alveolar epithelial cells (AECI) after injury [60]. Recently, lineage-labeling analysis of SPC cells further supports the hypothesis that AECII cells are the putative stem cell of the alveoli[21,29,55]. A great deal more work needs to be done to better understand the response of AECII cells (and the relative contributions of other progenitor populations) after various lung injuries.

Modeling IPF

IPF is a progressive disease with no known cure and, by definition, unknown etiology. There are, however, several mouse model systems that give rise to similar phenotypes in mice. One side effect of the antineoplastic drug Bleomycin in humans is pulmonary fibrosis. Intratracheal or systemic administration to rodents causes patchy fibrotic lesions[6,29,56]. Unlike in

humans, where pulmonary fibrosis is progressive and irreversible, mice generally show some degree of recovery. In mice, several cell types have been implicated in the repair from bleomycin-induced lung injury, although their relative contributions are not known due to technical limitations. AEC2 proliferate and give rise to AEC1 post-bleomycin. BASCs, which co-express Scgb1a1 and SPC, increase in number after bleomycin injury[16,49]. Several groups have demonstrated that SCGB1A1 lineage labeled cells contribute to new AECII and AECI cells 21 days after bleomycin injury[29,57]. Another cell type suggested to be involved in lung repair after bleomycin injury is a population of epithelial progenitors that express integrin alpha 6 beta 4[6]. There is a marked increase in both integrin beta 4 expression, quantified through western blot, and the number of alpha 6 beta 4 cells, analyzed by flow cytometry, after injury. In an in vivo culture system in which integrin alpha 6 beta 4+ cells were mixed with dissociated fetal lung and injected under the kidney capsule, these cells expanded and gave rise to either SCGB1A1+ or SPC+ cells. Their contribution to lung repair in vivo awaits further study. Similarly, more discriminating markers and new techniques that allow for the simultaneous assessment of multiple populations' behaviors post-bleomycin will allow us to refine hypotheses about the relative contributions of these populations in vivo.

In the mouse model of bleomycin-induced lung injury, PDGFRA expressing fibroblast cells proliferate within fibrotic patches and sometimes co-express the canonical myofibroblast marker aSMA[29,58]. Our lab looked to better define cell heterogeneity in these pdgfr-a expressing cells using single-cell sequencing. We identified a subpopulation of Tcf21+ cells that, when lineage labeled after bleomycin injury, gave rise to aSMA expressing cells in areas of fibrosis. Further discussion of this discovery is discussed in Chapter 5. Work by others has shown that

this lipofibroblast population found within the lung gives rise to myofibroblasts after bleomycin injury, and that this occurs through a transdifferentiation process by day 14 after injury[24].

In addition to their normal functions, pericytes have been described as the source of matrix-producing myofibroblasts in fibrotic diseases such as Scleroderma and in kidney and liver tissue[59,60,61,62]. In the mouse model of bleomycin-induced pulmonary fibrosis, we showed that lineage labeled NG2 expressing pericytes proliferated, but were not a significant source of aSMA expressing myofibroblasts[29]. Interestingly, a population of cells derived from Foxd1+ embryonic mesenchymal progenitors (that includes pericytes) was recently reported as a source of myofibroblasts in pulmonary fibrosis[58]. The contribution of adult pericytes to interstitial lung disease will require further investigation.

Mounting data suggest that mesenchymal stromal cells, either tissue resident or derived from the bone marrow, modulate lung injury as well as repair. This can be achieved either through modulation of the immune cell behavior or through direct effects on epithelial and stromal cells. Hyperoxia induced bronchopulmonary dysplasia, which prevents alveolar septation and reduces alveolar surface volume while causing pulmonary hypertension in infants, can be prevented through introduction of mesenchymal stromal cells. This positive effect on alveolar septation seemed to be induced through a paracrine effect, as just the conditioned media from bone marrow derived stem cells had a positive effect[63]. A more recent study using hyperoxia induced lung injury model demonstrated enhanced repair and increased numbers of BASCs after introduction of mesenchymal stromal cell conditioned media[49]. These data further support the paracrine mediated ameliorative effect of MSCs. Another population of mesenchymal cells is ABCG2+[64] that have been described to be present in the kidney, liver and testis, but little is known about their role in the lung[65].

Thoracic radiotherapy for treatment of lung cancer can result in pneumonitis and IPF in the regions where there is radiation exposure[66,67]. Radiation exposure in mice results in a similar fibrotic response[68]. Mutations in SPC and MUC5B are associated with familial forms of IPF in humans[69,70](Table 1). These mutations are thought to prevent proper protein processing and induce the unfolded protein response (UPR). UPR activation in AECIIs could contribute to lung fibrosis by impairing cell survival, the ability to re-epithelialize air spaces after injury and disrupt signaling between the epithelium and mesenchyme[71,72]. In mice, analogous activating mutations of these proteins are insufficient to cause spontaneous fibrosis, but potentiate the fibrotic response to bleomycin. Humans with short telomeres have a higher incidence of IPF than humans with normal length telomeres[42,73]. This phenotype though has not been able to be recapitulated in a mouse model system using either telomerase RNA null or telomerase reverse transcriptase null animals[74,75,76]. However, mice with shortened telomeres that were exposed to chronic cigarette smoke developed emphysematous air space enlargement, while the control group did not[77].

Other models-

Three model systems that highlight the lung's innate regenerative abilities are targeted cell depletion using diphtheria toxin, calorically restricted diet, and compensatory growth following partial pneumonectomy.

Inducible expression of diphtheria toxin allows for ablation of a subpopulation of cells and subsequent analysis of the response of remaining resident stem cell populations without causing broader insult to the organ system. This approach was recently used to demonstrate that surviving AECII expand in a clonal manner after targeted ablation of a fraction of AECIIs[21].

At some point during our evolutionary process, it was found to be favorable to reduce our O_2 consumption by reducing alveolar number during times of food shortages. This reduction in alveolar number though can be quickly replenished as soon as more food becomes abundant. Specifically, it has been well studied in small mammals that a calorically restricted diet over a period of about 2 weeks can reduce alveolar numbers by as much as 50%[78]. Once *ad libitum* refeeding begins, the alveolar numbers are completely regenerated within 72hrs[78]. Chapter 4 of this thesis sheds light on AECII behavior during the regenerative response after *ad libitum* feeding. This model system allows one to observe a natural, non-pathological response to lung repair and regeneration.

The regenerative response of the lung following a surgical reduction in lung volume (i.e., pneumonectomy) was studied as early 1970s[79,80,81]. Indeed, there is some data to suggest that this process occurs in animals ranging from rodents to humans, but the cellular and molecular processes involved remain poorly understood[82,83,84,85]. In this procedure, one (or more) lobe is ligated at the main stem bronchus and resected. In several model organisms, after removal of the entire left lobe, or approximately 40% of the total lung volume, the remaining right lobes have demonstrated an ability to completely regenerate the lost lung volume through expansion and suspected adult alveologenesis. In rodents, this occurs in as little as 14 days[82]. Recently, data suggest that a similar process can occur in adult humans with much slower kinetics[85]. One approach to understanding this in humans would be to study this process in non-human primates whose lung structure is more similar to the lungs of humans than those of mice (Figure 2). Some of our findings related to the compensatory response in non-human primates is discussed in Chapter 2.

A major stimulus in adult lung for post-PNX alveologenesis is stretch. Previous work has demonstrated filling the empty chest cavity with inert material prevents the mediastinal shift and in turn expansion of the remaining lobes. This attenuates the change in mass and cellular proliferation of the remaining lobe[86,87]. Another proposed stimulus for adult alveologenesis is cyclic expansion of the thorax resulting from diaphragmatic contraction. This hypothesis was further tested in a human study by comparing functional outcomes in patients after pneumonectomy who had their phrenic nerve accidentally damaged, thus causing hemi-diaphragmatic paralysis and loss of unilateral lung expansion on the side of pneumonectomy, versus patients with intact nerve function after pneumonectomy. This study showed that patients with hemidiaphragmatic paralysis had reduced lung function on the contralateral side of diaphragmatic paralysis compared to controls, thus suggesting a necessary role of stretch for compensatory lung growth[88]. The precise cellular and molecular mechanisms at play in the epithelial as well as stromal populations is still lacking.

Recent studies have demonstrated a necessary endothelial/epithelial vascular niche interaction regulated by FGF and VEGF for proper lung repair post-PNX (ding 2011). Specifically, knockout of fgfr-1 and Vegfr-2 results in a significantly reduced capacity for alveolar expansion post-pneumonectomy. These data suggest without proper angiogenesis, there is a reduced capacity for alveologenesis in the adult lung[18]. More recently Lee et al, using both in vivo and in vitro modeling, demonstrated a necessary role of a heterogeneous endothelial population in maintenance of BASC cell and lung repair after injury[19]. Recently, it has also been shown that CD11b+ macrophages in the regenerating lung are necessary for compensatory lung growth in mice following pneumonectomy. CD18 null mice demonstrated lack of leukocyte infiltration as well as impaired ability for lung growth compensation[89]. Lastly, work discussed in

Chapters 2 and 3 of this thesis begin to discuss the molecular players necessary for AECII differentiation into AECI cells post-PNX (Figure 3).

Restoring balance: stem cell approaches to treating lung disease

A better understanding of the cell types and molecules that mediate lung repair and regeneration has the potential to lead to novel cell and molecular therapeutic strategies for end-stage lung disease. Ideally, future strategies will prevent diagnosed lung diseases from progressing or reverse pathological remodeling. Areas of interest that are currently being investigated in the lung field include cell engraftment (or administration of MSCs/conditioned medium), recellularization of a decellularized lung with patient derived lung progenitor cells for transplantation, and molecular therapies.

Healthy adult lung tissue for transplantation is in short supply, but the possibility to repair damaged adult lung tissue could allow for more lung transplants. Currently, many potential donor lungs are discarded due to inability to match the recipient patient, or failing of quality control checks prior to transplant. One way to increase available lungs and to reduce waste of failed donor lungs is through de-celluarization and re-cellularization of the lung. Using a bio-rector and co-cultures of pulmonary epithelium and vascular endothelium with an acellular lung scaffold, several groups have seen remarkable remodeling of the lung with hierarchical epithelial organization within the matrix and through seeded endothelial cells, which have efficiently repopulating the vascular compartments[90]. This initial work used HUVEC cells as well as the immortallized lung adenoma carcinoma cell line A549 to recellularize a decellularzied rat lung. Both in-vitro and in-vivo work demonstrated general proof concept in the ability to create a functional, recellularized organ capable of supporting recipient rats for 6 hours post-transplant[90].

Recellularization with better-defined lung epithelial and stromal populations with long-term survival, self-renewal and differentiation potential could improve this strategy. In a step towards pre-clinical studies, Bonvillain et al have been able to scale the lung decellularization model system to use in non-human primate lungs[91].

Using a step-wise differentiation process, several groups have recently differentiated mouse and human embryonic stem cells (ES) and induced pluripotent stem cells (iPS) into lung progenitor cell lineages and mature epithelial cell types[92,93,94,95]. Taking cues from developmental biology, these protocols are constantly being refined to enhance the efficiency for generating lung cell lineages. These cells have been expanded and subsequently characterized in 2D and 3D in vitro models, transplantation under the kidney capsule of recipient animals, and seeding in decellularized lung scaffolds. These cells will undoubtedly prove useful in testing compounds for effects on patient-derived lung epithelial cells, a critical step towards the realization of personalized medicine. Whether these cells will prove useful for direct engraftment or seeding into bioengineered organ replacements remains to be seen.

Therapies designed to modulate endogenous progenitor cell populations of the lung potentially have the greatest near term therapeutic potential. In a recently published work, keratinocyte growth factor was demonstrated to support alveolar epithelium health when given to human patients who were subjected to LPS[96]. In this study, patients were either treated with placebo or Palifermin (KGF). Study subjects treated with KGF showed increased AECII proliferation, marked by increase in SP-D, and gelatinolytic enzyme activity, which has been suggested to support epithelial healing in organs, as compared to the placebo controls. Because decreased SP-D levels is correlated with poorer outcomes in patients with ARDS, it is possible that KGF therapy will benefit this population[96]. Another potential therapy designed to modulate

endogenous progenitor cells is the transplantation of mesenchymal stromal cells (or treatment with MSC conditioned medium) for the treatment of BPD. Newborn pups subjected to hyperoxia for a 14-day period were either treated once with pulmonary artery smooth muscle cell conditioned media or mesenchymal stem cell conditioned media. The pups treated with the mesenchymal stem cell conditioned media demonstrated less alveolar loss and maintained relatively normal volume density as compared to the pulmonary artery smooth muscle cell conditioned media[49]. Clinical trials are already underway to determine the safety of treating ARDS patients with allogeneic bone marrow-derived human mesenchymal stem cells. In a similar study, Zheng et al use adipose derived mesenchymal stem cells to treat ARDS. To date, they have demonstrated that these adipose derived mesenchymal are safe, but have only shown a weak effect at the current dose[97]. Clearly, there is great potential in the use of mesenchymal stem cells as a potential therapy, but further studies are necessary.

1.2 Conclusions

The field of lung stem cell biology, and specifically lung regenerative medicine, has come a long way since early work in the 1970s. Modern techniques have allowed us to define potential new lung epithelial stem cells other than the AECII and animal model systems have enabled controlled studies of progressive diseases and acute lung injuries. Great strides have been made toward understanding the cellular and molecular processes involved in the pathologic and reparative responses of endogenous progenitor cell populations, including new insights into the stem cell niche and cell:cell communication. The insights gleaned from studies like those described above, and discussed in the following chapters, have the potential to lead to new targeted and effective therapies to prevent or reverse pathological remodeling in lung disease.

1.3 References

1. Allen, J. *et al.* Statement on the care of the child with chronic lung disease of infancy and childhood. *Am. J. Respir. Crit. Care Med.* **168,** 356–396 (2003).

2. Van Cleave, J., Gortmaker, S. L. & Perrin, J. M. Dynamics of obesity and chronic health conditions among children and youth. *JAMA* **303,** 623–630 (2010).

3. Hoyert, D. L., Arias, E., Smith, B. L., Murphy, S. L. & Kochanek, K. D. Deaths: final data for 1999. *Natl. Vital Stat. Rep.* **49,** 1–113 (2001).

4. Thabut, G. *et al.* Survival benefit of lung transplantation for patients with idiopathic pulmonary fibrosis. *J. Thorac. Cardiovasc. Surg.* **126,** 469–475 (2003).

5. Bjoraker, J. A. *et al.* Prognostic significance of histopathologic subsets in idiopathic pulmonary fibrosis. *Am. J. Respir. Crit. Care Med.* **157,** 199–203 (1998).

6. Chapman, H. A. *et al.* Integrin α6β4 identifies an adult distal lung epithelial population with regenerative potential in mice. *J. Clin. Invest.* **121,** 2855–2862 (2011).

7. Kumar, P. A. *et al.* Distal airway stem cells yield alveoli in vitro and during lung regeneration following H1N1 influenza infection. *Cell* **147,** 525–538 (2011).

8. Rock, J. R. *et al.* Notch-dependent differentiation of adult airway basal stem cells. *Cell Stem Cell* **8,** 639–648 (2011).

9. Rawlins, E. L. *et al.* The role of Scgb1a1+ Clara cells in the long-term maintenance and repair of lung airway, but not alveolar, epithelium. *Cell Stem Cell* **4,** 525–534 (2009).

10. Rock, J. R., Randell, S. H. & Hogan, B. L. M. Airway basal stem cells: a perspective on their roles in epithelial homeostasis and remodeling. *Dis. Model. Mech.* **3,** 545–556 (2010).

11. Burri, P. H. in *Comprehensive Physiology* (John Wiley & Sons, Inc., 2011).

12. Rock, J. R. & Hogan, B. L. M. Epithelial progenitor cells in lung development, maintenance, repair, and disease. *Annu. Rev. Cell Dev. Biol.* **27,** 493–512 (2011).

13. Morrisey, E. E. & Hogan, B. L. M. Preparing for the first breath: genetic and cellular mechanisms in lung development. *Dev. Cell* **18,** 8–23 (2010).

14. Metzger, R. J., Klein, O. D., Martin, G. R. & Krasnow, M. A. The branching programme of mouse lung development. *Nature* **453,** 745–750 (2008).

15. Winkelmann, A. & Noack, T. The Clara cell: a 'Third Reich eponym'? *Eur. Respir. J.* **36,** 722–727 (2010).

16. Kim, C. F. B. *et al.* Identification of bronchioalveolar stem cells in normal lung and lung cancer. *Cell* **121,** 823–835 (2005).

17. Whitsett, J. A. & Weaver, T. E. Hydrophobic surfactant proteins in lung function and disease. *N. Engl. J. Med.* **347,** 2141–2148 (2002).

18. Ding, B.-S. *et al.* Endothelial-derived angiocrine signals induce and sustain regenerative lung alveolarization. *Cell* **147,** 539–553 (2011).

19. Lee, J.-H. *et al.* Lung stem cell differentiation in mice directed by endothelial cells via a BMP4-NFATc1-thrombospondin-1 axis. *Cell* **156,** 440–455 (2014).

20. Chen, L., Acciani, T., Le Cras, T., Lutzko, C. & Perl, A.-K. T. Dynamic regulation of platelet-derived growth factor receptor α expression in alveolar fibroblasts during realveolarization. *Am. J. Respir. Cell Mol. Biol.* **47,** 517–527 (2012).

21. Barkauskas, C. E. *et al.* Type 2 alveolar cells are stem cells in adult lung. *J. Clin. Invest.* **123,** 3025–3036 (2013).

22. McGowan, S. E. & Torday, J. S. THE PULMONARY LIPOFIBROBLAST (LIPID INTERSTITIAL CELL) AND ITS CONTRIBUTIONS TO ALVEOLAR

DEVELOPMENT. *Annu. Rev. Physiol.* **59,** 43–62 (1997).

23. Rehan, V. K. *et al.* Evidence for the presence of lipofibroblasts in human lung. *Exp. Lung Res.* **32,** 379–393 (2006).

24. El Agha, E. *et al.* Two-Way Conversion between Lipogenic and Myogenic Fibroblastic Phenotypes Marks the Progression and Resolution of Lung Fibrosis. *Cell Stem Cell* (2016). doi:10.1016/j.stem.2016.10.004

25. Boström, H., Gritli-Linde, A. & Betsholtz, C. PDGF-A/PDGF alpha-receptor signaling is required for lung growth and the formation of alveoli but not for early lung branching morphogenesis. *Dev. Dyn.* **223,** 155–162 (2002).

26. Cardoso, W. V. Molecular regulation of lung development. *Annu. Rev. Physiol.* **63,** 471–494 (2001).

27. Yamamoto, H. *et al.* Epithelial-vascular cross talk mediated by VEGF-A and HGF signaling directs primary septae formation during distal lung morphogenesis. *Dev. Biol.* **308,** 44–53 (2007).

28. Gerhardt, H. & Betsholtz, C. Endothelial-pericyte interactions in angiogenesis. *Cell Tissue Res.* **314,** 15–23 (2003).

29. Rock, J. R. *et al.* Multiple stromal populations contribute to pulmonary fibrosis without evidence for epithelial to mesenchymal transition. *Proc. Natl. Acad. Sci. U. S. A.* **108,** E1475–83 (2011).

30. Armulik, A., Genové, G. & Betsholtz, C. Pericytes: developmental, physiological, and pathological perspectives, problems, and promises. *Dev. Cell* **21,** 193–215 (2011).

31. Jostarndt-Fögen, K., Djonov, V. & Draeger, A. Expression of smooth muscle markers in the developing murine lung: potential contractile properties and lineal descent.

Histochem. Cell Biol. **110,** 273–284 (1998).

32. Featherstone, N. C. *et al.* Airway smooth muscle dysfunction precedes teratogenic congenital diaphragmatic hernia and may contribute to hypoplastic lung morphogenesis. *Am. J. Respir. Cell Mol. Biol.* **35,** 571–578 (2006).

33. Schittny, J. C., Miserocchi, G. & Sparrow, M. P. Spontaneous peristaltic airway contractions propel lung liquid through the bronchial tree of intact and fetal lung explants. *Am. J. Respir. Cell Mol. Biol.* **23,** 11–18 (2000).

34. Volckaert, T. *et al.* Parabronchial smooth muscle constitutes an airway epithelial stem cell niche in the mouse lung after injury. *J. Clin. Invest.* **121,** 4409–4419 (2011).

35. James, A. L. *et al.* Airway smooth muscle hypertrophy and hyperplasia in asthma. *Am. J. Respir. Crit. Care Med.* **185,** 1058–1064 (2012).

36. Baraldi, E. & Filippone, M. Chronic lung disease after premature birth. *N. Engl. J. Med.* **357,** 1946–1955 (2007).

37. Lahra, M. M., Beeby, P. J. & Jeffery, H. E. Intrauterine inflammation, neonatal sepsis, and chronic lung disease: a 13-year hospital cohort study. *Pediatrics* **123,** 1314–1319 (2009).

38. Mourani, P. M. & Abman, S. H. Pulmonary vascular disease in bronchopulmonary dysplasia: pulmonary hypertension and beyond. *Curr. Opin. Pediatr.* **25,** 329–337 (2013).

39. Miniño, A. M., Murphy, S. L., Xu, J. & Kochanek, K. D. Deaths: final data for 2008. *Natl. Vital Stat. Rep.* **59,** 1–126 (2011).

40. Shifren, A. & Mecham, R. P. The stumbling block in lung repair of emphysema: elastic fiber assembly. *Proc. Am. Thorac. Soc.* **3,** 428–433 (2006).

41. Rennard, S. I. COPD: overview of definitions, epidemiology, and factors influencing its development. *Chest* **113,** 235S–241S (1998).

42. Collard, H. R. & King, T. E., Jr. Demystifying idiopathic interstitial pneumonia. *Arch. Intern. Med.* **163,** 17–29 (2003).

43. du Bois, R. & King, T. E., Jr. Challenges in pulmonary fibrosis x 5: the NSIP/UIP debate. *Thorax* **62,** 1008–1012 (2007).

44. Travis, W. D. *et al.* An Official American Thoracic Society/European Respiratory Society Statement: Update of the International Multidisciplinary Classification of the Idiopathic Interstitial Pneumonias. *Am. J. Respir. Crit. Care Med.* **188,** 733–748 (2013).

45. Rubenfeld, G. D. *et al.* Incidence and outcomes of acute lung injury. *N. Engl. J. Med.* **353,** 1685–1693 (2005).

46. Ladha, F. *et al.* Sildenafil improves alveolar growth and pulmonary hypertension in hyperoxia-induced lung injury. *Am. J. Respir. Crit. Care Med.* **172,** 750–756 (2005).

47. Alejandre-Alcazar, M. A. *et al.* Hyperoxia modulates TGF-beta/BMP signaling in a mouse model of bronchopulmonary dysplasia. *AJP: Lung Cellular and Molecular Physiology* **292,** L537–L549 (2006).

48. Hansmann, G. *et al.* Mesenchymal stem cell-mediated reversal of bronchopulmonary dysplasia and associated pulmonary hypertension. *Pulm. Circ.* **2,** 170–181 (2012).

49. Tropea, K. A. *et al.* Bronchioalveolar stem cells increase after mesenchymal stromal cell treatment in a mouse model of bronchopulmonary dysplasia. *Am. J. Physiol. Lung Cell. Mol. Physiol.* **302,** L829–37 (2012).

50. Park, H.-S. *et al.* Sildenafil alleviates bronchopulmonary dysplasia in neonatal

rats by activating the hypoxia-inducible factor signaling pathway. *Am. J. Respir. Cell Mol. Biol.* **48,** 105–113 (2013).

51. Sandhaus, R. A. & Turino, G. Neutrophil elastase-mediated lung disease. *COPD* **10 Suppl 1,** 60–63 (2013).

52. Stevenson, C. S. & Birrell, M. A. Moving towards a new generation of animal models for asthma and COPD with improved clinical relevance. *Pharmacol. Ther.* **130,** 93–105 (2011).

53. Ferretti, S., Bonneau, O., Dubois, G. R., Jones, C. E. & Trifilieff, A. IL-17, produced by lymphocytes and neutrophils, is necessary for lipopolysaccharide-induced airway neutrophilia: IL-15 as a possible trigger. *J. Immunol.* **170,** 2106–2112 (2003).

54. Dhaliwal, K. *et al.* Monocytes control second-phase neutrophil emigration in established lipopolysaccharide-induced murine lung injury. *Am. J. Respir. Crit. Care Med.* **186,** 514–524 (2012).

55. Desai, T. J. & Krasnow, M. A. Stem cells: Differentiated cells in a back-up role. *Nature* **503,** 204–205 (2013).

56. Adamson, I. Y. Pulmonary toxicity of bleomycin. *Environ. Health Perspect.* **16,** 119–126 (1976).

57. Zheng, D. *et al.* Regeneration of alveolar type I and II cells from Scgb1a1-expressing cells following severe pulmonary damage induced by bleomycin and influenza. *PLoS One* **7,** e48451 (2012).

58. Hung, C. *et al.* Role of lung pericytes and resident fibroblasts in the pathogenesis of pulmonary fibrosis. *Am. J. Respir. Crit. Care Med.* **188,** 820–830 (2013).

59. Gabrielli, A., Avvedimento, E. V. & Krieg, T. Scleroderma. *N. Engl. J. Med.* **360,**

1989–2003 (2009).

60. Lin, S.-L., Kisseleva, T., Brenner, D. A. & Duffield, J. S. Pericytes and perivascular fibroblasts are the primary source of collagen-producing cells in obstructive fibrosis of the kidney. *Am. J. Pathol.* **173,** 1617–1627 (2008).

61. Greenhalgh, S. N., Iredale, J. P. & Henderson, N. C. Origins of fibrosis: pericytes take centre stage. *F1000Prime Rep.* **5,** 37 (2013).

62. Humphreys, B. D. *et al.* Fate tracing reveals the pericyte and not epithelial origin of myofibroblasts in kidney fibrosis. *Am. J. Pathol.* **176,** 85–97 (2010).

63. van Haaften, T. *et al.* Airway delivery of mesenchymal stem cells prevents arrested alveolar growth in neonatal lung injury in rats. *Am. J. Respir. Crit. Care Med.* **180,** 1131–1142 (2009).

64. Chow, K. *et al.* Dysfunctional resident lung mesenchymal stem cells contribute to pulmonary microvascular remodeling. *Pulm. Circ.* **3,** 31–49 (2013).

65. Fatima, S., Zhou, S. & Sorrentino, B. P. Abcg2 expression marks tissue-specific stem cells in multiple organs in a mouse progeny tracking model. *Stem Cells* **30,** 210–221 (2012).

66. Almeida, C. *et al.* The role of alveolar epithelium in radiation-induced lung injury. *PLoS One* **8,** e53628 (2013).

67. Haston, C. K., Begin, M., Dorion, G. & Cory, S. M. Distinct loci influence radiation-induced alveolitis from fibrosing alveolitis in the mouse. *Cancer Res.* **67,** 10796–10803 (2007).

68. Citrin, D. E. *et al.* Role of type II pneumocyte senescence in radiation-induced lung fibrosis. *J. Natl. Cancer Inst.* **105,** 1474–1484 (2013).

69. Lawson, W. E. & Loyd, J. E. The genetic approach in pulmonary fibrosis: can it provide clues to this complex disease? *Proc. Am. Thorac. Soc.* **3,** 345–349 (2006).

70. Peljto, A. L. *et al.* The pulmonary fibrosis-associated MUC5B promoter polymorphism does not influence the development of interstitial pneumonia in systemic sclerosis. *Chest* **142,** 1584–1588 (2012).

71. Zhong, Q. *et al.* Role of endoplasmic reticulum stress in epithelial-mesenchymal transition of alveolar epithelial cells: effects of misfolded surfactant protein. *Am. J. Respir. Cell Mol. Biol.* **45,** 498–509 (2011).

72. Lawson, W. E. *et al.* Endoplasmic reticulum stress in alveolar epithelial cells is prominent in IPF: association with altered surfactant protein processing and herpesvirus infection. *Am. J. Physiol. Lung Cell. Mol. Physiol.* **294,** L1119–26 (2008).

73. Chilosi, M., Carloni, A., Rossi, A. & Poletti, V. Premature lung aging and cellular senescence in the pathogenesis of idiopathic pulmonary fibrosis and COPD/emphysema. *Transl. Res.* **162,** 156–173 (2013).

74. Liu, T. *et al.* Telomerase activity is required for bleomycin-induced pulmonary fibrosis in mice. *J. Clin. Invest.* **117,** 3800–3809 (2007).

75. Liu, T. *et al.* Telomerase and telomere length in pulmonary fibrosis. *Am. J. Respir. Cell Mol. Biol.* **49,** 260–268 (2013).

76. Strong, M. A. *et al.* Phenotypes in mTERT+/- and mTERT-/- Mice Are Due to Short Telomeres, Not Telomere-Independent Functions of Telomerase Reverse Transcriptase. *Mol. Cell. Biol.* **31,** 2369–2379 (2011).

77. Alder, J. K. *et al.* Telomere length is a determinant of emphysema susceptibility. *Am. J. Respir. Crit. Care Med.* **184,** 904–912 (2011).

78. Massaro, D., Massaro, G. D., Baras, A., Hoffman, E. P. & Clerch, L. B. Calorie-related rapid onset of alveolar loss, regeneration, and changes in mouse lung gene expression. *Am. J. Physiol. Lung Cell. Mol. Physiol.* **286,** L896–906 (2004).

79. Brody, J. S. Time course of and stimuli to compensatory growth of the lung after pneumonectomy. *J. Clin. Invest.* **56,** 897–904 (1975).

80. Bennett, R. A., Colony, P. C., Addison, J. L. & Rannels, D. E. Effects of prior adrenalectomy on postpneumonectomy lung growth in the rat. *Am. J. Physiol.* **248,** E70–4 (1985).

81. Buhain, W. J. & Brody, J. S. Compensatory growth of the lung following pneumonectomy. *J. Appl. Physiol.* **35,** 898–902 (1973).

82. Nolen-Walston, R. D. *et al.* Cellular kinetics and modeling of bronchioalveolar stem cell response during lung regeneration. *Am. J. Physiol. Lung Cell. Mol. Physiol.* **294,** L1158–65 (2008).

83. Hsia, C. C. *et al.* Structural changes underlying compensatory increase of diffusing capacity after left pneumonectomy in adult dogs. *J. Clin. Invest.* **92,** 758–764 (1993).

84. Chamoto, K. *et al.* Alveolar epithelial dynamics in postpneumonectomy lung growth. *Anat. Rec.* **296,** 495–503 (2013).

85. Butler, J. P. *et al.* Evidence for adult lung growth in humans. *N. Engl. J. Med.* **367,** 244–247 (2012).

86. Brown, L. M., Rannels, S. R. & Rannels, D. E. Implications of post-pneumonectomy compensatory lung growth in pulmonary physiology and disease. *Respir. Res.* **2,** 340–347 (2001).

87. Hsia, C. C., Wu, E. Y., Wagner, E. & Weibel, E. R. Preventing mediastinal shift after pneumonectomy impairs regenerative alveolar tissue growth. *Am. J. Physiol. Lung Cell. Mol. Physiol.* **281,** L1279–87 (2001).

88. Dane, D. M., Johnson, R. L., Jr & Hsia, C. C. W. Dysanaptic growth of conducting airways after pneumonectomy assessed by CT scan. *J. Appl. Physiol.* **93,** 1235–1242 (2002).

89. Chamoto, K. *et al.* Migration of CD11b+ accessory cells during murine lung regeneration. *Stem Cell Res.* **10,** 267–277 (2013).

90. Ott, H. C. *et al.* Regeneration and orthotopic transplantation of a bioartificial lung. *Nat. Med.* **16,** 927–933 (2010).

91. Bonvillain, R. W. *et al.* A nonhuman primate model of lung regeneration: detergent-mediated decellularization and initial in vitro recellularization with mesenchymal stem cells. *Tissue Eng. Part A* **18,** 2437–2452 (2012).

92. Ghaedi, M. *et al.* Human iPS cell-derived alveolar epithelium repopulates lung extracellular matrix. *J. Clin. Invest.* **123,** 4950–4962 (2013).

93. Mou, H. *et al.* Generation of multipotent lung and airway progenitors from mouse ESCs and patient-specific cystic fibrosis iPSCs. *Cell Stem Cell* **10,** 385–397 (2012).

94. Yan, Q. *et al.* A Site-Specific Genetic Modification for Induction of Pluripotency and Subsequent Isolation of Derived Lung Alveolar Epithelial Type II Cells. *Stem Cells* **32,** 402–413 (2014).

95. Longmire, T. A. *et al.* Efficient derivation of purified lung and thyroid progenitors from embryonic stem cells. *Cell Stem Cell* **10,** 398–411 (2012).

96. Shyamsundar, M. *et al.* Keratinocyte growth factor promotes epithelial survival

and resolution in a human model of lung injury. *Am. J. Respir. Crit. Care Med.* **189,** 1520–1529 (2014).

97. Zheng, G. *et al.* Treatment of acute respiratory distress syndrome with allogeneic adipose-derived mesenchymal stem cells: a randomized, placebo-controlled pilot study. *Respir. Res.* **15,** 39 (2014).

98. Evans, M. J., Cabral-Anderson, L. J. & Freeman, G. Role of the Clara cell in renewal of the bronchiolar epithelium. *Lab. Invest.* **38,** 648–653 (1978).

99. Reynolds, S. D., Reynolds, P. R., Pryhuber, G. S., Finder, J. D. & Stripp, B. R. Secretoglobins SCGB3A1 and SCGB3A2 define secretory cell subsets in mouse and human airways. *Am. J. Respir. Crit. Care Med.* **166,** 1498–1509 (2002).

100. Evidence for Human Lung Stem Cells. *N. Engl. J. Med.* **365,** 464–466 (2011).

101. Hines, E. A., Jones, M.-K. N., Verheyden, J. M., Harvey, J. F. & Sun, X. Establishment of smooth muscle and cartilage juxtaposition in the developing mouse upper airways. *Proc. Natl. Acad. Sci. U. S. A.* **110,** 19444–19449 (2013).

102. Rock, J. & Königshoff, M. Endogenous lung regeneration: potential and limitations. *Am. J. Respir. Crit. Care Med.* **186,** 1213–1219 (2012).

103. Chen, G. *et al.* SPDEF is required for mouse pulmonary goblet cell differentiation and regulates a network of genes associated with mucus production. *J. Clin. Invest.* **119,** 2914–2924 (2009).

104. Hovenberg, H. W., Davies, J. R., Herrmann, A., Lindén, C. J. & Carlstedt, I. MUC5AC, but not MUC2, is a prominent mucin in respiratory secretions. *Glycoconj. J.* **13,** 839–847 (1996).

105. Rock, J. R. *et al.* Basal cells as stem cells of the mouse trachea and human airway

epithelium. *Proc. Natl. Acad. Sci. U. S. A.* **106,** 12771–12775 (2009).

106. Engelhardt, J. F. Stem cell niches in the mouse airway. *Am. J. Respir. Cell Mol. Biol.* **24,** 649–652 (2001).

107. Keith, I. M., Pelto-Huikko, M., Schalling, M. & Hökfelt, T. Calcitonin gene-related peptide and its mRNA in pulmonary neuroendocrine cells and ganglia. *Histochemistry* **96,** 311–315 (1991).

108. Bachar, O., Adner, M., Uddman, R. & Cardell, L.-O. Nerve growth factor enhances cholinergic innervation and contractile response to electric field stimulation in a murine in vitro model of chronic asthma. *Clin. Exp. Allergy* **34,** 1137–1145 (2004).

109. Weichselbaum, M., Sparrow, M. P., Hamilton, E. J., Thompson, P. J. & Knight, D. A. A confocal microscopic study of solitary pulmonary neuroendocrine cells in human airway epithelium. *Respir. Res.* **6,** 115 (2005).

110. Beers, M. F. *et al.* An antibody with specificity for surfactant protein C precursors: identification of pro-SP-C in rat lung. *Am. J. Respir. Cell Mol. Biol.* **7,** 368–378 (1992).

111. Bullard, J. E. & Nogee, L. M. Heterozygosity for ABCA3 mutations modifies the severity of lung disease associated with a surfactant protein C gene (SFTPC) mutation. *Pediatr. Res.* **62,** 176–179 (2007).

112. Desai, T. J., Brownfield, D. G. & Krasnow, M. A. Alveolar progenitor and stem cells in lung development, renewal and cancer. *Nature* **507,** 190–194 (2014).

113. Vanderbilt, J. N. *et al.* Directed expression of transgenes to alveolar type I cells in the mouse. *Am. J. Respir. Cell Mol. Biol.* **39,** 253–262 (2008).

114. McElroy, M. C. & Kasper, M. The use of alveolar epithelial type I cell-selective

markers to investigate lung injury and repair. *Eur. Respir. J.* **24,** 664–673 (2004).

115. Huang, S. X. L. *et al.* Efficient generation of lung and airway epithelial cells from human pluripotent stem cells. *Nat. Biotechnol.* **32,** 84–91 (2014).

1.4 Figures and Tables

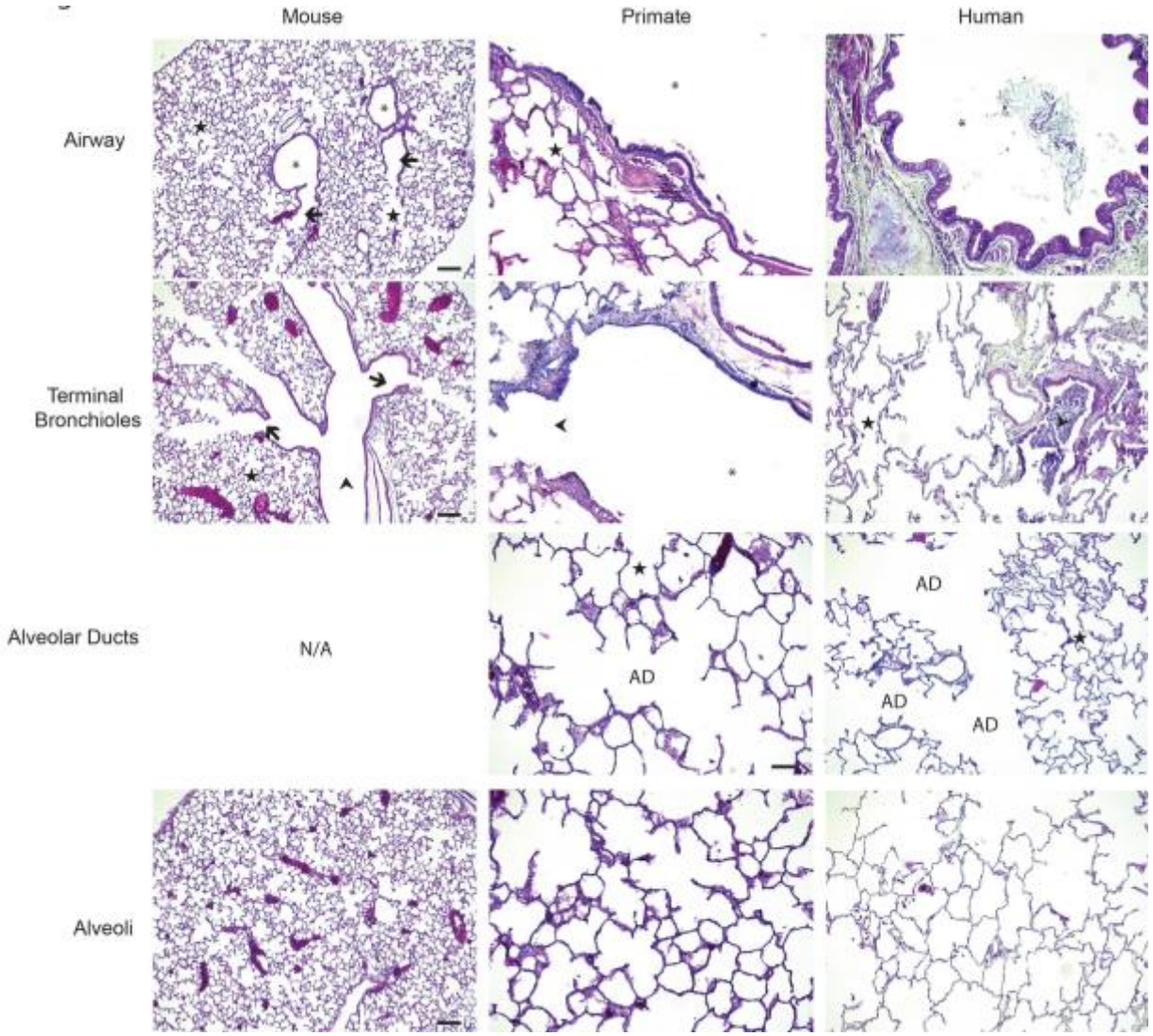

Figure 1. Comparison of Lung Airway and Airspace Morphology between Mouse, Primate, and Human

There are important differences between mouse and human lungs. For example, the lungs of humans are larger, with more generations of airway branches. Unlike mice, most of the intralobar airways of humans are lined with a pseudostratified epithelium containing submucosal glands and surrounded by airway smooth muscle and cartilage rings or plates. The smallest airways in humans, called terminal and respiratory bronchioles, are distinct from the bronchioalveolar duct junction in mice. Importantly, bronchioalveolar stem cells (BASCs) that were identified in mouse lungs have not been reported in human lungs. The lungs of rhesus macaques more closely resemble the lungs of humans, perhaps representing an improved model to study lung disease and injury/repair. Scale bars = 100um.

* Conducting airway
ç Bronchiolalveolar Duct Junction
… Terminal Bronchiole Airway
AD Alveolar Ducts
★ Alveoli

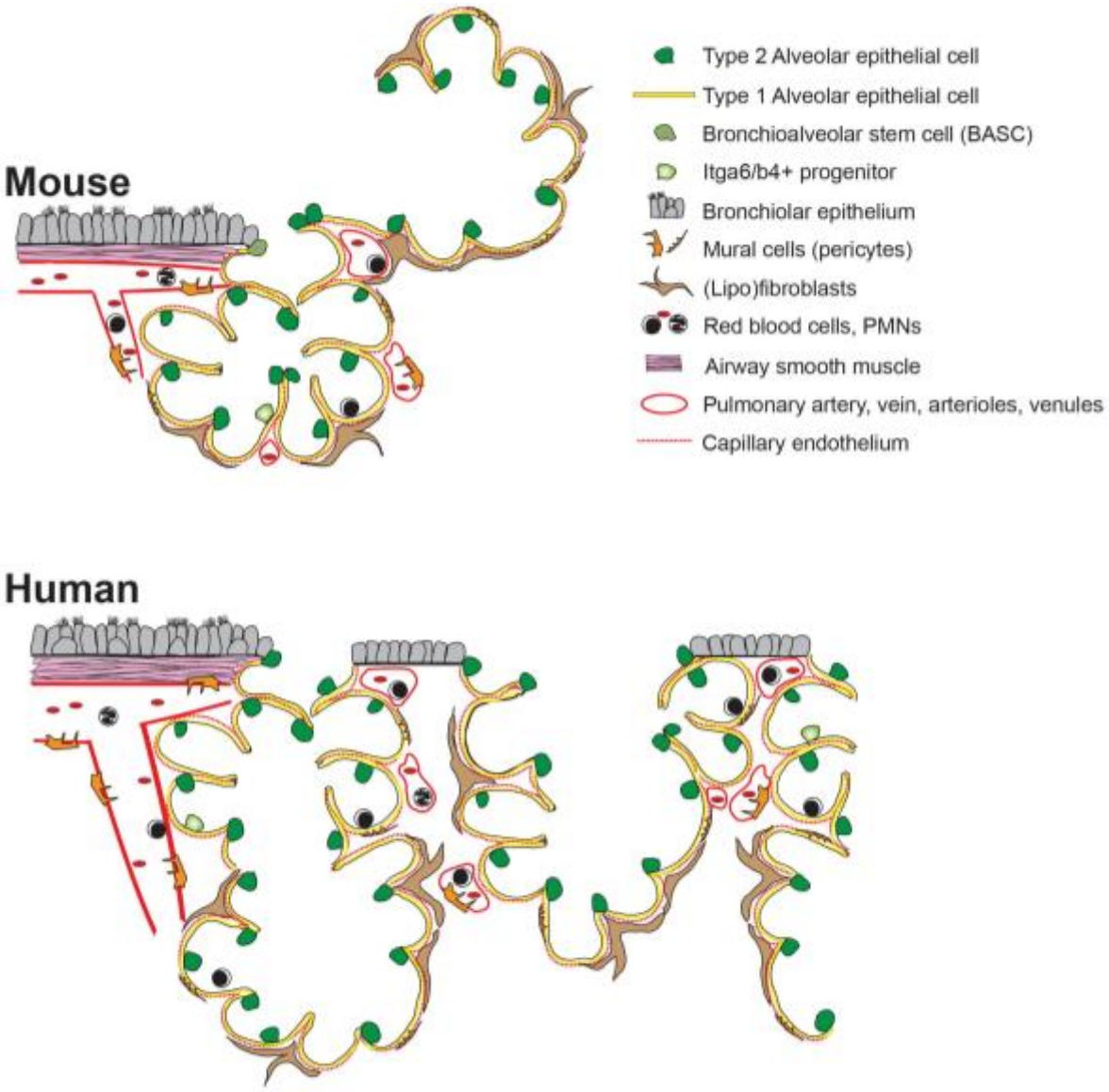
Mouse
Type 2 Alveolar epithelial cell
Type 1 Alveolar epithelial cell
Bronchioalveolar stem cell (BASC)
Itga6/b4+ progenitor
Bronchiolar epithelium
Mural cells (pericytes)
(Lipo)fibroblasts
Red blood cells, PMNs
Airway smooth muscle
Pulmonary artery, vein, arterioles, venules
Capillary endothelium
Human

Figure 2. Schematic of mouse and human/primate distal lung

Schematic of mouse and human/primate distal lung showing relative location of cell types discussed. Note the cuboidal epithelial lining of the respiratory bronchioles and the alveolar ducts that are not present in mice. BASCs, located at the bronchioalveolar duct junction in mice, have not been reported in mice.

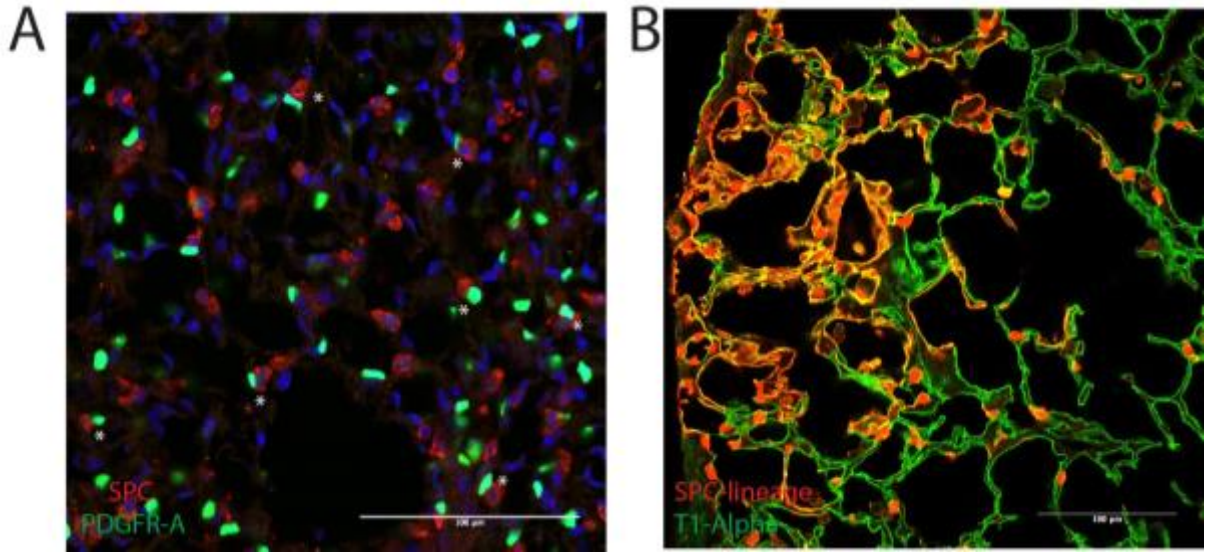
A
SPC
PDGFR-A
B
SPC lineage
T1-Alpha

Figure 3. Relative Location of Lipofibroblasts to AECIIs and Compensatory Lung Growth

Antibody staining of a section of lung from PDGFRA-HRB:GFP mice in which cells that express Pdgfra are marked with nuclear localized GFP. PDGFRA+ (lipo)fibroblasts are often found in close proximity to SPC+ AECII (*). Mounting data suggest that the fibroblasts constitute a component of the AECII "niche." Scale bars = 100uM

Compensatory lung growth following pneumonectomy in adults is one model that is useful to define the cellular and molecular processes that mediate distal lung regeneration. In the mouse, SPC-CreER lineage labeled cells (red) give rise to AECI (Pdpn, green) post-pneumonectomy, demonstrating that AECII have the capacity to generate new alveolar epithelium in this model. Scale bars = 100uM

Table 1- Selected Markers for Common Airway and Alveoli Cells

Cell Type	Gene Symbol
Airway Epithelium	
Club Cell	CCSP (CC10), Scgb1a1, Scgb3a2[98,99,9,100]
Ciliated Cell	TUBA1A[101]
Goblet Cell	MUC1, SPEDF, AGR2, MUC5AC, MUC5B[102,103,104]
Basal Cell	Krt5, P63, NGFR[105]
Neuroendocrine Cell	Cgrp, PGP9.5[106,107,108,109]
Bronchioalveolar Duct Junction	
Club Cell	CCSP (CC10), Scgb1a1, Scgb3a2
Bronchioalveolar Stem Cell (BASC)	CCSP/SPC[16]
Alveolar Epithelium	
Alveolar Type II Cell (AECII)	SPC, ABCA3,LYSM[105,110,111,112]
Alevolar Type I Cell (AECI)	PDPN, AQP5, HOPX[113,114,115,21]

Table 1. Selected markers for common airway and alveolar cells

Above is a table of commonly described cell types found in airways, brionchioalveolar duct junctions, and alveoli. We have compiled a list of previously published antibodies that can be used in mouse and human tissue.

Chapter 2

The role of the Notch signaling pathway in lung regeneration

2.1 Introduction

Defining resident stem cells in adult organ systems and determining the molecular regulators that drive stem cell proliferation and differentiation are necessary steps to developing regenerative therapies. There is an urgent need to address these questions in the lung because transplantable organs are scarce and lung disease has become the third leading cause of death in the US [1]. Classical and recent data demonstrate that type 2 alveolar epithelial cells (AECIIs) are capable of self-renewal and differentiation into AECIs in the adult lung [2-5]. Additional alveolar progenitor cell populations have recently been reported in the context of severe injury [6-8], but knowledge about the relative contributions of these populations and their ability to generate new functional alveolar epithelium awaits specific genetic lineage tracing.

Notch signaling regulates multiple aspects of embryonic lung development, adult homeostasis, and repair (reviewed in [9] [10,11] [12]. Several groups including our own have shown that Notch signaling is required for the differentiation of basal cells toward luminal lineages in the pseudostratified airway epithelium of adult lungs [13-15]. In addition to its role in progenitor cell differentiation, steady state Notch signaling in the conducting airway epithelium is required for the maintenance of club cells [16]. Less is known about Notch functions in the distal alveolar region of the lung. Recent data demonstrate that loss of Notch signaling in the alveolar epithelium during late embryonic/early post-natal development disrupts epithelial-mesenchymal interactions and leads to an emphysema-like phenotype [17]. In adult alveoli, data support a model

in which persistent Notch signaling in a recently described "lineage negative epithelial progenitor" prevents their differentiation into alveolar lineages [18]. Recent data suggest that the Notch ligand Jagged coming from pulmonary capillary endothelial cells contributes to the development of pulmonary fibrosis [19]. However, whether Notch directly regulates AECII behaviors in the adult has not been reported.

Here we use a pneumonectomy (PNX) model, or surgical reduction in lung volume, to identify cells and molecular processes that mediate the generation of new alveolar epithelium in adult lungs. This innate regenerative response post-PNX has been shown to occur in animals ranging from rodents to humans [20-24]. Previous studies have demonstrated that multiple epithelial populations, including AECIIs and BASCs, proliferate following PNX [20,25-28]. However, the extent to which different progenitor populations give rise to new alveolar epithelial cells remains unclear. For example, one recent report showed that lineage labeled AECI, long regarded as terminally differentiated and post-mitotic, gave rise to as many as 9% of AECII post-PNX[24]. Our work confirms that lineage-labeled AECII proliferate in response to PNX and generate AECI within 21-days post-surgery in mice. Our data support a model in which Notch signaling in AECIIs is required for this regenerative response and we provide evidence that PDGFRA+ fibroblasts are a component of the regenerative niche. Finally, we demonstrate for the first time an increase in AECII proliferation post-PNX in adult rhesus macaques.

2.2 Methods

Mice

Sftpc-CreERT2 (Sftpctm1(cre/ERT)Blh), ROSA-td-Tomato (Gt(ROSA)26Sortm2(CAG-tdTomato)Fawa), Rbpj flox (Rbpjtm1Hon), and Pdgfra-GFP (Pdgfratm11(EGFP)Sor) mice have

previously been described [3,29,30] All studies were approved by University of California, San Francisco (UCSF) Institutional Animal Care and Use Committees (IACUC).

Tamoxifen and EdU Administration

Tamoxifen (T5648; Sigma-Aldrich) was a 20 mg/ml stock solution in corn oil and given via intraperitoneal injection. Four 25mg/kg doses of TMX were given to each animal every other day for 4 days. EdU (Click-iT EdU Alexa Fluor 647 Imaging Kit C10340; Invitrogen) was administered via i.p. injection (50 mg/kg) three hours prior to sacrifice unless otherwise mentioned.

Pneumonectomy

10-14-week-old adult mice were anesthetized and intubated for ventilation using a Harvard mini-vent ventilator set at 200uL stroke volume at 200 strokes per minute. 2% isoflurane was administered via the ventilator throughout surgery. Once intubated and anesthetized, the left lung lobe was exposed through the rib cage and the pulmonary vasculature and left mainstem bronchus was ligated with a titanium clip. The left lobe was resected, and the ribs and skin closed. The left lobe was lifted through the rib cage and replaced but not resected in sham-operated animals.

Lung Dissociation and FACS

Mice were euthanized by CO_2 exposure and perfused with 20 mL cold PBS through the right ventricle. Lungs were inflated with protease solution [1–2 mL; Collagenase Type I (catalog #17100–017, 450 U/mL; Gibco), Elastase (catalog #LS002279, 4 U/mL; Worthington

Biochemical Corporation), Dispase (catalog #354235, 5 U/mL; BD Biosciences) and DNaseI (catalog #10104159001, 0.33 U/mL; Roche) in DMEM/F12], cut into small pieces (<2 mm2), and incubated in 2 mL protease solution for 20 min at 37 °C with frequent agitation. DMEM/F12 + 10% FBS was added, and tissue was disrupted by pipetting, washed with DMEM/F12, and incubated for 5 min at 37 °C in 2 mL 0.1% Trypsin-EDTA + 0.325 mg DNaseI with intermittent agitation. An equal volume of DMEM-F12 + 10% FBS was added, and tissue was dissociated by pipetting. Cells were washed with 5 mL DMEM/F12, incubated at room temperature for 1.5 min in warmed 2 mL red blood cell lysis buffer (catalog #00–4333-57; eBioscience), filtered through a 40-μm strainer, centrifuged, and resuspended in PBS + 2% BSA. Sorting was performed on FACS ARIA II, and data was analyzed with FACS Diva (BD Biosciences).

qPCR

RNA was purified from cell collected by FACS for qPCR using Trizol (Invitrogen). RNA pellets were resuspended in TE pH 8.0 (ambion) and RNA quantity and quality was measured using a Nanodrop. cDNA was made with Vilo Mastermix (Invitrogen 11755250) and qPCR master mix was SYBR GreenEr (Invitrogen 11762). 384 well plates were run on a Viia7 and RNA expression was measured using the $2^{\wedge-(\Delta\Delta CT)}$ in which each of the three PNX mice were compared to an average of all three sham animals. All reactions were run in triplicate. Statistical analysis and graphing was then produced by Prism 6 software.

Cell Culture

FACS sorted SFTPC+ cells and PDGFRA+ cells were plated in the upper chamber of .4uM transwell wells in 24 well tissue culture plates at a ratio of 2,500 SFTPC+ cells to 50,000

PDGFRA+ cells. Cells were seeded in 48uL of growth factor reduced Matrigel (BD Biosciences 356230) and 48uL of pneumosphere media: DMEM/F12 +10% FBS containing FGF 50ng/mL, EGF 40ng/mL, KGF 20ng/mL, HGF 20ng/mL, PDGF-B 20ng/mL, ITS (1x Gibco), Cholera toxin (0.25mg/ml). 500uL of pneumosphere media was then placed in the lower chamber and changed every two days after plating. Gamma Secretase Inhibitor DAPT (Sigma D5942) was diluted in DMSO (.1%) and used at a final concentration of 50uM.

Mouse Tissue Preparation

Animals were injected with 50mg/kg of EdU resuspended in PBS three hours prior to sacrifice to label proliferating cells. Mice were euthanized by CO_2 exposure, and pulmonary perfusion was performed with 20 mL cold PBS through the right ventricle. Lungs and trachea were removed and inflated to 20 cm H_2O pressure with 4% paraformaldehyde. Lungs were fixed for 30 minutes at 4ºC in 4% paraformaldehyde and washed 3x15 minutes in PBS.

Immunohistochemistry of Mouse Tissue

Wax slides were dewaxed and rehydrated. Antigen retrieval was performed using Dako unmasking solution (Dako S169984). Samples were pressure cooked for 15 minutes at 110ºC. Samples were washed 3x in PBS. Cryosections (100 μm) and paraffin sections (7 μm) were stained by standard protocols. Rabbit anti-SFTPC (catalog #ab3786, 1:500; Millipore), goat anti-secretoglobin1a1 (SCGB1A1; 1:10,000; kind gift from Barry Strip), were used without antigen retrieval on cryosections. Hamster anti-PDPN (clone 8.1.1, 1:1,000; DSHB) was used without antigen retrieval on paraffin sections. Rabbit anti-RFP (catalog #600– 4013791:250; Rockland) and Rabbit anti-NICD2 (Millipore 07-1233) was used with antigen retrieval on paraffin sections.

Rabbit anti-SFTPC (see above) was used with antigen retrieval on paraffin sections. EdU staining performed per manufacturer recommendations. Alexa-Fluor–coupled secondary antibodies (Invitrogen) were used at 1:500. A Zeiss Imager M2 was used for normal fluorescent imaging. A Zeiss Lumar V12 stereoscope was used to image alveolospheres in culture. Z stacks of optical sections were captured on a Leica Sp5 laser-scanning confocal microscope. Unless otherwise noted, sections from at least three mice were analyzed for each data point.

Primates-

All monkeys selected for these studies were California National Primate Research Center colony-born rhesus macaques (*Macaca mulatta*). All monkeys were given a comprehensive physical examination, including a chest radiograph and complete blood count, and were determined to be healthy monkeys. Care and housing of animals complied with the provisions of the Institute of Laboratory Animal Resources and conformed to practices established by the Association for Assessment and Accreditation of Laboratory Animal Care (AAALAC). Animal studies conformed to applicable provisions of the Animal Welfare Act and other federal statutes and regulations relating to animals (*Guide for the Care and Use of Laboratory Animals*; National Institutes of Health, revised 1985). Experimental protocols were reviewed and approved by the University of California, Davis Institutional Animal Care and Use Committee. 12 adult female rhesus monkeys (aged 4years 5months to 9years 2month, weights from 4.9 to 11.22kg) underwent PNX or sham operation in the CNPRC surgery suite. 7 days or 7 weeks later, animals were euthanized with an overdose of pentobarbital after being sedated with Telazol (8 mg/kg im) and anesthetized with Diprivan (0.1–0.2 mg/kg^{1} $/min^{1}$ iv) with the dose adjusted as necessary by the attending veterinarian. The monkeys were necropsied following exsanguination through the

posterior vena cava. The lungs were fixed via the airways through a tracheal cannula with 4% paraformaldehyde at 30-cm fluid pressure (8 h). Estimated alveolar volume was performed using Euler Characteristics [31,32] and estimated lung volume was performed using an immersion technique [33]. Wax sections were dewaxed and rehydrated for immunostaining. Antigen retrieval was performed using Dako unmasking solution (Dako S169984). Samples were pressure cooked for 15 minutes at 110ºC. Samples were washed 3x in PBS. Paraffin sections (7 μm) were stained by standard protocols with rabbit anti-pro-SPC (#ab3786, 1:500; Millipore).

2.3 Results

AECII proliferate and give rise to AECI post-PNX

We generated adult Sftpc-CreER/+;ROSA-Tomato/+ mice and administered 4 doses of tamoxifen to label ~85% of the total AECII population with a heritable RFP reporter as previously described [3]. Two weeks after the final dose of tamoxifen, mice either underwent a left lobe pneumonectomy (PNX) or a sham operation. All mice were given EdU 3 hours prior to euthanasia 7-days post-operation. Immunofluorescence analysis shows that 0.28 ± 0.17% of lineage labeled cells incorporated EdU in the lungs of sham operated mice compared to 7.81 ± 1.97% in the lung of mice post-PNX. (Figure 1 A-C).

It has previously been reported that AECII give rise to AECI following PNX and are therefore one source of new alveolar epithelium [4]. To confirm this, we dosed Sftpc-CreER; ROSA-Tomato mice with tamoxifen and performed sham operations or PNX as described above. Animals were sacrificed for analysis 3-weeks post-operation, when the compensatory response is complete [34]. Thick sections were stained with antibodies against RFP (lineage-label) and

podoplanin (PDPN, AECI marker) and analyzed by confocal microscopy. We focused on the periphery of the accessory lobe as previous morphometric data demonstrates greatest expansion of this lobe [35,36]. In sham operated animals, approximately 3.33 ± 1.17% of lineage-labeled cells co-express PDPN (Figure 1 D, E, G). This is in stark contrast to the post-PNX lungs in which 40.33 ± 1.05% of lineage-labeled cells expressed PDPN (Figure1 D, F, H). These data confirm that AECII, as a population, are a major contributor to the formation of new alveolar epithelium in the remaining right lobes following PNX.

Notch receptors and downstream targets are upregulated in the lung post-PNX

Next, we sought to identify molecular regulators of AECII proliferation and differentiation. Because the Notch signaling pathway regulates many adult stem cell populations, including basal cells of the conducting airway epithelium, and controls embryonic alveologenesis, we hypothesized that this pathway would also play a role in adult alveologenesis [11,13,17,37]. Sftpc-CreER; ROSA-Tomato lineage-labeled cells were isolated by FACS from the lungs of mice 4-days post-PNX or sham operation for qPCR analysis. We detected increased *Pdpn* expression in the lineage-labeled population compared to sham controls, consistent with increased generation of AECI from lineage-labeled cells post-PNX (Figure 2A). We also detected increased expression of the Notch receptors 1 and 2 and the downstream target *Hey2* in lineage labeled cells 4-days post-PNX compared to sham operated lungs (Figure 2A).

Several lines of evidence suggest that resident PDGFRA+ fibroblasts, often observed adjacent to AECII (Figure S1A, B), constitute a component of the AECII niche in vivo [4,38,39]. To determine if this population is a source of Notch ligand following PNX, we isolated GFP+ cells from mice in which a histone-tagged GFP is knocked into the *Pdgfra* locus. Expression of the

Notch ligand *Jag2* was increased in PDGFRA+ fibroblasts 4-days post-PNX compared to fibroblasts from sham operated animals (Figure 2B). Together, these data suggest that Notch signaling regulates AECII behaviors post-PNX and implicate PDGFRA+ fibroblasts as a component of the regenerative niche.

Notch signaling regulates colony formation in an in vitro assay of alveologensis

To begin characterizing the epithelial:mesenchymal interactions that regulate progenitor cell behaviors in the alveoli, we modified a co-culture system in which AECII co-cultured with PDGFRA+ fibroblasts clonally expand to self-renew and give rise to AECI [4] (Figure S1). AECII and fibroblasts are isolated by FACS from Sftpc-CreER; Rosa-Tomato mice and Pdgfra-GFP mice, respectively. The cells are mixed and seeded in a mixture of growth factor reduced Matrigel and growth medium. Within 7-days, individual AECII give rise to multicellular "alveolospheres" (Figure S1C). No colonies formed after 14 days in culture if PDGFRA+ cells were not added to the system (Figure S1D). Alveolospheres were fixed and stained after 14 days of culture with antibodies against pro-Sftpc (AECII), PDPN (AECI), and SCGB1A1 (Club cells). Pro-Sftpc and luminal PDPN were detected in the alveolospheres. We did not observe any colonies that expressed SCGB1A1 (Figure S1E-F).

As a first step to test the effect of Notch on AECII proliferation and differentiation, Sftpc lineage-labeled cells and PDGFRA+ fibroblasts were isolated by FACS as described above and seeded in the alveolosphere assay. The gamma secretase inhibitor DAPT (50 um) or DMSO (.1%) vehicle control was added at the time of plating. At both 7 and 14-days post-plating, DAPT reduced the colony forming efficiency (0.66 ± 0.12%) of AECII compared to vehicle controls (3.13 ± 0.10%) (Figure 2C-E and data not shown). These data suggest that Notch

regulates the survival, proliferation or differentiation of AECII; however, this conclusion was limited by the caveat that DAPT treatment would affect Notch signaling in both AECII and PDGFRA+ fibroblasts.

To address this issue, we generated Sftpc-CreER; $RBPJ^{Fx/Fx}$; ROSA-tomato mice and Sftpc-CreER; $RBPJ^{Fx/+}$; Rosa-tomato mice as negative controls. We gave 4 doses of tamoxifen to induce lineage labeling and deletion of one or both copies of the Notch transcriptional cofactor Rbpj in control and experimental mice, respectively. Two weeks after the final dose of tamoxifen, the mice were sacrificed and lineage-labeled cells were isolated by FACS and co-cultured with normal PDGFRA+ fibroblasts. Lineage-labeled RBPJ-deficient AECII ("RBPJ KO") had a reduced CFE (6.25 ± 0.09%) compared to RBPJ heterozygous ("RBPJ Het") AECII 14-days post-plating (8.39 ± 0.12%) (Figure 2F-H). These data suggest that the Notch pathway regulates cell survival or proliferation of AECII in vitro.

Notch signaling regulates proliferation and differentiation of AECII post-PNX in vivo

To determine if Notch regulates AECII behaviors during adult alveologenesis in vivo, we generated Sftpc-CreER; $RBPJ^{Fx/Fx}$; ROSA-Tomato mice and Sftpc-CreER; $RBPJ^{Fx/+}$; ROSA-Tomato controls as described above. Adult mice were given 4 doses of tamoxifen to induce lineage-labeling and deletion of one or both alleles of *Rbpj*. 2-weeks later, mice underwent PNX. In control animals, 9 ± 0.44% of lineage-labeled RBPJ heterozygous cells incorporated EdU 7-days post-PNX compared to only 2.3 ± 1.5% of lineage-labeled RBPJ-deficient cells (Figure 3A-C).

Next, we analyzed cohorts of Sftpc-CreER; $RBPJ^{Fx/Fx}$; ROSA-Tomato mice and Sftpc-CreER; $RBPJ^{Fx/+}$; ROSA-Tomato controls by immunofluorescence 21-days post-PNX to

determine if Notch regulates the differentiation of AECII into AECI. In control mice, 30 ± 4.3% of lineage-labeled cells expressed markers of AECI (Figure 3D, E, G). In stark contrast, only 6.4± 2.3% of RBPJ-deficient lineage-labeled AECII gave rise to AECI (Figure 3D, F, H). Together, these data support a model in which Notch signaling is involved with regulating AECII proliferation and differentiation during compensatory lung growth in adult mice.

AECII proliferate in a nonhuman primate model of adult alveologenesis

We sought to determine whether AECII proliferate following PNX in nonhuman primates because their lungs are structurally and physiologically more similar to human lungs than those of mice. One young adult female rhesus macaque underwent a sham operation and one age-matched female macaque underwent PNX. CT scans were performed pre-operation, immediately post-operation, 2-weeks post-operation and 4-weeks post-operation to assess changes in lung size (Figure 4A-D). Within two weeks of PNX, the remaining right lobes shifted and expanded into the left chest cavity. Within 4 weeks, the remaining right lobes completely filled the chest cavity (Figure 4D). The accessory lobe of one macaque at 7 weeks post-PNX displaced a volume of 42,500mm^3 compared to a sham operated accessory lobe that displaced only 22,400mm^3 (Figure 4E).

To determine whether this expansion was attributable to the generation of new alveoli, we processed the accessory lobes for morphometric analysis as described [32]. We used the Euler characteristic and fractionator design to estimate the number of alveoli in each accessory lobe [31]. There was a ~2-fold increase in the total number of alveoli in the post-PNX accessory lobe compared to the sham operated control, consistent with compensatory lung growth following PNX in nonhuman primates (Figure 4F).

In a follow up study, four young adult female rhesus macaques underwent a sham operation and four age-matched female macaques underwent PNX. Animals were injected with 50mg/kg of EdU prior to euthanasia on day 7 post operation. Tissue sections were stained with antibodies against EdU and the AECII marker SPC. We did not observe any proliferating AECII in the lungs of 4 sham operated animals that were analyzed; in contrast, 12.34±1.63% of AECII in pneumonectomized primates incorporated EdU (Fig4 I).

2.4 Discussion

Our lineage-tracing analysis confirm that Sftpc+ AECII are a source of new alveolar epithelium, including AECI, post-PNX. Our data do not exclude the possibility that other epithelial progenitor populations also contribute to new alveolar epithelium. However, we did not observe proliferation around bronchoalveolar duct junctions (BADJ) and clones of lineage labeled cells did not emanate from the BADJ. Together, this suggests that BASCs are not a major source of alveolar epithelium post-PNX. In contrast to what has been reported in the context of bleomycin and influenza induced injury/repair [13,40], we did not observe p63 or KRT5 staining in lungs post-PNX (data not shown).

Unlike some organ systems, the distal lung does not have a discreet anatomical stem cell niche. Proposed components of the alveolar niche include smooth muscle [41], vasculature [25], and cells of the immune system [42]. Mounting data suggest that fibroblasts are an essential component of the alveolar stem cell niche [4,38]. Indeed, we show that fibroblasts are essential for AECII self-renewal and differentiation in vitro. Our data also support a model in which PNX either directly or indirectly induces *Jag2* expression in PDGFRA+ fibroblasts, and that loss of the downstream Notch co-activator RBPJ specifically in AECII reduces their proliferation and differentiation.

Understanding the capacity for alveologenesis in adult human lungs and the cell and molecular mechanisms that drive this process will hold great potential for regenerative medicine in the future. There has been one case study providing evidence that compensatory lung growth occurs in humans following PNX [23]. However, this study was primarily radiographic and provided little mechanistic insight. To our knowledge, these are the first data regarding AECII proliferation following PNX in nonhuman primates. These data have the potential to inform future efforts at stimulating adult alveologenesis to reverse pathological remodeling and improve the quality of life for patients with lung disease.

2.5 References

1 Hoyert, D. L., Arias, E., Smith, B. L., Murphy, S. L. & Kochanek, K. D. National vital statistics reports. *Deaths: Final Data for 1999* **49**, doi:papers2://publication/uuid/95F9C87D-0BE6-4459-A8CC-05E254B3BD74 (2012).

2 Evans, M. J., Cabral, L. J., Stephens, R. J. & Freeman, G. Transformation of alveolar type 2 cells to type 1 cells following exposure to NO2. *Exp. Mol. Pathol.* **22**, 142-150, doi:papers2://publication/uuid/3B2B19AD-25D4-4320-A64C-8F8F94DB5556 (1975).

3 Rock, J. R. *et al.* Multiple stromal populations contribute to pulmonary fibrosis without evidence for epithelial to mesenchymal transition. *Proc. Natl. Acad. Sci. U.S.A.* **108**, E1475-1483, doi:papers2://publication/doi/10.1073/pnas.1117988108 (2011).

4 Barkauskas, C. E. *et al.* Type 2 alveolar cells are stem cells in adult lung. *J. Clin. Invest.*, doi:papers2://publication/doi/10.1172/JCI68782DS1 (2013).

5 Desai, T. J., Brownfield, D. G. & Krasnow, M. A. Alveolar progenitor and stem cells in lung development, renewal and cancer. *Nature* **507**, 190-194, doi:10.1038/nature12930 (2014).

6 Kim, C. F. *et al.* Identification of bronchioalveolar stem cells in normal lung and lung cancer. *Cell* **121**, 823-835, doi:10.1016/j.cell.2005.03.032 (2005).

7 Chapman, H. A. *et al.* Integrin α6β4 identifies an adult distal lung epithelial population with regenerative potential in mice. *J. Clin. Invest.* **121**, 2855-2862, doi:papers2://publication/doi/10.1172/JCI57673DS1 (2011).

8 Kumar, P. A. *et al.* Distal airway stem cells yield alveoli in vitro and during lung regeneration following H1N1 influenza infection. *Cell* **147**, 525-538, doi:10.1016/j.cell.2011.10.001 (2011).

9 Morrisey, E. E. & Hogan, B. L. M. Preparing for the First Breath: Genetic and Cellular Mechanisms in Lung Development. *Developmental Cell* **18**, 8-23, doi:papers2://publication/doi/10.1016/j.devcel.2009.12.010 (2010).

10 Tsao, P.-N. *et al.* Gamma-secretase activation of notch signaling regulates the balance of proximal and distal fates in progenitor cells of the developing lung. *J. Biol. Chem.* **283**, 29532-29544, doi:papers2://publication/doi/10.1074/jbc.M801565200 (2008).

11 Guseh, J. S. *et al.* Notch signaling promotes airway mucous metaplasia and inhibits alveolar development. *Development* **136**, 1751-1759, doi:10.1242/dev.029249 (2009).

12 Tsao, P.-N. *et al.* Notch signaling controls the balance of ciliated and secretory cell fates in developing airways. *Development* **136**, 2297-2307, doi:papers2://publication/doi/10.1242/dev.034884 (2009).

13 Rock, J. R. *et al.* Notch-dependent differentiation of adult airway basal stem cells. *Cell Stem Cell* **8**, 639-648, doi:papers2://publication/doi/10.1016/j.stem.2011.04.003 (2011).

14 Gomi, K., Arbelaez, V., Crystal, R. G. & Walters, M. S. Activation of NOTCH1 or NOTCH3 Signaling Skews Human Airway Basal Cell Differentiation toward a Secretory Pathway. *PLoS ONE*, doi:10.1371/journal.pone.0116507 (2015).

15 Guseh, J. *et al.* Notch signaling promotes airway mucous metaplasia and inhibits alveolar development. *Development* **136**.

16 Pardo-Saganta, A. *et al.* Injury induces direct lineage segregation of functionally distinct airway Basal stem/progenitor cell subpopulations. *Cell Stem Cell* **16**, 184-197, doi:10.1016/j.stem.2015.01.002 (2015).

17 Tsao, P.-N. N. *et al.* Epithelial Notch signaling regulates lung alveolar morphogenesis and airway epithelial integrity. *Proc. Natl. Acad. Sci. U.S.A.* **113**, 8242-8247, doi:10.1073/pnas.1511236113 (2016).

18 Vaughan, A. E. *et al.* Lineage-negative progenitors mobilize to regenerate lung epithelium after major injury. *Nature* **517**, 621-625, doi:10.1038/nature14112 (2015).

19 Cao, Z. *et al.* Targeting of the pulmonary capillary vascular niche promotes lung alveolar repair and ameliorates fibrosis. *Nat. Med.* **22**, 154-162, doi:10.1038/nm.4035 (2016).

20 Nolen-Walston, R. D. *et al.* Cellular kinetics and modeling of bronchioalveolar stem cell response during lung regeneration. *Am. J. Physiol. Lung Cell Mol. Physiol.* **294**, L1158-1165, doi:papers2://publication/doi/10.1152/ajplung.00298.2007 (2008).

21 Hsia, C. C. *et al.* Structural changes underlying compensatory increase of diffusing capacity after left pneumonectomy in adult dogs. *J. Clin. Invest.* **92**, 758-764, doi:papers2://publication/doi/10.1172/JCI116647 (1993).

22 Mentzer, S. J. Alveolar Epithelial Dynamics in Postpneumonectomy Lung Growth. 1-9, doi:papers2://publication/doi/10.1002/ar.22659 (2013).

23 Butler, J. P. *et al.* Evidence for adult lung growth in humans. *N. Engl. J. Med.* **367**, 244-247, doi:papers2://publication/doi/10.1056/NEJMoa1203983 (2012).

24 Jain, R. *et al.* Plasticity of Hopx(+) type I alveolar cells to regenerate type II cells in the lung. *Nat Commun* **6**, 6727, doi:10.1038/ncomms7727 (2015).

25 Ding, B.-S. *et al.* Endothelial-Derived Angiocrine Signals Induce and Sustain Regenerative Lung Alveolarization. *Cell* **147**, 539-553, doi:papers2://publication/doi/10.1016/j.cell.2011.10.003 (2011).

26 Brody, J. S., Burki, R. & Kaplan, N. Deoxyribonucleic acid synthesis in lung cells during compensatory lung growth after pneumonectomy. *Am Rev Respir Dis* **117**, 307-316, doi:10.1164/arrd.1978.117.2.307 (1978).

27 Brody, J. S. Time course of and stimuli to compensatory growth of the lung after pneumonectomy. *J. Clin. Invest.* **56**, 897-904, doi:papers2://publication/doi/10.1172/JCI108169 (1975).

28 Barkauskas, C. E. *et al.* Type 2 alveolar cells are stem cells in adult lung. *J. Clin. Invest.* **123**, 3025-3036, doi:10.1172/JCI68782 (2013).

29 Hamilton, T. G., Klinghoffer, R. A., Corrin, P. D. & Soriano, P. Evolutionary divergence of platelet-derived growth factor alpha receptor signaling mechanisms. *Molecular and Cellular Biology* **23**, 4013-4025, doi:papers2://publication/uuid/8BF39E31-800D-49AD-AAC0-4421CCABDCB4 (2003).

30 Tanigaki, K. *et al.* Notch-RBP-J signaling is involved in cell fate determination of marginal zone B cells. *Nat Immunol* **3**, 443-450, doi:10.1038/ni793 (2002).

31 Hyde, D. M., Tyler, N. K., Putney, L. F., Singh, P. & Gundersen, H. J. G. Total number and mean size of alveoli in mammalian lung estimated using fractionator sampling and unbiased estimates of the Euler characteristic of alveolar openings. *Anat Rec A Discov Mol Cell Evol Biol* **277A**, 216-226, doi:papers2://publication/doi/10.1002/ar.a.20012 (2004).

32 Hyde, D. M. *et al.* Alveoli increase in number but not size from birth to adulthood in rhesus monkeys. *Am. J. Physiol. Lung Cell Mol. Physiol.* **293**, L570-579, doi:papers2://publication/doi/10.1152/ajplung.00467.2006 (2007).

33 Hsia, C. C. W., Hyde, D. M., Ochs, M. & Weibel, E. R. An Official Research Policy Statement of the American Thoracic Society/European Respiratory Society: Standards for Quantitative Assessment of Lung Structure. *Am. J. Respir. Crit. Care Med.* **181**, 394-418, doi:papers2://publication/doi/10.1164/rccm.200809-1522ST (2010).

34 Fehrenbach, H. *et al.* Neoalveolarisation contributes to compensatory lung growth following pneumonectomy in mice. *Eur. Respir. J.* **31**, 515-522, doi:papers2://publication/doi/10.1183/09031936.00109407 (2008).

35 Filipovic, N. *et al.* Mapping Cyclic Stretch in the Post-Pneumonectomy Murine Lung. *Journal of Applied Physiology*, doi:papers2://publication/doi/10.1152/japplphysiol.00635.2013 (2013).

36 Ackermann, M. *et al.* Sprouting and intussusceptive angiogenesis in postpneumonectomy lung growth: mechanisms of alveolar neovascularization. *Angiogenesis*, doi:papers2://publication/doi/10.1007/s10456-013-9399-9 (2013).

37 Lafkas, D. *et al.* Therapeutic antibodies reveal Notch control of transdifferentiation in the adult lung. *Nature* **528**, 127-131, doi:10.1038/nature15715 (2015).

38 Chen, L., Acciani, T., Le Cras, T., Lutzko, C. & Perl, A.-K. T. Dynamic Regulation of Platelet-Derived Growth Factor Receptor α Expression in Alveolar Fibroblasts during Realveolarization. *American Journal of Respiratory Cell and Molecular Biology* **47**, 517-527, doi:papers2://publication/doi/10.1165/rcmb.2012-0030OC (2012).

39 Green, J., Endale, M., Auer, H. & Perl, A.-K. T. Diversity of Interstitial Lung Fibroblasts Is Regulated by Platelet-Derived Growth Factor Receptor α Kinase Activity. *American Journal of Respiratory Cell and Molecular Biology* **54**, 532-545, doi:10.1165/rcmb.2015-0095OC (2016).

40 Kumar, P. A. *et al.* Distal airway stem cells yield alveoli in vitro and during lung regeneration following H1N1 influenza infection. *Cell* **147**, 525-538, doi:papers2://publication/doi/10.1016/j.cell.2011.10.001 (2011).

41 Volckaert, T. *et al.* Parabronchial smooth muscle constitutes an airway epithelial stem cell niche in the mouse lung after injury. *J. Clin. Invest.* **121**, 4409-4419, doi:papers2://publication/doi/10.1172/JCI58097 (2011).

42 Chamoto, K. *et al.* Migration of CD11b(+) accessory cells during murine lung regeneration. *Stem Cell Res* **10**, 267-277, doi:papers2://publication/doi/10.1016/j.scr.2012.12.006 (2013).

2.6 Figures and Tables

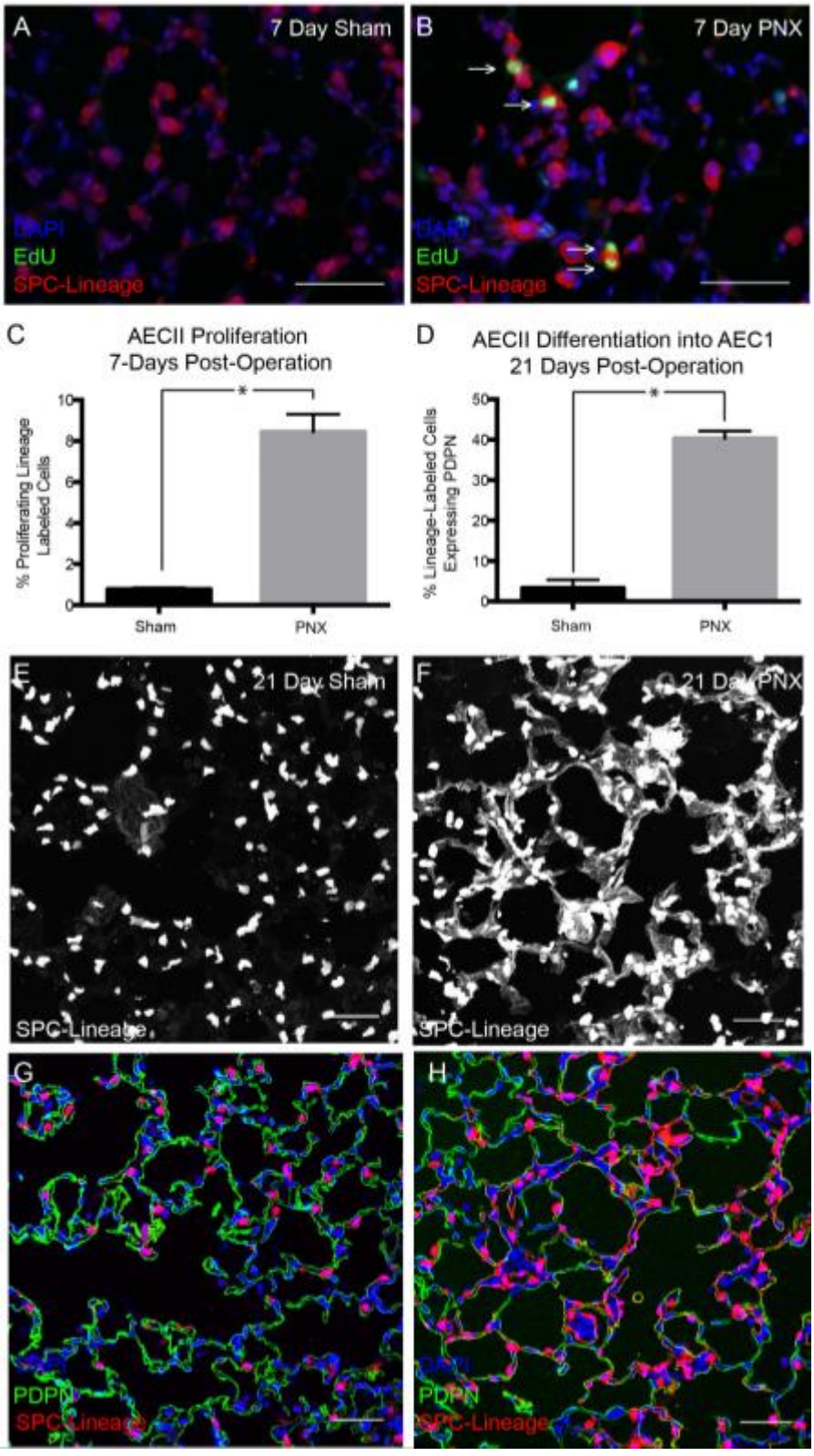

Figure 1. AECII self-renew and generate AECI during adult lung regeneration

(A-C) 7 days post-PNX there is an increase in the proportion of Sftpc lineage-labeled cells that incorporate EdU compared to sham operated animals (*p=0.0189). (D-H) 21 days post-PNX the number of Sftpc lineage-labeled cells which co-express the AECI marker PDPN was significantly increased compared to sham operated animals ($p \leq 0.0001$). (E-H) Immunofluorescent staining of thick sections demonstrating differentiation of Sftpc lineage-labeled cells (red) into AECI (green, PDPN) 21d post-PNX (F, H). Very little turnover of AECII into AECI occurred in sham operated animals (E,G). Arrows indicate proliferating lineage-labeled cells. Scale bars=50uM n=3

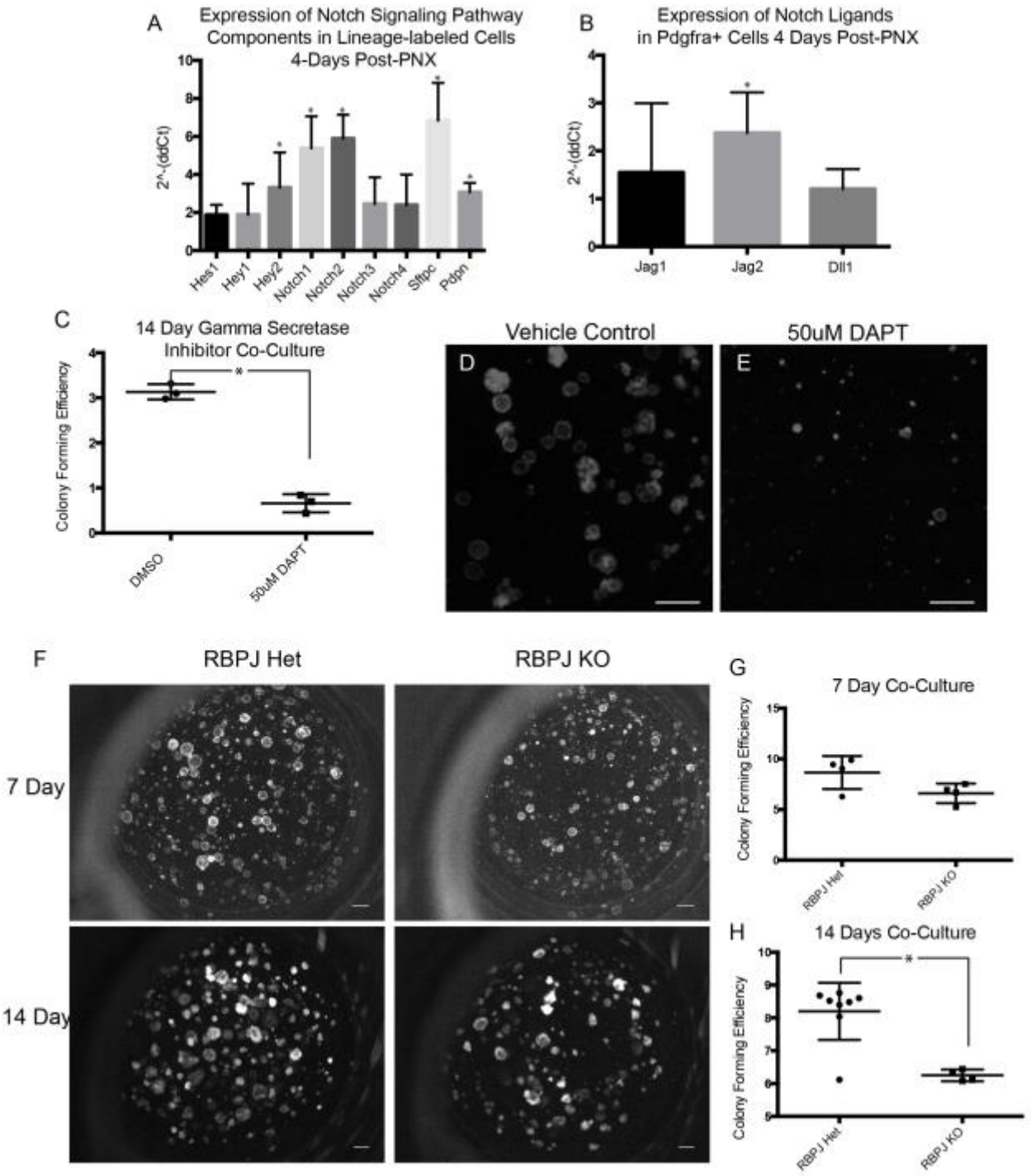
A
Expression of Notch Signaling Pathway Components in Lineage-labeled Cells 4-Days Post-PNX
2^-(ddCt)
Hes1
Hey1
Hey2
Notch1
Notch2
Notch3
Notch4
Sftpc
Pdpn
B
Expression of Notch Ligands in Pdgfra+ Cells 4 Days Post-PNX
2^-(ddCt)
Jag1
Jag2
Dll1
C
14 Day Gamma Secretase Inhibitor Co-Culture
Colony Forming Efficiency
DMSO
50uM DAPT
Vehicle Control
50uM DAPT
D
E
F
RBPJ Het
RBPJ KO
7 Day
14 Day
G
7 Day Co-Culture
Colony Forming Efficiency
RBPJ Het
RBPJ KO
H
14 Days Co-Culture
Colony Forming Efficiency
RBPJ Het
RBPJ KO

Figure 2. Notch is required for AECII colony formation in vitro

(A) qPCR analysis of Sftpc lineage-labeled cells demonstrates an increase in the expression of Notch receptors and downstream targets as well as markers of AECII (*Sftpc*) and AECI (*Pdpn*) 4d post-PNX compared to sham operated animals (*p <0.05). (B) The expression of *Jag2* is upregulated in PDGFRA+ fibroblasts 4d post-PNX compared to sham operated lungs. (C-E) Treatment of alveolosphere co-cultures with the gamma secretase inhibitor DAPT (50 uM) reduces colony forming efficiency of AECII compared to vehicle controls at 14d ($p \leq 0.0001$). (F-H) Alveolosphere co-cultures of lineage labeled RBPJ-deficient AECIIs with PDGFRA-GFP+ fibroblasts had a reduced colony forming efficiency at 14d compared to lineage labeled AECII that were heterozygous for RBPJ (*p=0.0015). Scale bars=500uM n=>3

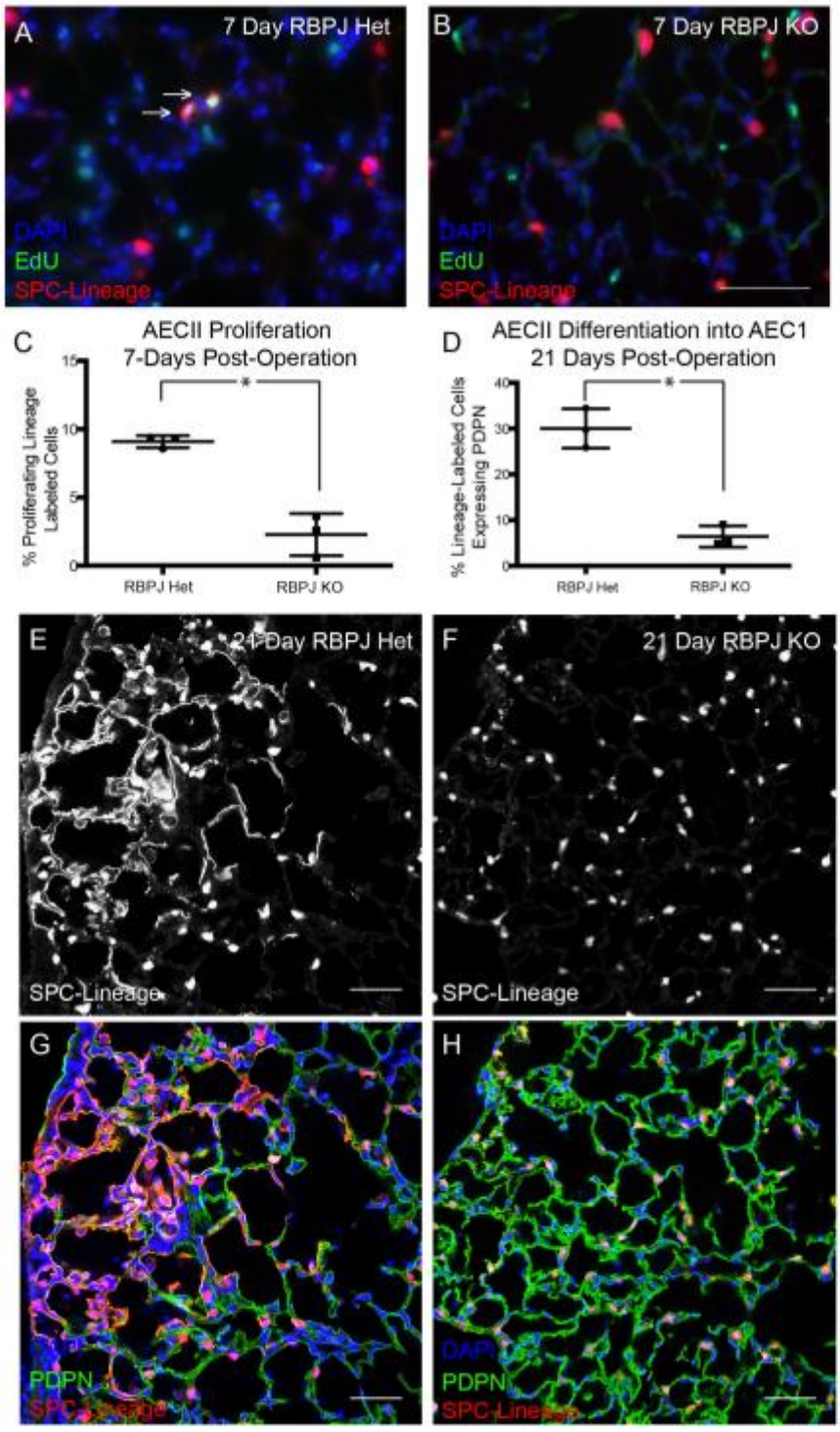
A
7 Day RBPJ Het
DAPI
EdU
SPC-Lineage
B
7 Day RBPJ KO
DAPI
EdU
SPC-Lineage
C
AECII Proliferation
7-Days Post-Operation
% Proliferating Lineage Labeled Cells
15
10
5
0
*
RBPJ Het
RBPJ KO
D
AECII Differentiation into AEC1
21 Days Post-Operation
% Lineage-Labeled Cells Expressing PDPN
40
30
20
10
0
*
RBPJ Het
RBPJ KO
E
21 Day RBPJ Het
SPC-Lineage
F
21 Day RBPJ KO
SPC-Lineage
G
PDPN
SPC-Lineage
H
DAPI
PDPN
SPC-Lineage

Figure 3. Notch regulates proliferation and differentiation of AECII in vivo

(A-C) Conditional deletion of RBPJ from lineage-labeled AECII resulted in reduction of the total number of EdU+ (green, proliferative cells), lineage-labeled (red) cells 7d post-PNX compared to conditionally heterozygous controls (*p= 0.0018). (D-H) Conditional deletion of RBPJ from lineage-labeled AECII resulted in reduced differentiation into AECI (green, PDPN) 21d post-PNX compared to conditionally heterozygous controls (*p=0.0011). Arrows indicate proliferating lineage-labeled cells. Scale bars= 50uM n=3

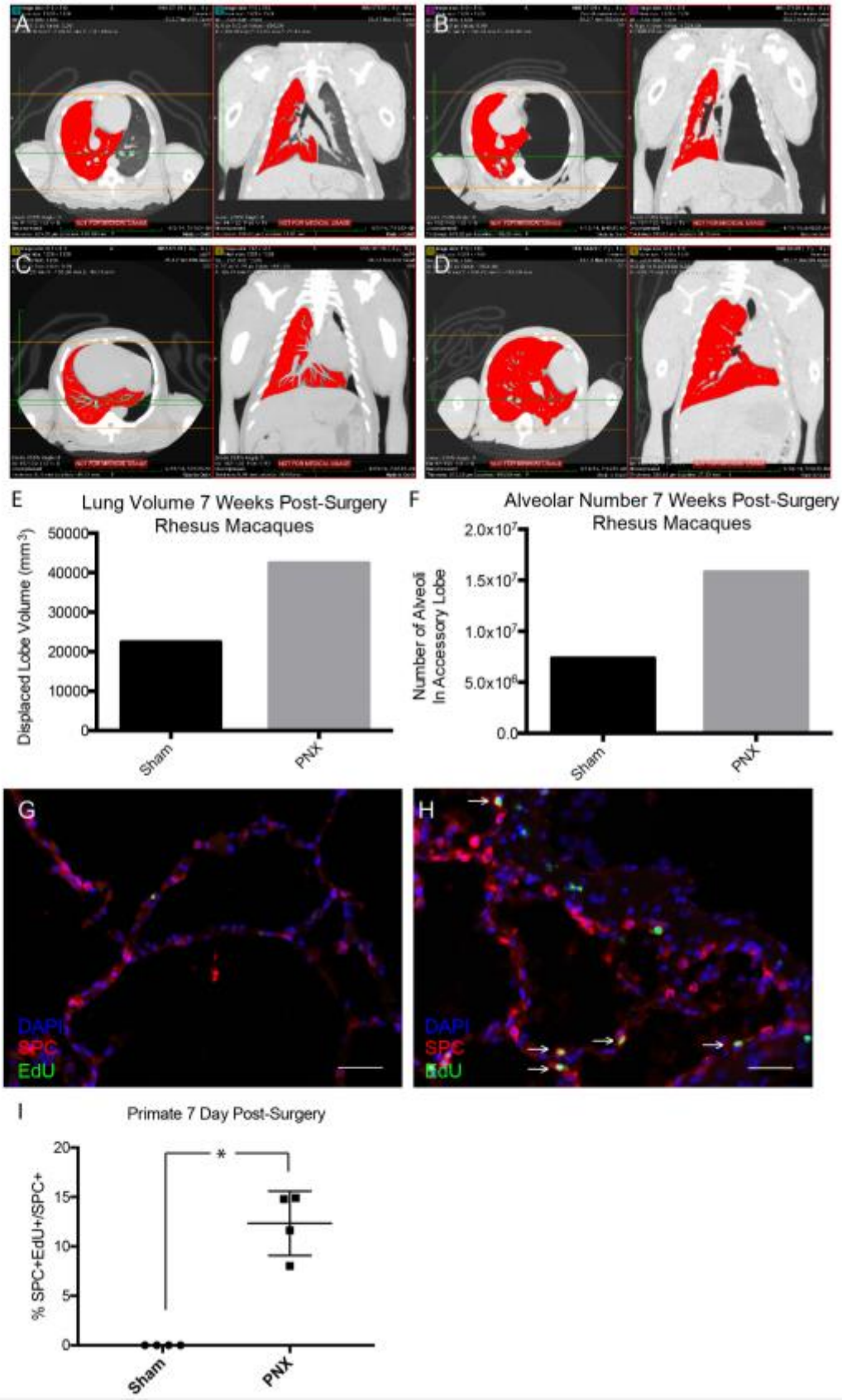
A
B
C
D
E
Lung Volume 7 Weeks Post-Surgery
Rhesus Macaques
Displaced Lobe Volume (mm3)
50000
40000
30000
20000
10000
0
Sham
PNX
F
Alveolar Number 7 Weeks Post-Surgery
Rhesus Macaques
Number of Alveoli In Accessory Lobe
2.0x10^7
1.5x10^7
1.0x10^7
5.0x10^6
0.0
Sham
PNX
G
DAPI
SPC
EdU
H
DAPI
SPC
EdU
I
Primate 7 Day Post-Surgery
% SPC+EdU+/SPC+
20
15
10
5
0
*
Sham
PNX

Figure 4. Adult alveologenesis occurs in non-human primates

CT scans of adult female rhesus macaques at steady state (A) or PNX (B-D). The right lobes have been pseudo-colored red. The remaining right lobes began to expand into the left chest cavity within 2 weeks (C) and filled the left chest cavity by 4wk post-PNX (D). Total displaced lung volume (E) and estimated alveolar number (F) were increased in the accessory lobe of the PNX animal by 7 weeks compared to the sham operated animal. (G-I) There was an increase in the proportion of proliferative (*) AECII cells 7 days post-PNX compared to the sham operated control. Arrows indicate proliferating SPC+ cells (*p=.0003, n=4) (H, I). Scale bars=50uM

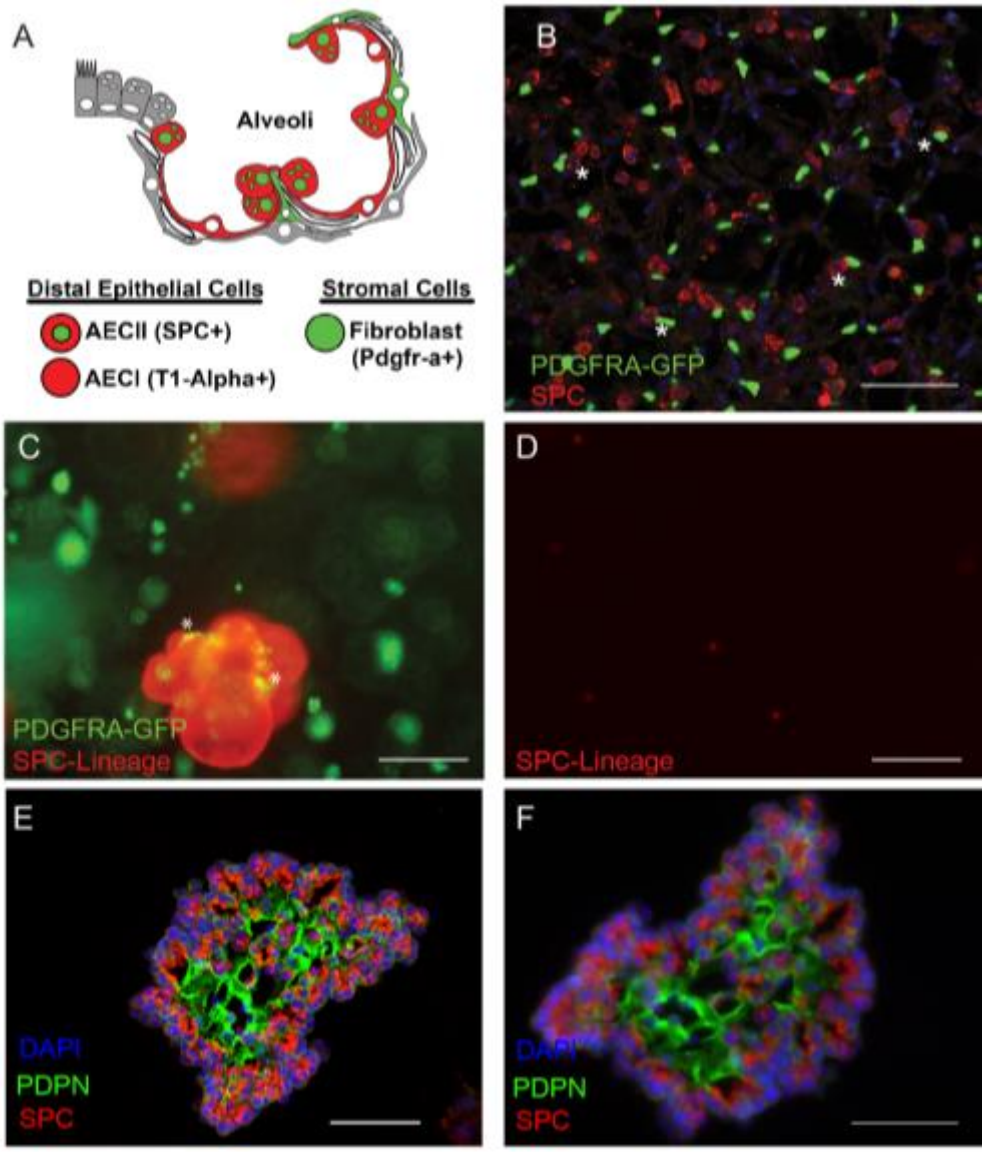
A
Alveoli
Distal Epithelial Cells
AECII (SPC+)
AECI (T1-Alpha+)
Stromal Cells
Fibroblast
(Pdgfr-a+)
B
PDGFRA-GFP
SPC
C
PDGFRA-GFP
SPC-Lineage
D
SPC-Lineage
E
DAPI
PDPN
SPC
F
DAPI
PDPN
SPC

Supplement 1. PDGFRA+ fibroblasts are a component of the alveolar stem cell niche

(A) Schematic of AECII and PDGFRA+ fibroblasts in the distal lung. (B) Immunofluorescent staining showing proximity of some Pdgfra-GFP+ cells to AECIIs in adult alveoli. (C) Individual AECII co-cultured with PDGFRA+ fibroblasts give rise to multicellular alveolospheres. (D) No alveolospheres form when PDGFRA+ fibroblasts are not added at the time of plating. (E-F) Histological sections of alveolospheres 14-days after culture showing expression of pro-Sftpc (AECII) and PDPN (AECI) markers. Scale bars=50uM

Chapter 3

The role of the Wnt signaling pathway in lung regeneration

3.1 Introduction

It is well established that the Wnt signaling pathway plays a necessary role during embryonic lung development [1,2]. As early as E9.0, Wnt found in the ventral interior mesoderm signals to the Nkx2.1+ progenitor cells of the anterior foregut endoderm to separate and begin to form the lung buds. Specifically, it has been shown that loss of Wnt2 and Wnt2b from the mesenchyme results in a failure to form these initial lung buds[3]. After initial lung budding has begun to occur, a predetermined patterning of lung branching morphogenesis [4] takes place which begins to separate the lung into proximal, airway, and distal, alveolar, cell types.

In a study involving the targeted deletion of beta-catenin from SPC and CCSP expressing cells starting at E.5, mice which had beta-catenin deleted from SPC expressing cells develop abnormal pulmonary structure, such as enlarged and elongated airways and almost no formation of alveolar sacs[5]. On the other hand, mice which had beta-catenin deleted from CCSP expressing cells exhibited no change[5]. Interestingly the SPC;beta-catenin null mice had little to no positive staining for proSP-C, a marker of AECIIs[5].

Most recently, Wnt signaling has been suggested to be involved in alveologenesis that occurs postnatally. Specifically, a subgroup of axin2+ AECIIs were found to increase 2-fold in number between the periods of E18.5 and P4. This increase in axin2+ AECIIs correlated with a significant decrease in AECI numbers[6]. When observing axin+ AECII behavior during early postnatal alveologenesis, the axin2+ cell group had increased clonal potential as compared to

non-axin2+ AECIIs. Further analysis of Wnt signaling during the same time period, through overexpression of beta-catenin, increased AECII clones[6]. Lastly, overexpression of beta-catenin demonstrated a marked increase in AECII into AECI conversion [6]. These data, however, do not address the role of the Wnt signaling pathway during adult alveologenesis.

The following data begin to elucidate the role of the Wnt pathway during adult alveologenesis. This is achieved through utilizing the pneumonectomy model system on SPC-CreER;Rosa:Tomato mice which were crossed into a $Ctnnb1^{flx/flx}$ mouse. These SPC-CreEr;$Ctnnb1^{flx/flx}$;Rosa:Tomato mice were compared to SPC-CreEr;$Ctnnb1^{flx/+}$;Rosa:Tomato mice for differences in cell proliferation as well as differentiation. We also followed up with a lung dry weight analysis to determine if loss of beta-catenin would result in a reduction in overall lung mass. These data ultimately demonstrated a reduction in AECII proliferation, a loss in AECII into AECI conversion, and a reduction in lung weight.

3.2 Methods

Pneumonectomy

All animal experiments were performed in accordance with UCSF and CNPRC IACUC-approved protocols. 10-14 week old adult mice were anesthetized and intubated for ventilation using a Harvard mini-vent ventilator set at 200uL stroke volume at 200 strokes per minute. 2% isoflurane was administered via the ventilator throughout surgery. Once intubated and anesthetized, the left lung lobe was exposed through the rib cage and the pulmonary vasculature and left mainstem bronchus was ligated with a titanium clip. The left lobe was resected, and the ribs and skin closed. The left lobe was lifted through the rib cage and replaced but not resected in sham-operated animals.

Lung Dissociation and FACS

Mice were euthanized by CO_2 exposure and perfused with 20 mL cold PBS through the right ventricle. Lungs were inflated with protease solution [1–2 mL; Collagenase Type I (catalog #17100–017, 450 U/mL; Gibco), Elastase (catalog #LS002279, 4 U/mL; Worthington Biochemical Corporation), Dispase (catalog #354235, 5 U/mL; BD Biosciences) and DNaseI (catalog #10104159001, 0.33 U/mL; Roche) in DMEM/F12], cut into small pieces (<2 mm2), and incubated in 2 mL protease solution for 20 min at 37 °C with frequent agitation. DMEM/F12 + 10% FBS was added, and tissue was disrupted by pipetting, washed with DMEM/F12, and incubated for 5 min at 37 °C in 2 mL 0.1% Trypsin-EDTA + 0.325 mg DNaseI with intermittent agitation. An equal volume of DMEM-F12 + 10% FBS was added, and tissue was dissociated by pipetting. Cells were washed with 5 mL DMEM/F12, incubated at room temperature for 1.5 min in warmed 2 mL red blood cell lysis buffer (catalog #00–4333-57; eBioscience), filtered through a 40-μm strainer, centrifuged, and resuspended in PBS + 2% BSA. Sorting was performed on FACS ARIA II, and data was analyzed with FACS Diva (BD Biosciences).

qPCR

RNA was purified from cell collected by FACS for qPCR using Trizol (Invitrogen). RNA pellets were resuspended in TE pH 8.0 (ambion) and RNA quantity and quality was measured using a Nanodrop. cDNA was made with Vilo Mastermix (Invitrogen 11755250) and qPCR master mix was SYBR GreenEr (Invitrogen 11762). 384 well plates were run on a Viia7 and RNA expression was measured using the $2^{\wedge-(\Delta\Delta CT)}$ in which each of the three PNX mice were

compared to an average of all three sham animals. All reactions were run in triplicate. Statistical analysis and graphing was then produced by Prism 6 software.

Mouse Tissue Preparation

Animals were injected with 50mg/kg of EdU resuspended in PBS three hours prior to sacrifice to label proliferating cells. Mice were euthanized by CO_2 exposure, and pulmonary perfusion was performed with 20 mL cold PBS through the right ventricle. Lungs and trachea were removed and inflated to 20 cm H_2O pressure with 4% paraformaldehyde. Lungs were fixed for 30 minutes at 4ºC in 4% paraformaldehyde and washed 3x15 minutes in PBS.

Immunohistochemistry of Mouse Tissue

Cryosections (10-100 μm) were cut and then stained with hamster anti-PDPN (clone 8.1.1, 1:1,000; DSHB) and Rabbit anti-RFP (catalog #600– 4013791:250; Rockland). EdU staining was performed according to manufacturer recommendations. Alexa-Fluor–coupled secondary antibodies (Invitrogen) were used at 1:500. Z stacks of optical sections were captured on a Leica Sp5 laser-scanning confocal microscope. Unless otherwise noted, sections from at least three mice were analyzed for each data point.

3.3 Results

Wnt Ligands and Downstream Targets are Up-Regulated Post-PNX

To determine if AECIIs up-regulated the Wnt pathway post-PNX, we generated Sftpc-CreER;ROSA-Tomato mice and administered 4 doses of tamoxifen to label ~85% of the total AECII population as described[7]. Two weeks after the last dose of tamoxifen, the mice either

underwent a left lobe pneumonectomy (PNX) or a sham operation. We then took the sham and PNX operated lungs, dissociated them into single cells and sorted for lineage labeled AECIIs at day 4 post-operation, as it has been previously described that proliferation begins to significantly increase by this timepoint. We found significant increases in Wnt signaling pathway genes such Ctnnb1, GSK3B, Wnt2, Wnt5a, and Lef1 (Fig.1). These data led us to believe that the Wnt pathway might be involved in the preceding neo-alveolarization that occurs post-pneumonectomy.

Loss of Ctnnb1 results in a Decrease in AECII Proliferation and Differentiation

To determine if the Wnt signaling pathway regulates AECII behavior during adult alveologenesis in vivo, we generated SPC-CreEr;Ctnnb1$^{flx/+}$;Rosa:Tomato and SPC-CreEr;Ctnnb1$^{flx/flx}$;Rosa:Tomato. Loss of Ctnnb1, or beta-catenin, prevents co-activation of transcription factors related to the TCF/LEF family, and therefore inhibits further activation of the Wnt signaling pathway. Adult SPC-CreEr;Ctnnb1$^{flx/+}$;Rosa:Tomato and SPC-CreEr;Ctnnb1$^{flx/flx}$;Rosa:Tomato mice were given 4 doses of tamoxifen to induce maximum lineage labeling of AECIIs and deletion of Ctnnb1. Two weeks after the final dose of tamoxifen, mice either underwent a sham operation or full left lobe pneumonectomy. 7 days after operation, animals were injected with EdU, a BrdU analog, three hours prior to sacrifice to label actively dividing cells. We then quantified the number of lineage labeled cells that also incorporated EdU in the two groups. The data showed a significant decrease in proliferation in the SPC-CreEr;Ctnnb1$^{flx/flx}$;Rosa:Tomato mice as compared to the SPC-CreEr;Ctnnb1$^{flx/+}$;Rosa:Tomato mice. Specifically, we found 12.08±1.534% of AECIIs proliferation in the control animals, and just 4.133±0.822% of AECIIs in the Ctnnb1 KOs (Fig. 2 A-C).

We then asked whether there was a change in AECII into AECI conversion 21-days post pneumonectomy. Using the same lineage tracing and surgery approach as above, we then allowed the animals to recover for 21-days post-operation before taking the lungs for analysis. After sectioning and staining the tissue, we found that the control animals had 35.47±4.05% of lineage labeled AECIIs co-stained for PDPN, a marker of AECIs. When we analyzed the Ctnnb1 KO animals, we found only 4.232±1.768% of lineage labeled AECIIs co-staining for PDPN (Fig 3. A-F). Collectively, these data demonstrate that the Wnt signaling pathway is necessary for both proliferation and differentiation of AECIIs in the adult mouse lung.

Loss of the Wnt Signaling Pathway Prevents Neo-Alveolarization Post-PNX

To further determine the extent of how loss of the Wnt signaling pathway disrupts neo-alveolarization post-pneumonectomy in the adult mouse, we performed a lung dry weight analysis. SPC-CreEr;Ctnnb1$^{flx/+}$;Rosa:Tomato and SPC-CreEr;Ctnnb1$^{flx/flx}$;Rosa:Tomato mice underwent full left lobe pneumonectomies. 14 days post-operation, animals were euthanized and the accessory lobes were collected for lyophilization and weighing. Accessory lobe weights were then normalized to the length of the animal, and Ctnnb1 KO lungs were then compared to the Ctnnb1 hets for differences in lung weights. We found that there was a statistically significant decrease in the Ctnnb1 KO lung weights as compared to the heterozygote animals, with approximately a 25% reduction in weight (Fig. 4).

3.4 Discussion

The above data suggest that the Wnt signaling pathway is involved in AECII proliferation as well as differentiation during adult alveologenesis post-pneumonectomy. These initial

findings were further reinforced through a lung dry weight analysis in which we found a significant reduction in accessory lobe weight in the Ctnnb1 KO animals as compared to the Ctnnb1 heterozygotes.

Despite these findings, further investigation into the Wnt signaling pathway's role in adult alveologenesis is necessary. As mentioned in the introduction, a recent publication by the Morrisey Lab[6] demonstrated the role of a unique Axin2+ AECII cell, which was found to play a dominate role in post-natal alveolarization. Using a similar breeding scheme of Spc-CreER animals crossed to $Ctnnb1^{flx/flx}$ and $Ctnnb1^{flx/+}$ mice, they suggested that loss of Wnt signaling forces AECII into AECI conversion.

The Morrisey Lab data are somewhat in conflict with what we have shown above, however it must be taken into consideration they were looking at neo-alveolarization in the context of postnatal development, and not adult neo-alveolarization. A few ways to further address these questions would be to perform FACS analysis on lineage labeled AECIIs post-pnx which have been stained for PDPN, and compare numbers between the two groups. It remains unanswered whether there is a dominant cell of origin from which Wnt signals to the AECIIs to proliferate post-pnx. It would also be an interesting project to determine if there is cross-talk between the Wnt and Notch signaling pathway's. Work in other organ systems, such as the small intestine[8], show a necessary interaction to maintain proper progenitor cell maintenance and differentiation. Further investigation of the Wnt signaling pathway's involvement in adult alveologenesis could potentially be utilized for drug therapies in individuals suffering from such diseases as COPD.

3.5 References

1. Morrisey, E. E. & Hogan, B. L. M. Preparing for the first breath: genetic and cellular mechanisms in lung development. *Dev. Cell* **18,** 8–23 (2010).

2. Herriges, M. & Morrisey, E. E. Lung development: orchestrating the generation and regeneration of a complex organ. *Development* **141,** 502–513 (2014).

3. Goss, A. M. *et al.* Wnt2/2b and beta-catenin signaling are necessary and sufficient to specify lung progenitors in the foregut. *Dev. Cell* **17,** 290–298 (2009).

4. Metzger, R. J., Klein, O. D., Martin, G. R. & Krasnow, M. A. The branching programme of mouse lung development. *Nature* **453,** 745–750 (2008).

5. Mucenski, M. L. *et al.* β-Catenin Is Required for Specification of Proximal/Distal Cell Fate during Lung Morphogenesis. *J. Biol. Chem.* **278,** 40231–40238 (2003).

6. Frank, D. B. *et al.* Emergence of a Wave of Wnt Signaling that Regulates Lung Alveologenesis by Controlling Epithelial Self-Renewal and Differentiation. *Cell Rep.* **17,** 2312–2325 (2016).

7. Rock, J. R. *et al.* Multiple stromal populations contribute to pulmonary fibrosis without evidence for epithelial to mesenchymal transition. *Proc. Natl. Acad. Sci. U. S. A.* **108,** E1475–83 (2011).

8. Tian, H. *et al.* Opposing activities of Notch and Wnt signaling regulate intestinal stem cells and gut homeostasis. *Cell Rep.* **11,** 33–42 (2015).

3.6 Figures and Tables

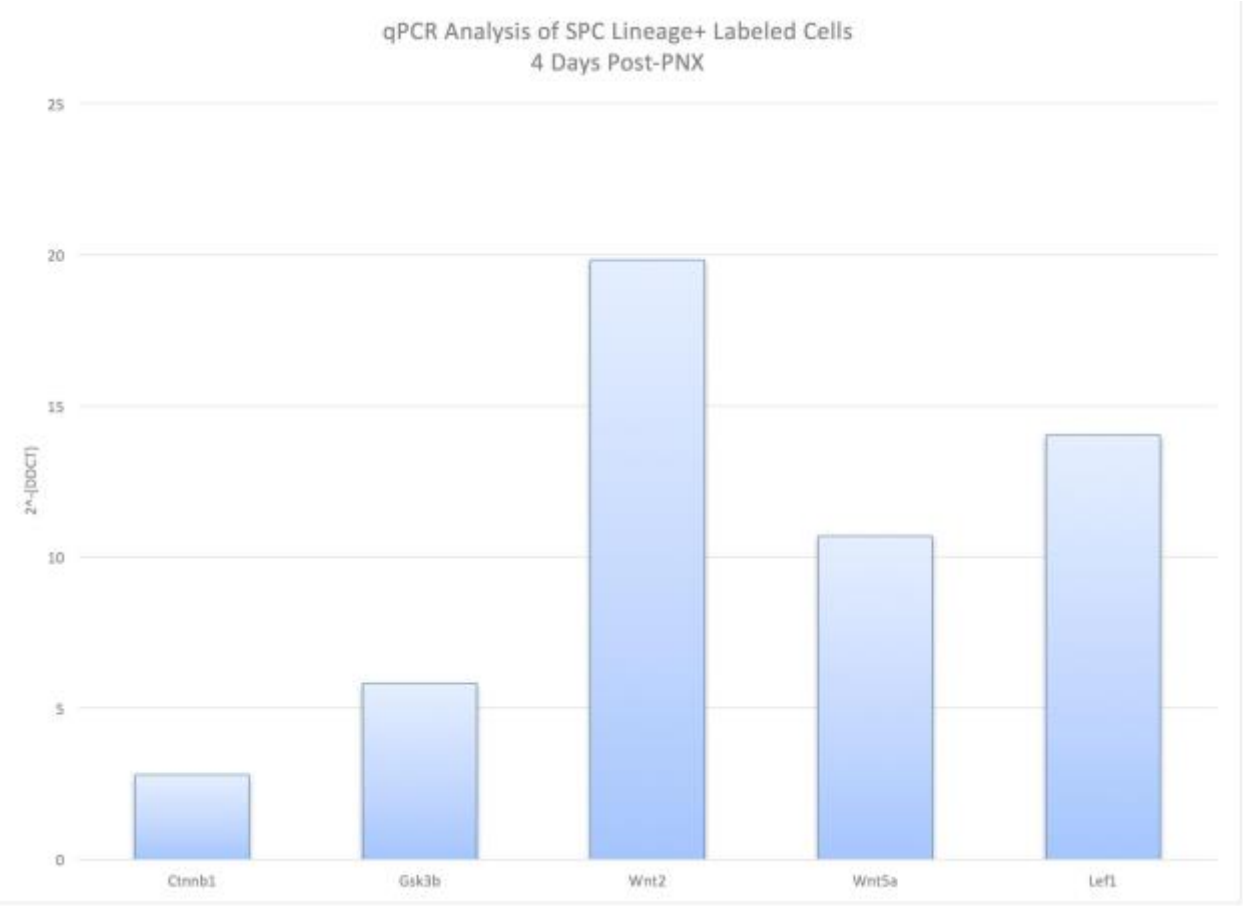

Figure 1. qPCR Analysis of Lineage Labeled AECIIs 4 days Post-PNX

qPCR analysis of lineage labeled AECIIs 4-days post-pnx vs sham demonstrated an increase in Wnt signaling pathway genes. These data led us to believe that the Wnt pathway might play a role in adult alveologenesis.

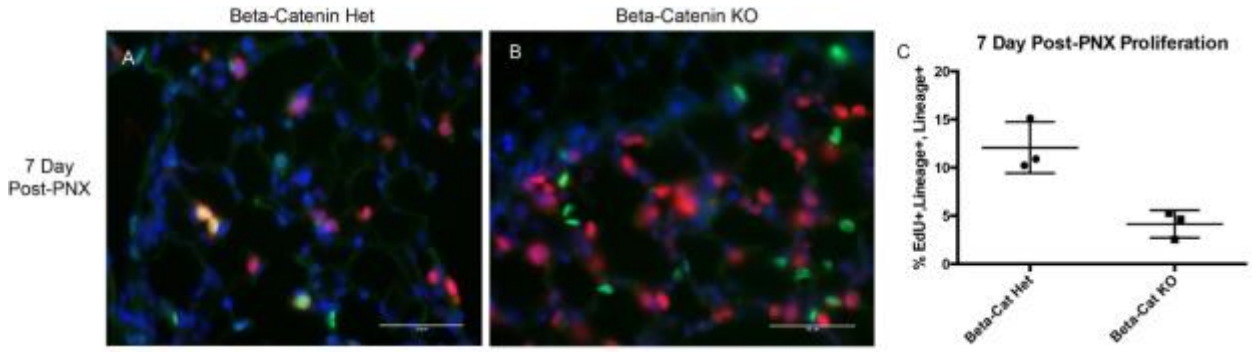
Beta-Catenin Het
Beta-Catenin KO
7 Day
Post-PNX
A
B
C
7 Day Post-PNX Proliferation
% EdU+,Lineage+, Lineage+
20
15
10
5
0
Beta-Cat Het
Beta-Cat KO

Figure 2. Loss of Beta-Catenin Results in a Decrease in AECII Proliferation

SPC-CreEr;Ctnnb1$^{flx/+}$;Rosa:Tomato and SPC-CreEr;Ctnnb1$^{flx/flx}$;Rosa:Tomato mice underwent full left lobe pneumonectomies. 7 days post-operation, lungs were taken for analysis of AECII proliferation (A-B). We found that 12.08±1.534% of AECIIs proliferate in the control animals, while the Ctnnb1 KOs had only 4.133±0.822% of AECIIs proliferating (C). Scale bars=50uM p=.0103 N=3

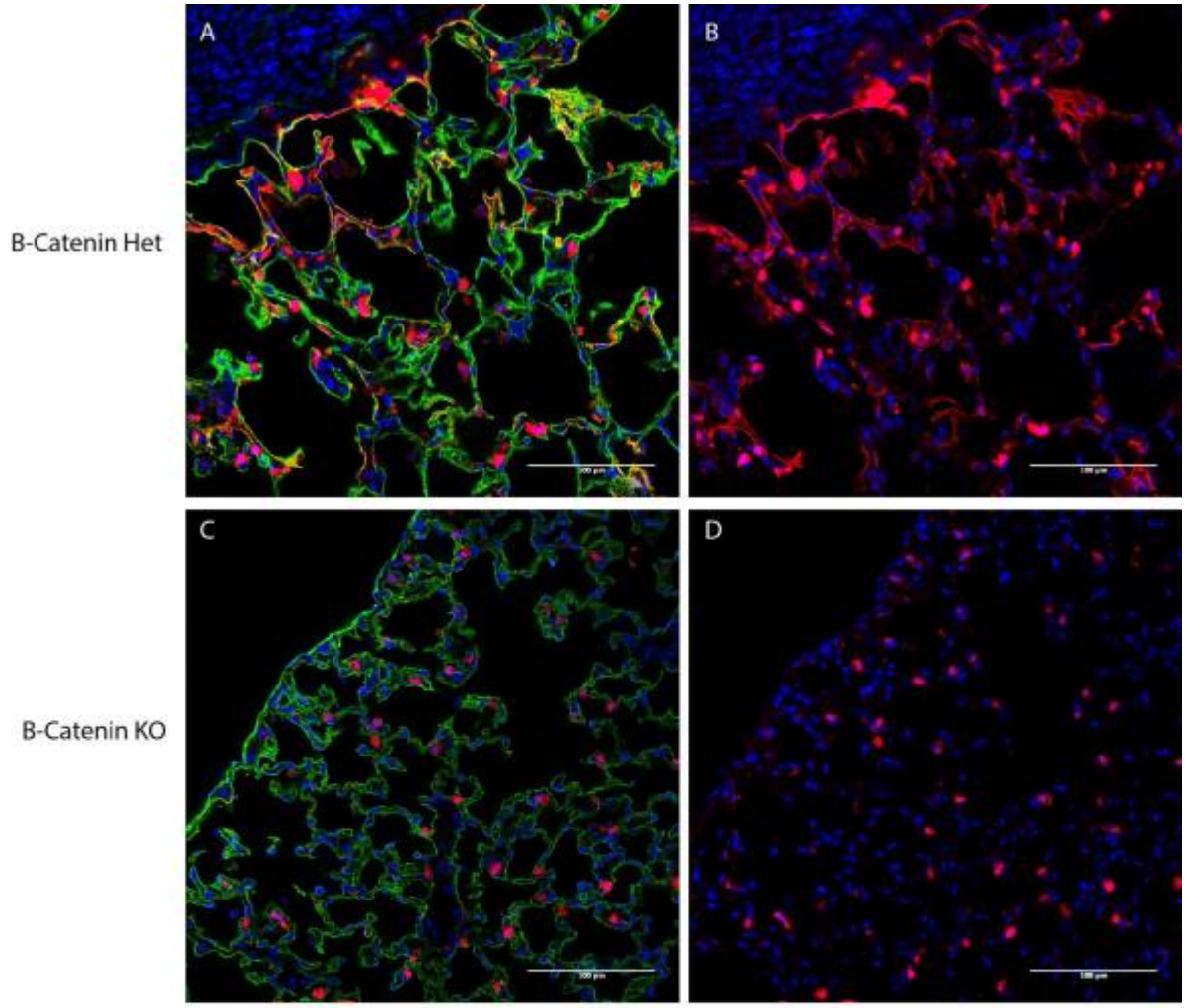
B-Catenin Het
B-Catenin KO
A
B
C
D

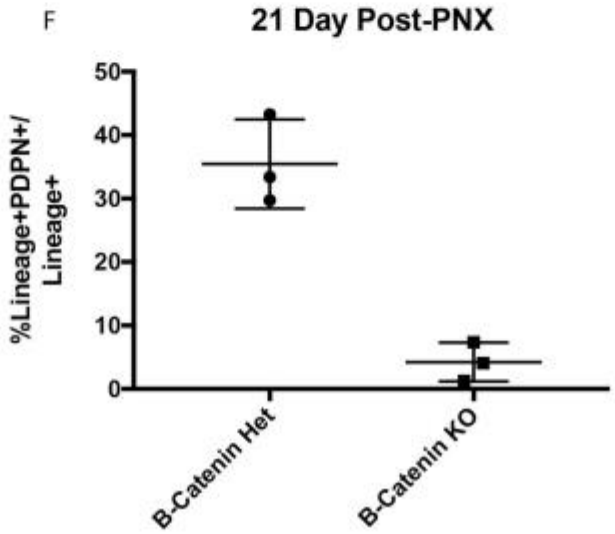
F
21 Day Post-PNX
%Lineage+PDPN+/ Lineage+
50
40
30
20
10
0
B-Catenin Het
B-Catenin KO

Figure 3. Loss of Beta-Catenin Results in a Reduction of AECII into AECI Conversion

SPC-CreEr;Ctnnb1$^{flx/+}$;Rosa:Tomato and SPC-CreEr;Ctnnb1$^{flx/flx}$;Rosa:Tomato mice underwent full left lobe pneumonectomies. 21 days post-operation, lungs were taken for analysis of AECII into AECI conversion using the AECI marker PDPN. 35.47±4.05% of lineage labeled AECIIs co-stained for PDPN in the control animals while only 4.232±1.768% of AECIIs in the Ctnnb1 KO animal co-stained for PDPN. Scale bars=50uM p=.0021 N=3

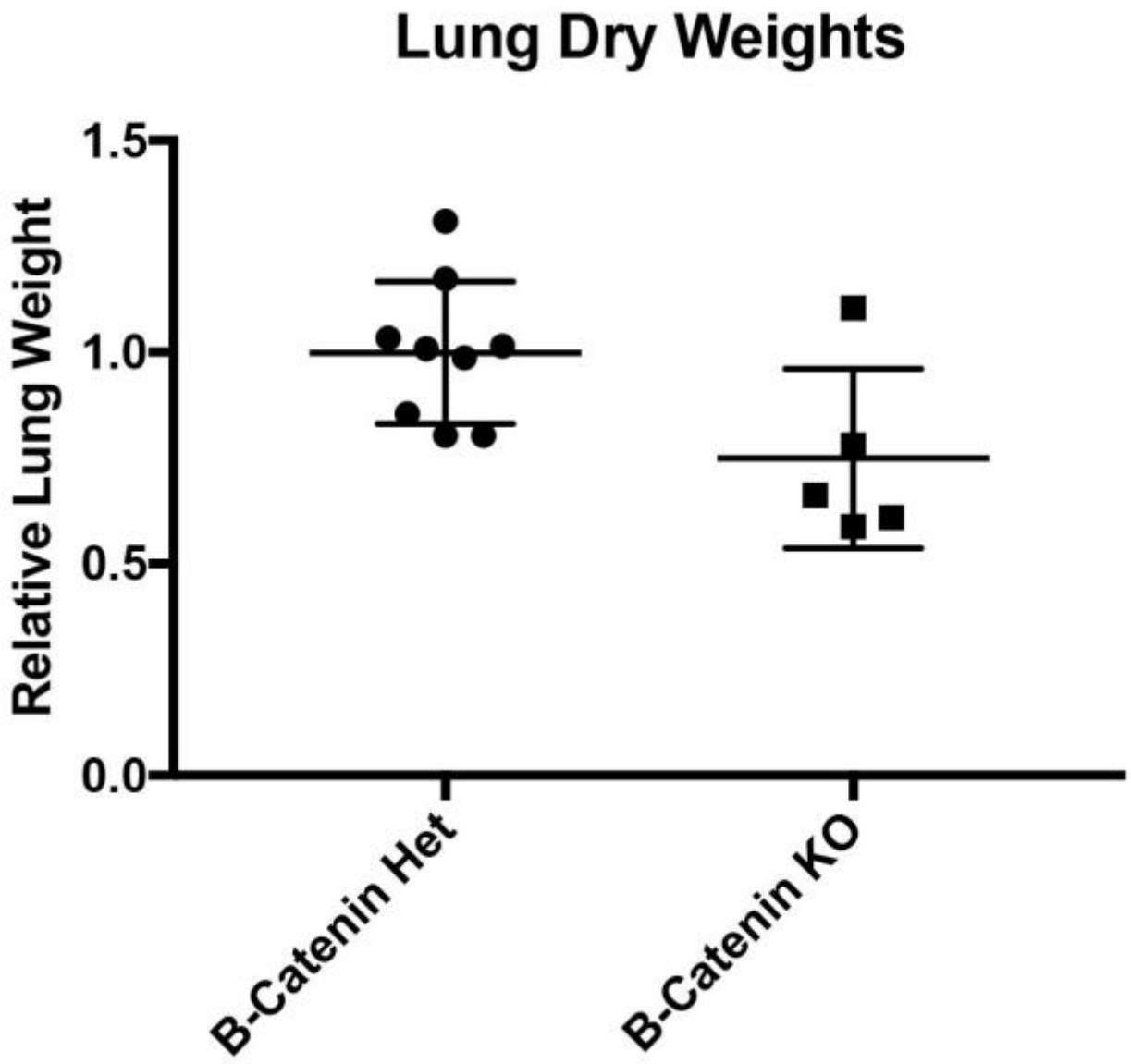
Lung Dry Weights
Relative Lung Weight
1.5
1.0
0.5
0.0
B-Catenin Het
B-Catenin KO

Figure 4. Loss of Beta-Catenin Results in a Reduction in Accessory Lobe Dry Weight

SPC-CreEr;Ctnnb1$^{flx/+}$;Rosa:Tomato and SPC-CreEr;Ctnnb1$^{flx/flx}$;Rosa:Tomato mice underwent full left lobe pneumonectomies. 14 days post-operation, accessory lobes were taken for dry weight analysis. Accessory lobes were lyophilized, weighed, and then normalized to each mouse by mouse length. Ctnnb1 KO accessory lobe weights were then compared to Ctnnb1 Hets. Ctnnb1 KO accessory lobes had on average a 25% reduction in weight. p=.0314 Ctnnb1 Het N=9 Ctnnb1 KO N=5

Chapter 4

Caloric restriction diet as a model of lung regeneration

4.1 Introduction

During the dark times of World War II, 500,000 Jewish people were confined in an area of Warsaw that was only 5% of the city's total area[1]. In this encampment, it was decided that the Jewish occupants would be slowly starved to death by feeding them a diet of only 800 calories a day[2]. A group of doctors, lead by Dr. Israel Milejowski, took it upon themselves to take detailed records of the metabolic, physiological, and autopsy studies of individuals suffering from starvation in an attempt to determine best practice of treatment given the situation. From these data, it was discovered that individuals on this restricted caloric diet had reduced body temperatures, hyperlucent lungs, and reduction in O_2 consumption by 30-40%[2]. Lastly, they found upwards of 13.5% of individuals who had died from starvation also suffered from emphysema[2]. More recently, similar findings have been seen in individuals suffering from anorexia nervosa[3].

Previous studies, using various mammalian model animals, have shown a similar effect; 35% of alveoli were found to be lost as quickly as 72 hours after starting the calorically restricted diet in a mouse model system. Further continuation of the diet over a 12-day period resulted in an additional 12% loss of alveoli[4]. Interestingly, within a short window of just 72 hours of *ad libitum* refeeding the number of alveoli had regrown to normal levels[4]. When a microarray analysis was performed on animals that had been calorically restricted then re-fed versus mice who ate *ad libitum*, various pro-angiogenic, cell-cycle, and extracellular matrix remodeling genes

were upregulated. Of particular interest to my work HeyL, a direct target of the Notch signaling pathway, was also found to be up-regulated[5].

To determine if AECIIs behave similarly in this model as in the pneumonectomy model system, I initially established that the caloric restriction model can significantly decrease the lung dry weight as compared to the *ad libitum* fed animals. Next, we used SPC-CreER;Rosa:Tomato animals to lineage trace AECII into AECI conversion after a period of caloric restriction and re-feeding. Lastly, I then used the SPC-CreER;RBP-$J^{fl/+}$;Rosa:Tomato and SPC-CreER;RBP-$J^{fl/fl}$;Rosa:Tomato to compare if loss of the Notch signaling pathway resulted in a reduction of AECII into AECI conversation.

4.2 Methods

Caloric Restriction Diet

All animal experiments were performed in accordance with UCSF and CNPRC IACUC-approved protocols. 8-12 week adult mice were singularly housed and observed for 5 days to determine their daily food consumption. A calorically restricted diet was then implemented by reducing available food by 2/3rd compared to the average intake from the previous 5 days. After 15 days of on a restricted diet, mice were either euthanized through CO_2 exposure or fed *ad libitum* for an additional 5 days before euthanization. To compensate for loss of retinoic acid intake for the animals with reduced caloric intake, animals were fed Ralston Purina Laboratory Chow 5001. Control animals were allowed to eat *ad libitum* throughout the entirety of the experiment.

Mouse Tissue Preparation

Animals were injected with 50mg/kg of EdU resuspended in PBS three hours prior to sacrifice to label proliferating cells. Mice were euthanized by CO_2 exposure, and pulmonary perfusion was performed with 20 mL cold PBS through the right ventricle. Lungs and trachea were removed and inflated to 20 cm H_2O pressure with 4% paraformaldehyde. Lungs were fixed for 30 minutes at 4ºC in 4% paraformaldehyde and washed 3x15 minutes in PBS.

Immunohistochemistry of Mouse Tissue

Cryosections (10-100 μm) were cut and then stained with hamster anti-PDPN (clone 8.1.1, 1:1,000; DSHB) and Rabbit anti-RFP (catalog #600– 4013791:250; Rockland). Alexa-Fluor–coupled secondary antibodies (Invitrogen) were used at 1:500. Z stacks of optical sections were captured on a Leica Sp5 laser-scanning confocal microscope. Unless otherwise noted, sections from at least three mice were analyzed for each data point.

4.3 Results

Reduction in Daily Caloric Intake Reduces Total Lung Weight

Initially, we were interested to see if the calorically restricted diet can show significant weight decrease and then increase over the previously reported time period [4]. Figure 1-A shows that over a period of 15 days the mice undergo significant weight decrease. Immediately upon re-feeding on day-15, we see a sharp increase in mouse weight by day-16, with most mice showing an increasing trend in weight from day 16 forward. Despite previously reported pathological changes of the alveolar regions of the lung after an extended period of reduced caloric intake, it

was not yet established that this reduction in alveolar number also resulted in a decrease in lung weight.

To determine if lung weight decreases after a reduction in caloric intake, adult littermate mice were either put on a calorically restricted diet or feed *ad libitum* for a period of 15 days. On day 15 mice were euthanized, whole lungs were lyophilized overnight and then weighed the next day. The dry lung weights were then normalized to mouse length, and mice on the calorically restricted diet were then compared to the mice fed *ad libitum*. Mice which were fed the calorically restricted diet had an average normalized lung weight which was only 85%±0.01583 of the mice fed *ad libitum*.

AECIIs Differentiate into AECIs During Lung Regeneration

We next wanted to learn if the AECIIs differentiate into AECIs similar to our pneumonectomy model system. Similar to what was described above, adult SPC-CreER;Rosa:Tomato mice were put on a calorically restricted diet for a period of 15 days. After this 15 day period, SPC-CreER;Rosa:Tomato mice were allowed to eat *ad libitum* for three more days before euthanization. After lungs were perfused and embedded in OCT for cryosectioning, thick sections (~50-100uM) were cut and stained for RFP, the AECII lineage trace marker, and PDPN, a marker of AECIs. As expected, we found patches throughout the lung where the AECII lineage trace marker co-stained for PDPN (Fig 2-A). When images were shown in a max projection view, the formation of what looks to be new alveolar epithelium could be seen (Fig 2-B).

Loss of RBPJ Reduces AECII into AECI Conversion after Caloric Restriction and then Feeding *Ad Libitum*

Finally, we asked whether loss of RBPJ results in a reduction in AECII into AECI conversion in the caloric restriction model system. SPC-CreER;RBP-$J^{fl/+}$;Rosa:Tomato and SPC-CreER;RBP-$J^{fl/fl}$;Rosa:Tomato littermates were put on a calorically restricted diet for a period of 15 days before being fed *ad libitum* for another three more days. On day-18, mice were euthanized and lungs were collected for histological analysis. Thick cryosections (50-100uM) were cut and tissue was stained for RFP and PDPN. After analysing sections for number of lineage labeled cells which also co-stained for PDPN, we found on average 15.04%±0.5771 lineage labeled+PDPN+ cells in the RBPJ Het mice (Fig 3 A-E). There was a statistically significant decrease in the rate of AECII into AECI differentiation in the RBPJ KO animals, in which only 3.887%±.3393 lineage labeled cells also co-stained for PDPN(Fig 3 A-E).

4.4 Discussion

The work started by Dr. Israel Milejowski's group in the Jewish Ghetto over 70 years ago to better understand the body, and specifically the lung's behavior under extreme duress, is still relevant and necessary knowledge today. As the field of basic science and medicine moves towards this idea of "regenerative medicine", it is important for us to understand how the body naturally degenerates and regenerates. The above data demonstrate definitively that the AECII gives rise to AECIs during neo-alveolarization post-caloric restriction. We also uncover that the Notch signaling pathway plays a role in the regenerative response, similar to our previous work demonstrating a role for Notch post-pneumonectomy. Further work will be necessary to unlock whether this regenerative response is exactly the same as seen in the pneumonectomy model

system, or if there is a different interplay between progenitor cell populations found within the adult lung. Ultimately, these data will continue to provide the necessary base from which to develop potential therapeutics in the future.

4.5 References:

1. D., M. W. M. & Winick, M. *Final Stamp: The Jewish Doctors in the Warsaw Ghetto*. (AuthorHouse, 2007).

2. Yudkin, J. Hunger Disease: Studies by the Jewish Physicians in the Warsaw Ghetto. *J. R. Soc. Med.* **72,** 790 (1979).

3. Massaro, D. & Massaro, G. D. Hunger disease and pulmonary alveoli. *Am. J. Respir. Crit. Care Med.* **170,** 723–724 (2004).

4. Massaro, D., Massaro, G. D., Baras, A., Hoffman, E. P. & Clerch, L. B. Calorie-related rapid onset of alveolar loss, regeneration, and changes in mouse lung gene expression. *Am. J. Physiol. Lung Cell. Mol. Physiol.* **286,** L896–906 (2004).

5. Massaro, D. *et al.* Rapid onset of gene expression in lung, supportive of formation of alveolar septa, induced by refeeding mice after calorie restriction. *Am. J. Physiol. Lung Cell. Mol. Physiol.* **292,** L1313–26 (2007).

4.6 Figures and Tables

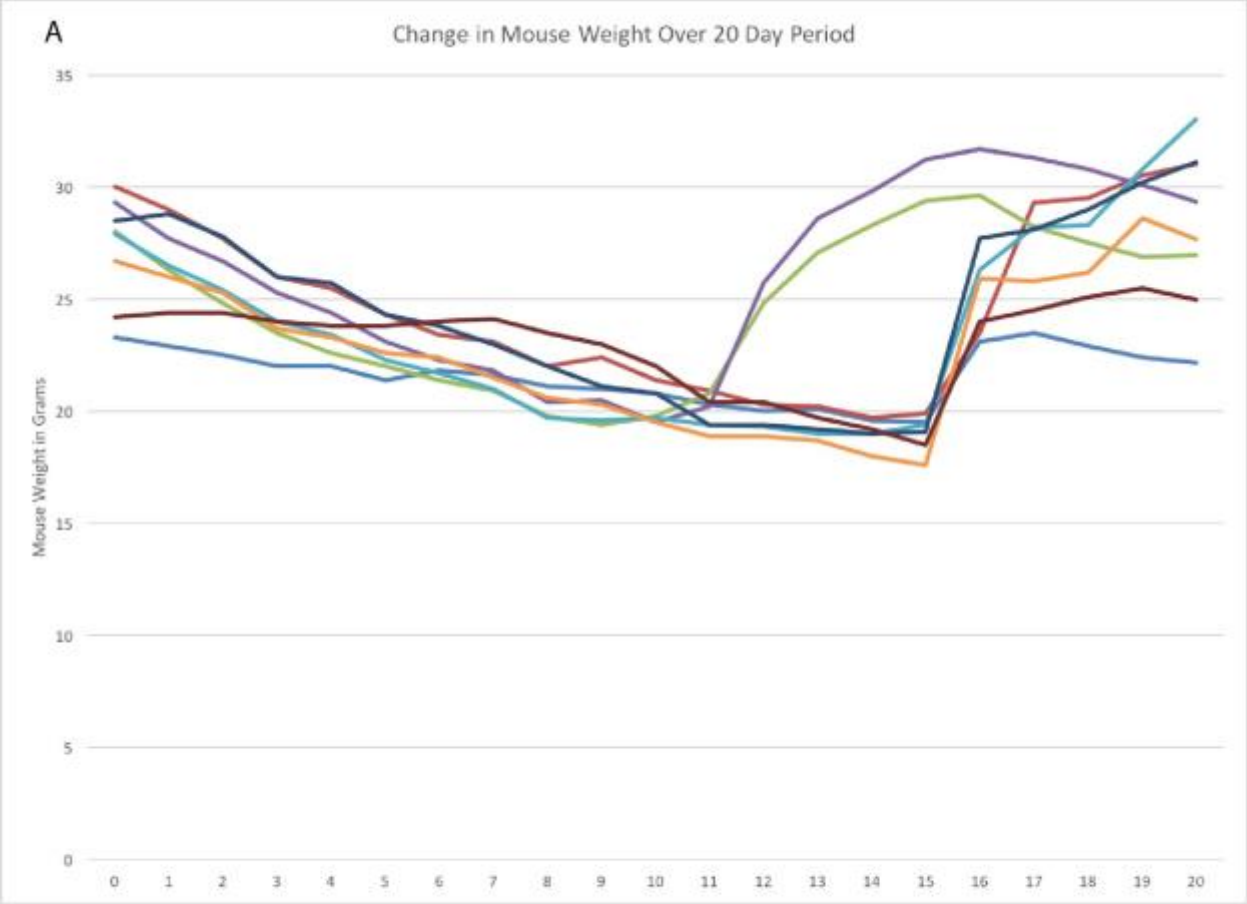

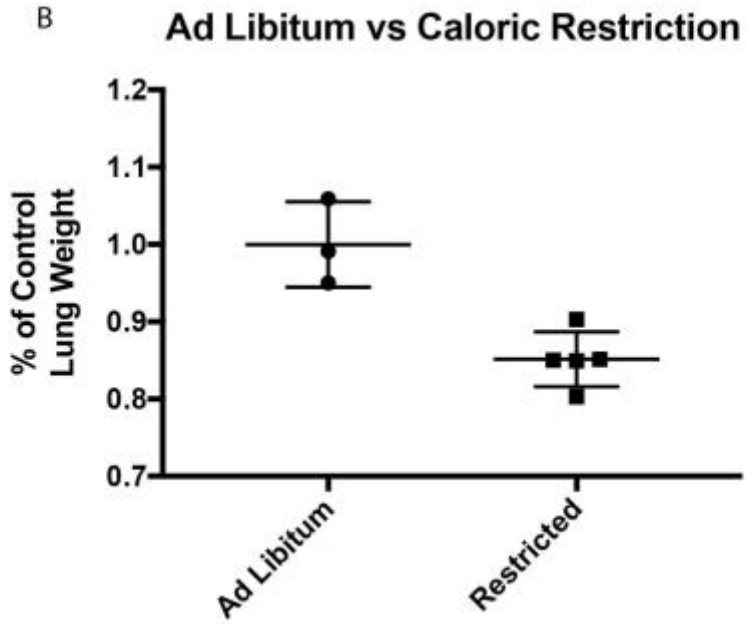

Figure 1. Reduction in Daily Caloric Intake Reduces Total Lung Weight

A) Adult B6 mice underwent a 2/3rd reduction in caloric intake over a 15-day period before being fed *ad libitum*. There was a sharp increase in body weight seen between days 15 and 16 once caloric intake was no longer restricted. B) Adult mice were euthanized and lungs were taken for dry weight measurements after 15 days of either feeding *ad libitum* or calorically restricted. A statistically significant decrease in lung weight was found in animals which had a reduced daily caloric intake (85±0.01583% of *ad libitum* mouse lung weight). *Ad libitum* n= 3. Restricted n=5. P=.0032

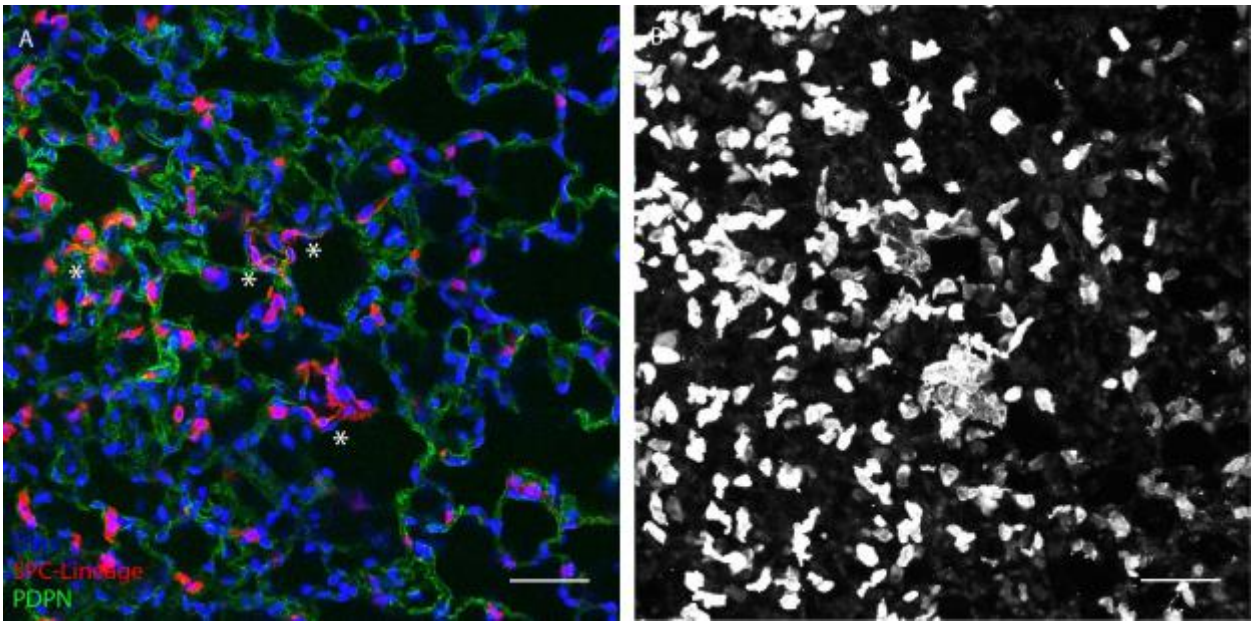
A
B
LPC-Lineage
PDPN

Figure 2. AECIIs Give Rise to New Alveolar Epithelium within 3 Day post-*Ad Libitum* Feeding

A single cross section taken from a confocal z-series stack which shows that new alveolar epithelium (*) formation has occurred within 3 days after mice were allowed to eat freely after a 15 day calorically restricted diet (Fig A). This is a max projection of the z-series from panel A showing, in greater detail, several new areas of alveolar epithelial regeneration (Fig. B).

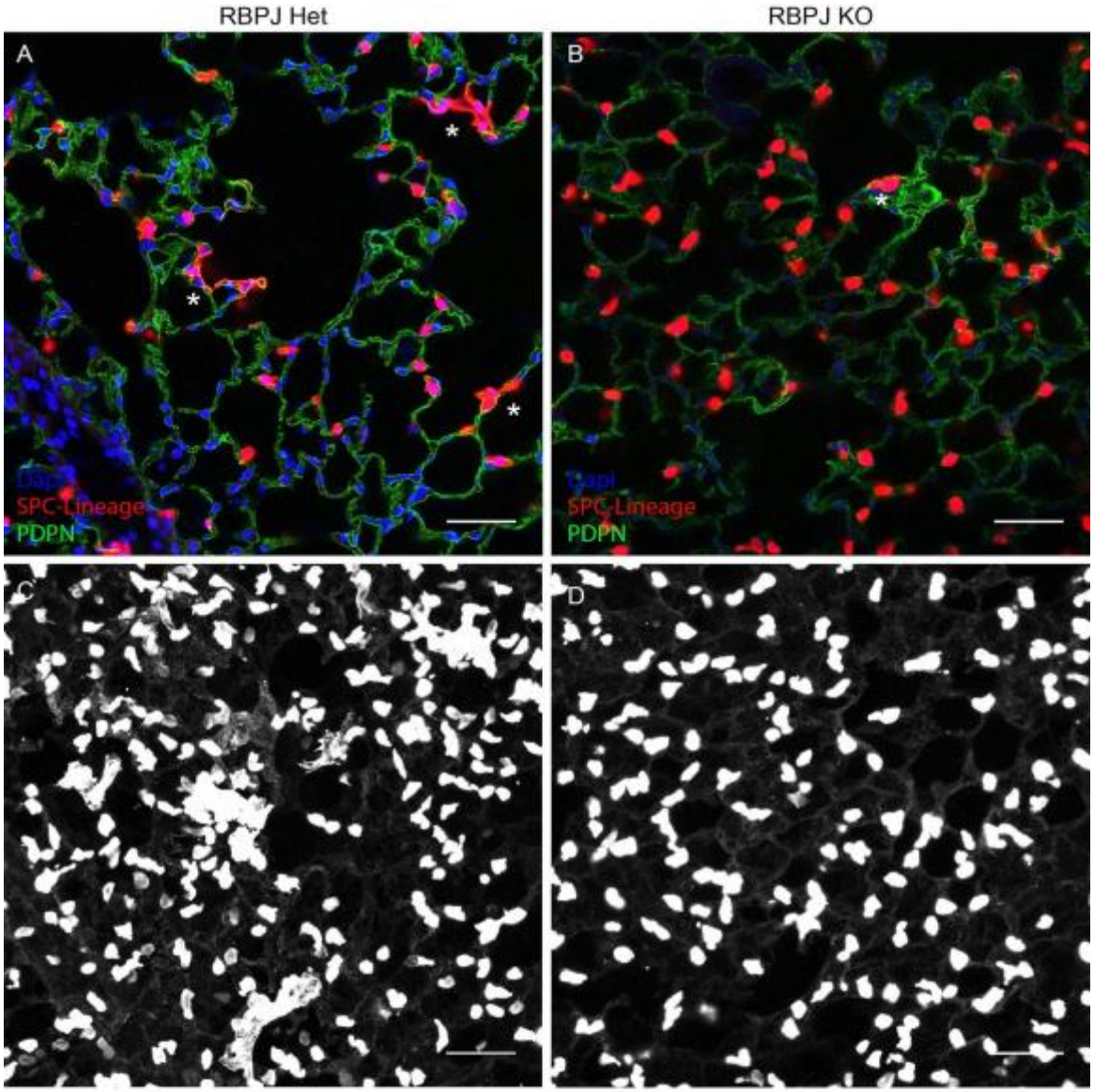
RBPJ Het
RBPJ KO
A
B
C
D
Dapi
SPC-Lineage
PDPN
Dapi
SPC-Lineage
PDPN

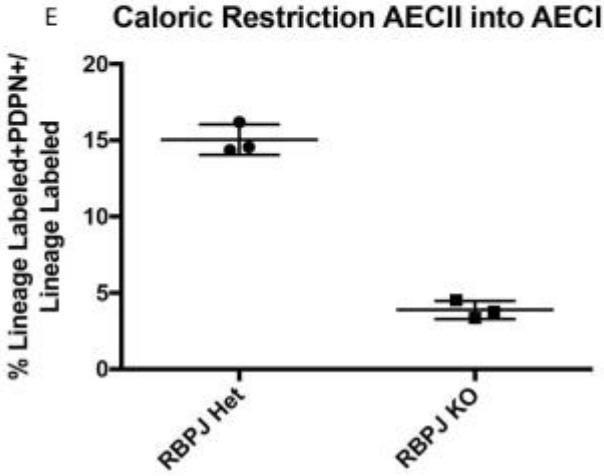
E
Caloric Restriction AECII into AECI
% Lineage Labeled+PDPN+/ Lineage Labeled
20
15
10
5
0
RBPJ Het
RBPJ KO

Fig 3. Loss of RBPJ Results in a Reduction of AECII into AECI Conversion.

Adult SPC-CreER;RBP-$J^{fl/+}$;Rosa:Tomato and SPC-CreER;RBP-$J^{fl/fl}$;Rosa:Tomato were compared post-caloric restriction and then *ad libitum* feeding to look for differences in AECII into AECI differentiation. SPC-CreER;RBP-$J^{fl/+}$;Rosa:Tomato mice had 15.04±0.5571% lineage labeled cells that co-stained for PDPN (Fig 3 A, E). This was in contrast to the SPC-CreER;RBP-$J^{fl/fl}$;Rosa:Tomato mouse in which only 3.887±0.3393% of lineage labeled cells co-stained for PDPN (Fig 3 B,E). Max projection of the z-series show in greater detail several new areas of alveolar epithelium regeneration in the RBPJ Het animals. p=.0001 n=3 for each animal group. Scale bar= 50uM

Chapter 5

Single cell sequencing reveals lung fibroblast heterogeneity

5.1 Introduction

The heterogeneity of mammalian lung fibroblasts is evident from the diverse functions that have been shown during development and disease. During development, fibroblasts are essential as signaling centers, secreting growth factors and organizing lung branching and sacculation, providing the extracellular matrix for epithelial growth and mechanical support for forces of adult respiratory function[1-7]. Fibroblasts are also central to the pathology of fibrotic lung diseases as they produce and remodel ECM, modulate the immune response, and alter the mechanical properties of the lung with debilitating consequences[8,9].

Alveolar fibroblasts in healthy adult lungs have been studied mostly as controls prior to Bleomycin or surgical intervention[10,11]. The low level of proliferation observed (0% using 3h BrdU pulse) has led to the general conclusion that fibroblasts exist at steady state from the conclusion of sacculation until disease onset[11,12]. As a result, accurate assessment of heterogeneity, turnover and lineage relationships between fibroblast subsets in healthy lungs has been limited. Additional limitations exist due to a lack of genetic tools and markers to allow the isolation of primary fibroblast cells, especially in humans. A number of studies have addressed the expression of Pdgfra, showing its role in postnatal lung maturation[12-14] and showing that expression of GFP knocked into the Pdgfra locus can be used to discriminate between fibroblast subsets in mice[10,12-15]. During septation (up to P8) GFP-low fibroblasts are classified as predominantly lipofibroblast and the GFP-high cells as myofibroblasts[14]. In adult lungs the

Pdgfra-GFP-high are described as matrix-like and the Pdgfra-low as myofibroblast-like[10]. This could reflect temporal changes in fibroblasts at the molecular level or technical limitations of bulk sorting and sequencing these populations.

Two recent papers have established two additional markers of lung fibroblasts, Adrp (Plin2) and Tbx4, that can give rise to myofibroblasts (Acta2+, Col1a1+) cells in the lung[16,17]. These genetic models provide clear evidence of the lineage relationship between fibroblast subpopulations, but many open questions remain about the exact molecular signature of the different fibroblast subsets and the overlap between markers that have been proposed.

We have previously shown that resident fibroblasts in mouse lungs that express Pdgfra can express the myofibroblast marker Acta2 (aSMA) in the context of bleomycin-induced pulmonary fibrosis[11]. Using a recently described transplant assay[18], we show that aSMA negative Pdgfra+ fibroblasts of the adult lung can give rise to aSMA+ myofibroblasts in fibrotic lesions of recipient lungs. We perform single cell RNA sequencing to assess the heterogeneity amongst the Pdgfra+ fibroblast population. Expression of already established genes such as Pdgfra, Fgf10, Plin2, Tbx4, and Col1a1, confirm that the Pdgfra+ population at baseline contains a heterogeneous population of fibroblasts containing both lipofibroblast like and myofibroblast like cells. We report the identification of four subpopulations of cells that can be classified by the divergent expression of genes associated with lipid production/trafficking or matrix deposition and inflammation.

One of the genes identified as enriched in the lipid population is the transcription factor Tcf21, a marker of kidney podocytes that has previously been shown to be required for lung branching during development[2,19,20]. Tcf21+ cells have also been implicated as a cell of origin

for cardiac myofibroblasts[21]. Using a Tcf21-CreER allele for lineage tracing, we show that the Tcf21+ population of fibroblasts in the lung proliferates and give rise to aSMA+ fibroblasts in the context of bleomycin-induce pulmonary fibrosis[22]. We also show that a similar Tcf21+ fibroblast population exists in the adult human lung. In summary, this study demonstrates the utility of single cell sequencing for identifying subsets of cells within a defined population and discovering both novel markers and gene networks that characterize those cells. In addition, these data provide context regarding many of markers that have been used to characterize lung fibroblasts.

5.2 Methods

Mice

Mouse strains used in this study were as follows: Tcf21tm3.1(cre/Esr1*)Eno[23], ROSA-td-Tomato (Gt(ROSA)26Sortm2(CAG-tdTomato)Fawa) have been described in[11] and its construction is was identical to the ROSA-fGFP[24]. PDGFRA-GFP (Pdgfratm11(EGFP)Sor) and NG2-DSRed Tg(Cspg4-DsRed.T1)1Akik mice have previously been described[25,26]. University of California, San Francisco (UCSF) Institutional Animal Care and Use Committees (IACUC) approved all studies.

Tamoxifen and EdU administration

Tamoxifen (T5648; Sigma-Aldrich) was a 20 mg/ml stock solution in corn oil and given via intraperitoneal injection. Four 25mg/kg doses of TMX were given to each animal every other

day for 4 days. EdU (Click-iT EdU Alexa Fluor 647 Imaging Kit C10340; Invitrogen) was administered via i.p. injection (50 mg/kg) 24 hours prior to sacrifice unless otherwise mentioned.

Bleomycin Injury and Cell Transplant

8 to 12 week old B6 adult mice were given one dose of Bleomycin (2.5units per gram) intratracheally. 7 days post-Bleomycin treatment, mice received either 200K PDGFR-A GFP+ or 200K NG2-dsRed cells administered intratracheally. Mice were then housed for 7 more days before sacrifice. 8 to 12 week old adult B6 TCF21: CreER/+; Rosa: tomato/+ mice were given one dose of Bleomycin (2.5units per gram), and allowed to recover for 7 to 14 days before sacrifice.

Single Cell Isolation

Mice were euthanized by CO_2 exposure, and pulmonary perfusion was performed with 20 mL cold PBS through the right ventricle. The lungs were then inflated with 1mL of dissociation buffer for 1 minute. Lungs were extracted and minced with a razor blade and then placed in a 15mL conical with 4mL of dissociation buffer and incubated at 37∘C for 45 minutes. Cells were washed twice in PBS and filtered using a 70um filter. Cells collected by FACS that were negatively gate on Pacific-blue Live/Dead stain and CD45 and positive for Pdgfra-GFP.

RNA Sequencing

Pdgfra-GFP+ live cells were sorted into DMEM 10% FBS as detailed in Single cell isolation procedure. Fluidigm C1 and C1 integrated fluidic circuits (IFCs) were used to capture live cells,

lyse, convert polyA+RNA into full length cDNA, amplify cDNA and generate a cDNA library according to their detailed protocol ("Using C1 to Generate Single-Cell cDNA Libraries for mRNA Sequencing", Fluidigm, PN 100-7168). Lysis, reverse transcription and PCR was performed on the C1 system. Library preparation for sequencing was performed following a "modified Illumina Nextera XT DNA library preparation protocol" for cDNA acquired from the C1 system. The concentration of cDNA was determined using Quant-iT™ PicoGreen® dsDNA Assay Kit (Life Technologies) and measured using a FLUOstar OPTIMA (BMG Labtech). Sequencing was performed by Elim BioPharm (Oakland, CA) on 2 lanes of an Illumina HiSeq Flow cell. In total 662 million 50 bp reads were sequenced for each end.

Bioinformatics and Statistics

Reads were aligned and mapped using Tophat2 (version 2.1.0) and Bowtie2 (version 2.2.6) software[27]. 662 million reads were sequenced per end and 603 million were aligned with an average of 3.1 million reads per cell per end and a average 91% alignment rate. All of the accepted hits in bam files output from Tophat2 were processed using Picard tools (http://broadinstitute.github.io/picard/) FixMateInformation command and then counts were compiled using HTSeq-count (http://www-huber.embl.de/users/anders/HTSeq/doc/count.html) using the UCSC mm10 mouse assembly. All of the gene counts for each cell were compiled into a single file. Filtering was then performed to remove any cell that did not have at least a 50% alignment rate. Then all genes that did not have a least one read aligned in at least 3 cells were removed. The resulting cell/gene matrix file was then normalized using DESeq2 (https://bioconductor.org/packages/release/bioc/html/DESeq2.html). The clustering, PCA and

significance testing were performed using scicast (details and a walkthrough can be found at https://github.com/iandriver/scicast).

Mouse Tissue Preparation

Mice were euthanized by CO_2 exposure, and pulmonary perfusion was performed with 20 mL cold PBS through the right ventricle. Lungs and trachea were removed and inflated to 20 cm H_2O pressure with 4% paraformaldehyde. Lungs were fixed for 30 minutes at 4ºC in 4% paraformaldehyde and washed 3x15 minutes in PBS.

Human tissues.

All human tissue samples were obtained from UCSF Interstitial Lung Disease Blood and Tissue Repository and are classified as Non-identifiable Otherwise Discarded Human Tissues.

Immunohistochemistry of Mouse and Human Tissue

Cryosections (50 μm) were stained by standard protocols. Rabbit anti-RFP (catalog# 401379, 1:250; Rockland), Mouse anti-SMA (catalog# MA137027, 1:500; Thermo), Rat anti-PDGFR-A (catalog# 3174p, 1:250; Cell Signal), TCF21 (abcam 32981, 1:100), G0S2 (ThermoFischer PA523087, 1:100), PkiG (protein-tech 21371-1-AP, 1:100), Vimentin (Santa Cruz sc7557, 1:400) followed by alexa-fluor coupled secondary antibodies (Invitrogen) used at 1:500. Z stacks of optical sections were captured on a Leica Sp5 laser-scanning confocal microscope and reconstructed with Fiji.

Lung Dissociation and FACS and Flow Cytometry

Mice were euthanized by CO_2 exposure and perfused with 20 ml cold PBS through the right ventricle. Lungs were inflated with protease solution [1–2 ml; Collagenase Type I (catalog #17100–017, 450 U/ml; Gibco), Elastase (catalog #LS002279, 4 U/ml; Worthington Biochemical Corporation), Dispase (catalog #354235, 5 U/ml; BD Biosciences) and DNaseI (catalog #10104159001, 0.33 U/ml; Roche) in DMEM/F12], cut into small pieces (<2 mm^2), and incubated in 2 ml protease solution for 20 min at 37 °C with frequent agitation. DMEM/F12 + 10% FBS was added, and tissue was disrupted by pipetting, washed with DMEM/F12, and incubated for 5 min at 37 °C in 2 ml 0.1% Trypsin-EDTA + 0.325 mg DNaseI with intermittent agitation. An equal volume of DMEM-F12 + 10% FBS was added, and tissue was dissociated by pipetting. Cells were washed with 5 ml DMEM/F12, incubated at room temperature for 1.5 min in warmed 2 ml red blood cell lysis buffer (catalog #00–4333-57; eBioscience), filtered through a 40-μm strainer, centrifuged, and resuspended in PBS + 2% BSA. Sorting was performed on FACS ARIA II, and data was analyzed with FACS Diva (BD Biosciences). Flow cytometry was performed using a BD LSRII. Cells were fixed and permeabilized with Thermofisher Fix and Perm kit (GAS003). Primary anti-bodies used at 1:100 included TCF21 (abcam 32981), CD45 (BioLegend 303115), CD31 (BioLegend 304009), Epcam (BioLegend 324206), G0S2 (ThermoFischer PA523087), PkiG (protein-tech 21371-1-AP), chicken anti-Integrin-Alpha8 (Gift of Dr. Yasuyuki Yokosaki, Hiroshima). EdU staining performed according to manufacturer recommendations.

RNA Isolation and qPCR

After FACS isolation cells were 50,000 cells were pelleted and resuspended in 1ml of Trizol Reagent (catalog # 15596018 Thermo Fisher) and RNA was isolated per the manufacturers protocol. RNA was resuspended in 40ul of TE and 10ul of RNA was mixed with SuperScript VILO MasterMix (catalog # 11755050 Thermo Fisher) in a total reaction of 20ul per the manufacturers protocol. The resulting cDNA product was diluted 1:4 in TE and 1ul was used per 20ul reaction. qPCR was carried out using SYBR GreenER qPCR SuperMix Universal (catalog # 11762100 Thermo Fisher) and run on a ABI 7500 system (Thermo Fisher) according to the SYBR GreenER protocol. Each reaction was run in triplicate and averaged and all points with more than one melting temperature were discarded. Data was analyzed using delta-Ct counts against GAPDH for each sample prior to calculation of fold change. Boxplots for qPCR data were created using seaborn (https://github.com/mwaskom/seaborn) and the code for their generation can be found at (https://github.com/iandriver/RNA-sequence-tools/boxplot.py). Significance for all qPCR plots was calculated using a one-way anova test. * $p < 0.05$, ** $p < 0.01$, *** $p < 0.001$, **** $p < 0.0001$

5.3 Results

In vivo characterization of myofibroblast potential

To provide further evidence that Pdgfra+ cells give rise to myofibroblasts in the lung[11], we modified a recently described cell transplant protocol[18]. GFP+ cells were isolated by FACS from the lungs of knock-in mice that express a histone-tagged GFP under control of the endogenous PDGFRA regulatory elements. GFP+ cells ($2x10^5$) were delivered by intratracheal

instillation to recipient wild type mice 7 days after they had been given a single intratracheal dose of bleomycin. Fourteen days after cell injection, we performed immunofluorescence on lung sections from recipient mice and detected GFP+ cells in fibrotic lesions that were co-stained with an antibody against the myofibroblast marker aSMA (Fig1 A-C, Sup1 A). This suggests that at least a subset of Pdgfra+ fibroblasts are a cell of origin for aSMA myofibroblasts. In contrast, Ng2+ pericyte-like cells from donor lungs were not found in fibrotic lesions of recipient mice, suggesting either that these cells are not a source of myofibroblasts or that they do not survive and engraft in recipient lungs (Fig1 D-F).

Single cell transcriptome profiling of Pdgfra+ fibroblasts

We have shown that the Pdgfra-GFP allele marks spatially distinct populations of cells in the lung and there is some evidence that this population is contains transcriptionally distinct subpopulations that can be distinguished by high or low expression of the GFP transgene[10,12]. To profile the heterogeneity of this fibroblast population in an unbiased manner, we performed single cell RNA sequencing on Pdgfra-GFP+ cells isolated from the lungs of a healthy 2-month old mouse by FACS. Using the Fluidigm C1 platform, we captured 68 cells on one integrated fluidics circuit (IFC, "all"). Because Pdgfra-GFP "low" cells are less abundant[10], we reasoned that this population would be underrepresented in our single cell sequencing data. Therefore, we purified Pdgfra-GFP low cells by FACS and captured 79 of these cells on a second IFC ("low"). Barcoded cDNA was generated and sequenced. After sequencing and filtering out cells that did not pass quality control metrics (see methods), a total of 128 cells remained, 55 from "all" Pdgfra-GFP and 73 from "low" Pdgfra-GFP.

Hierarchical clustering of these cells based on sequencing data reveals that at least four subpopulations exist. Differences in gene expression between cells of these subpopulations (Figure 2A) show that they can be clustered into two groups: lipofibroblast-like (Lipofibroblasts and Intermediate) and matrix fibroblasts (Matrix and Matrix+). Lipofibroblasts are enriched for Plin2, G0s2, and Pdgfra and a number of genes that regulate adipogenesis and lipolysis[28,29]. This group also expresses Tcf21 (Pod1), a marker of kidney podocytes that regulates myofibroblast differentiation[30] and is necessary for lung morphogenesis[31,32] (Figure 2A,2H). The Intermediate cells have significantly lower Plin2, Tcf21, and G0s2 expression. Intermediate cells express a number of genes absent from lipofibroblasts that are expressed in matrix cells, such as Pdgfrb, Dcn, and Eln. Matrix and matrix+ cells express a number of adhesion, extracellular matrix and cytokines that are largely absent from lipofibroblasts, such as Has1, Col14a1, Lum, Ly6a and IL33. The matrix+ subpopulation is distinguished from matrix cells by the significantly decreased expression of genes like Fgf10, Itga8, and Tbx4, that are common among all other fibroblasts and further decreased expression of lipofibroblast-enriched genes such as G0s2, Plin2, Sphk2 compared to the matrix subset. These data shed light on the heterogeneity within the adult lung Pdgfra+ fibroblast population with respect to some commonly used fibroblast markers and identify a spectrum of fibroblast functions: lipid metabolism and adipogenesis (Plin2, G0s2, Sphk2), extracellular matrix production and degradation (Eln, Dcn, Lum), immune signaling (Il33, Cxcl1, Ccl12) and growth factors (Fgf10, Bmp3) (Figure 2).

Given the recent findings in El Agha, et al. and Ting Xie, et al.[16,17], we paid close attention to Plin2, Fgf10 and Tbx4 distributions among the fibroblast subpopulation. Plin2 is most enriched in the lipofibroblast subset whereas Fgf10 and Tbx4 are highest in the

intermediate subset and slightly lower in the lipofibroblast and matrix subpopulations. Analysis using the monocle software package[33] reveals a "pseudotime" relationship between fibroblasts where the intermediate subpopulation lies between the lipofibroblast and matrix populations (Fig2C). The direction of the relationship is not implied by pseudotime as each direction is equally likely mathematically. To further characterize the lipofibroblast subpopulation, we identified genes that are high in this subpopulation and lower in the intermediate and matrix populations (Fig 2). This revealed a number of novel potential markers of lipofibroblasts including G0s2, Gyg, Shpk2, and Tcf21.

Tcf21 is a marker of fibroblast progenitors

The transcription factor Tcf21 is a marker of white adipocytes[19], and is required for lung development[32]. Our sequencing data showed that this gene is expressed in lipofibroblasts of the lung (Figure 2H). To verify that Tcf21 marks a subset of Pdgfra+ fibroblasts in the lung, we administered tamoxifen to adult Pdgfra-GFP, Tcf21-CreER;ROSA-TdTomato mice. One week later we analyzed lung sections by immunofluorescence. Indeed, 41±12% (95% confidence interval) of Pdgfra-GFP+ cells in the adult mouse lung was also TdTomato+, confirming that Tcf21-CreER is expressed in a subset of Pdgfra+ fibroblasts (Fig S2A-B). A subset of cells labeled with Tcf21-CreER (25±3%) express very little or no Pdgfra-GFP. These cells have a similar morphology and localization to the Pdgfra-GFP+, Tcf21+ cells (Fig S2A-B) and are Pecam-, Pdgfra+, and Rage- fibroblasts (S3A,C,E).

To assess the capacity of Tcf21+ fibroblasts to give rise to myofibroblasts in the context of pulmonary fibrosis, we administered a single intratracheal dose of bleomycin (or saline

control) to Tcf21-CreER;ROSA-TdTomato mice two weeks after the final dose of tamoxifen. Two weeks after the administration of bleomycin, mice were euthanized and the lungs were analyzed by flow cytometry, immunofluorescence and qPCR. In the lungs of bleomycin treated mice, 20-30% of the Tcf21 lineage traced cells were positive for aSMA by FACS, compared to 10% of cells in the saline injected controls (Figure 3G). Immunofluorescence showed that many of the lineage traced cells in bleomycin treated animals were aSMA+ myofibroblasts within fibrotic foci (Figure 3D-F). qPCR analysis showed that aSMA (Acta2) expression is upregulated 2.3 fold in FACS purified Tcf21 lineage traced cells 14 days after Bleomycin compared to saline controls. Col3a1 and Col1a1 were also upregulated in lineage traced cells following bleomycin (Figure 3I). In contrast Pdgfra, G0s2, and Tcf21 had decreased expression in Tcf21+ lineage cells 14 days after Bleomycin. These data are consistent with the hypothesis that Tcf21+ cells in bleomycin treated lungs undergo a transition away from a Pdgfra+ Tcf21+ lipofibroblast towards an aSMA positive myofibroblast.

Next we sought to assess the proliferative capacity of fibroblast subpopulations in response to bleomycin. Four days after saline injection, the percent of Tcf21 lineage traced cells and Pdgfra-GFP+ cells that incorporated EdU in a 24 hour pulse was ~1%. Four days after Bleomycin injection, 6% of the Tcf21+ cells incorporated EdU whereas only 2% of the Pdgfra-GFP+cells were proliferative (Fig3 H). These data suggest that the Tcf21+ cells are highly proliferative compared to the overall Pdgfra+ fibroblast population. Both the lineage tracing and qPCR data strongly suggest that Tcf21+ lung fibroblasts are capable of proliferating and differentiating towards a myofibroblast fate. Whether proliferation is required for this differentiation from lipofibroblast to myofibroblast is still under investigation.

ITGA8 marks a subset of human lung fibroblasts

To determine whether a similar cell population exists in the human lung, we identified several candidate surface markers from the mouse single cell RNA sequencing data for FACS enrichment of live human cells. Itga8 expression is highest in the lipofibroblast group cells with decreasing levels in Intermediate and Matrix cells and correlates with G0s2 expression, the top marker of lipofibroblasts (Sup Figure 4). Staining for ITGA8 in healthy human lungs shows that ITGA8 and Tcf21 stain a subset of Vimentin+ cells (Fig4 A-B). We sorted ITGA8+ and ITGA8- cells from the total population of live CD45-, CD31-, EPCAM- cells isolated from non-utilized donor lung tissue. Analysis revealed that 5-6.5% of the total population is ITGA8+ and of those cells 14.2% are also Tcf21+ and 29.9% are G0S2+. Of the Tcf21+ cells 80% are ITGA8+ and 86% of the G0S2+ cells are ITGA8+. Together, these data indicate that ITGA8 is a viable surface marker for sorting a highly enriched population of lipofibroblasts from human lungs. qPCR performed on sorted human ITGA8+ cells shows that ITGA8+ cells are enriched for ITGA8 along with TCF21 and PDGFRB (Fig 4E). In one out of three lungs both G0S2 and PLIN2 were greatly enriched in the ITGA8+ population, but overall enrichment in ITGA8+ cells was small and not statistically significant. The enrichment of COL14A1 in ITGA8 agrees with the expression data from mice, where Tcf21 lineage cells decreased Col14a1 expression after Bleomycin treatment (Figure 3I), suggesting Col14a1 is enriched in healthy Tcf21+ fibroblasts in both mice and humans.

5.4 Discussion

These data demonstrate the utility of single cell sequencing for elucidating the heterogeneity within populations of cells in the lung. We show that the Pdgfra+ population of mouse lung fibroblasts contains at least four transcriptionally distinct subpopulations. These populations can be described along a transcriptional spectrum of two classical fibroblast subsets: lipofibroblast and matrix/myofibroblast. The single cell transcriptional profiles generated both support these classical definitions and allow us to further characterize and subdivide fibroblast identity. In this paper we focus on describing the overall trends in gene expression across populations and the identification of novel markers of cell identity. These data also offer potential insights into the signaling networks that are mediate fibroblast cross-talk with other epithelial, immune and fibroblast populations. Examples include Bmp3 expression in lipofibroblasss, and Il33 and Ccl11 (eotaxin) expression in the matrix fibroblasts. One caveat of our study is the fact that these cells were isolated from healthy 2 month old mice and so do not encompass the full range of fibroblasts in the lung, specifically the activated myofibroblast that emerges in pathological fibrotic lesions.

Our data and the recent work from[16] and[17] clearly demonstrate a lineage relationship between fibroblast subtypes, specifically the reversible interconversion of lipofibroblasts to myofibroblasts. We analyzed our single cell transcriptome data using the Monocle software package[33] to order the cells in "pseudotime." Directionality cannot be inferred from this analysis of single cell sequencing data, so one cannot assign a progenitor cell identity or assess whether this differentiation is bi-directional. However, our data support previous lineage tracing data, whereby cells genetically labeled by Tcf21, Plin2, Tbx4, or Fgf10 can reversibly give rise to

aSMA positive myofibroblasts. Our data show that Tcf21 and Plin2 are expressed at higher levels in the lipofibroblast population and Tbx4 and Fgf10 are slightly higher in the Intermediate population. Therefore, we hypothesize that either the "Intermediate" cells represent a progenitor cell population, capable of giving rise to both lipofibroblast and myofibroblast or that the lipofibroblast is a progenitor with the "Intermediate" cell as a transitory state along myofibroblast differentiation.

One of the goals of this work was to identify novel markers for human fibroblasts where there has been a lack of tools for sorting fibroblasts. The ITGA8+ subpopulation in adult human lungs contains a majority of the Tcf21+ and G0s2+ cells, but is not restricted to these fibroblast subpopulations. This fits with mouse data, where Itga8 is expressed at the highest level in lipofibroblasts but is also expressed in all of the populations except the Matrix+ cells. The donor human lungs used in this study are heterogeneous with respect to age, genetics and environmental exposure. Further study is needed to characterize the population of fibroblasts marked by ITGA8+ and how this population changes with age and disease states. Furthermore, our data reveal other novel cell surface markers of fibroblast subpopulations that remain to be studied. In addition to demonstrating applications of single cell sequencing, these data reveal novel markers of clinically relevant fibroblast subpopulations and provide important insights into fibroblast plasticity and the etiology of pulmonary fibrosis.

5.5 References

1 Hines, E. A. & Sun, X. Tissue crosstalk in lung development. *J Cell Biochem* **115**, 1469-1477, doi:10.1002/jcb.24811 (2014).

2 McGowan, S. E. & McCoy, D. M. Regulation of fibroblast lipid storage and myofibroblast phenotypes during alveolar septation in mice. *American Journal of Physiology - Lung Cellular and Molecular Physiology* **307**, doi:10.1152/ajplung.00144.2014 (2014).

3 McGowan, S. E. & McCoy, D. M. Fibroblast growth factor signaling in myofibroblasts differs from lipofibroblasts during alveolar septation in mice. *American Journal of Physiology - Lung Cellular and Molecular Physiology* **309**, doi:10.1152/ajplung.00013.2015 (2015).

4 Ruiz-Camp, J. & Morty, R. E. Divergent fibroblast growth factor signaling pathways in lung fibroblast subsets: where do we go from here? *American Journal of Physiology - Lung Cellular and Molecular Physiology*, doi:10.1152/ajplung.00298.2015 (2015).

5 Tschumperlin, D. J. Matrix, mesenchyme, and mechanotransduction. *Ann Am Thorac Soc* **12 Suppl 1**, S24-29, doi:10.1513/AnnalsATS.201407-320MG (2015).

6 De Langhe, S. P., Carraro, G., Warburton, D., Hajihosseini, M. K. & Bellusci, S. Levels of mesenchymal FGFR2 signaling modulate smooth muscle progenitor cell commitment in the lung. *Dev Biol* **299**, 52-62, doi:10.1016/j.ydbio.2006.07.001 (2006).

7 Metzger, R. J., Klein, O. D., Martin, G. R. & Krasnow, M. A. The branching programme of mouse lung development. *Nature* **453**, 745-750, doi:papers2://publication/doi/10.1038/nature07005 (2008).

8 Chambers, R. C. & Mercer, P. F. Mechanisms of alveolar epithelial injury, repair, and fibrosis. *Ann Am Thorac Soc* **12 Suppl 1**, S16-20, doi:10.1513/AnnalsATS.201410-448MG (2015).

9 Hinz, B. Mechanical aspects of lung fibrosis: a spotlight on the myofibroblast. *Proc Am Thorac Soc* **9**, 137-147, doi:10.1513/pats.201202-017AW (2012).

10 Green, J., Endale, M., Auer, H. & Perl, A. T. Diversity of Interstitial Lung Fibroblasts is Regulated by PDGFRalpha Kinase Activity. *Am J Respir Cell Mol Biol*, doi:10.1165/rcmb.2015-0095OC (2015).

11 Rock, J. R. *et al.* Multiple stromal populations contribute to pulmonary fibrosis without evidence for epithelial to mesenchymal transition. *Proc. Natl. Acad. Sci. U.S.A.* **108**, E1475-1483, doi:papers2://publication/doi/10.1073/pnas.1117988108 (2011).

12 Kimani, P. W., Holmes, A. J., Grossmann, R. E. & McGowan, S. E. PDGF-Ralpha gene expression predicts proliferation, but PDGF-A suppresses transdifferentiation of neonatal mouse lung myofibroblasts. *Respir Res* **10**, 119, doi:10.1186/1465-9921-10-119 (2009).

13 Boström, H. *et al.* PDGF-A signaling is a critical event in lung alveolar myofibroblast development and alveogenesis. *Cell* **85**, 863-873, doi:papers2://publication/uuid/0E9A332C-7B05-4DE9-B4F7-A63C0CFB3201 (1996).

14 McGowan, S. E. & McCoy, D. M. Platelet derived growth factor-A and sonic hedgehog signaling direct lung fibroblast precursors during alveolar septal formation. *... Journal of Physiology-Lung ...*, doi:papers2://publication/uuid/53AD138B-0A2B-4BF9-980E-31162F9F5779 (2013).

15 McGowan, S. E. & McCoy, D. M. Fibroblast growth factor signaling in myofibroblasts differs from lipofibroblasts during alveolar septation in mice. *Am J Physiol Lung Cell Mol Physiol* **309**, L463-474, doi:10.1152/ajplung.00013.2015 (2015).

16 El Agha, E. *et al.* Two-Way Conversion between Lipogenic and Myogenic Fibroblastic Phenotypes Marks the Progression and Resolution of Lung Fibrosis. *Cell Stem Cell*, doi:10.1016/j.stem.2016.10.004 (2016).

17 Xie, T. *et al.* Transcription factor TBX4 regulates myofibroblast accumulation and lung fibrosis. *Journal of Clinical Investigation*, doi:10.1172/JCI85328 (2016).

18 Tsukui, T., Ueha, S., Shichino, S., Inagaki, Y. & Matsushima, K. Intratracheal cell transfer demonstrates the profibrotic potential of resident fibroblasts in pulmonary fibrosis. *Am J Pathol* **185**, 2939-2948, doi:10.1016/j.ajpath.2015.07.022 (2015).

19 de Jong, J. M., Larsson, O., Cannon, B. & Nedergaard, J. A stringent validation of mouse adipose tissue identity markers. *Am J Physiol Endocrinol Metab* **308**, E1085-1105, doi:10.1152/ajpendo.00023.2015 (2015).

20 Maezawa, Y. *et al.* Loss of the Podocyte-Expressed Transcription Factor Tcf21/Pod1 Results in Podocyte Differentiation Defects and FSGS. *Journal of the American Society of Nephrology* **25**, 2459-2470, doi:10.1681/ASN.2013121307 (2014).

21 Braitsch, C. M., Combs, M. D., Quaggin, S. E. & Yutzey, K. E. Pod1/Tcf21 is regulated by retinoic acid signaling and inhibits differentiation of epicardium-derived cells into smooth muscle in the developing heart. *Developmental Biology* **368**, 345-357, doi:10.1016/j.ydbio.2012.06.002 (2012).

22 Maezawa, Y. *et al.* A new Cre driver mouse line, Tcf21/Pod1-Cre, targets metanephric mesenchyme. *PLoS ONE* **7**, doi:10.1371/journal.pone.0040547 (2012).

23 Song, H. *et al.* Functional characterization of pulmonary neuroendocrine cells in lung development, injury, and tumorigenesis. *Proc. Natl. Acad. Sci. U.S.A.* **109**, 17531-17536, doi:papers2://publication/doi/10.1073/pnas.1207238109 (2012).

24 Rawlins, E. L. *et al.* The role of Scgb1a1+ Clara cells in the long-term maintenance and repair of lung airway, but not alveolar, epithelium. *Cell Stem Cell* **4**, 525-534, doi:10.1016/j.stem.2009.04.002 (2009).

25 Hamilton, T. G., Klinghoffer, R. A., Corrin, P. D. & Soriano, P. Evolutionary divergence of platelet-derived growth factor alpha receptor signaling mechanisms. *Molecular and Cellular Biology* **23**, 4013-4025, doi:papers2://publication/uuid/8BF39E31-800D-49AD-AAC0-4421CCABDCB4 (2003).

26 Zhu, X., Bergles, D. E. & Nishiyama, A. NG2 cells generate both oligodendrocytes and gray matter astrocytes. *Development* **135**, 145-157, doi:10.1242/dev.004895 (2008).

27 Trapnell, C. *et al.* Differential gene and transcript expression analysis of RNA-seq experiments with TopHat and Cufflinks. *Nat Protoc* **7**, 562-578, doi:10.1038/nprot.2012.016 (2012).

28 Choi, H. *et al.* G0/G1 switch gene 2 has a critical role in adipocyte differentiation. *Cell Death & Differentiation* **21**, 1071-1080, doi:10.1038/cdd.2014.26 (2014).

29 Schweiger, M. *et al.* G0/G1 switch gene-2 regulates human adipocyte lipolysis by affecting activity and localization of adipose triglyceride lipase. *J Lipid Res* **53**, 2307-2317, doi:10.1194/jlr.M027409 (2012).

30 Plotkin, M. & Mudunuri, V. Pod1 induces myofibroblast differentiation in mesenchymal progenitor cells from mouse kidney. *Journal of cellular biochemistry* **103**, 675-690, doi:10.1002/jcb.21441 (2008).

31 Costa, R. H., Kalinichenko, V. V. & Lim, L. Transcription factors in mouse lung development and function. *Am J Physiol Lung Cell Mol Physiol* **280**, L823-838 (2001).

32 Quaggin, S. E. *et al.* The basic-helix-loop-helix protein pod1 is critically important for kidney and lung organogenesis. *Development* **126**, 5771-5783 (1999).

33 Trapnell, C. *et al.* The dynamics and regulators of cell fate decisions are revealed by pseudotemporal ordering of single cells. *Nat Biotechnol* **32**, 381-386, doi:10.1038/nbt.2859 (2014).

5.6 Figures and Tables

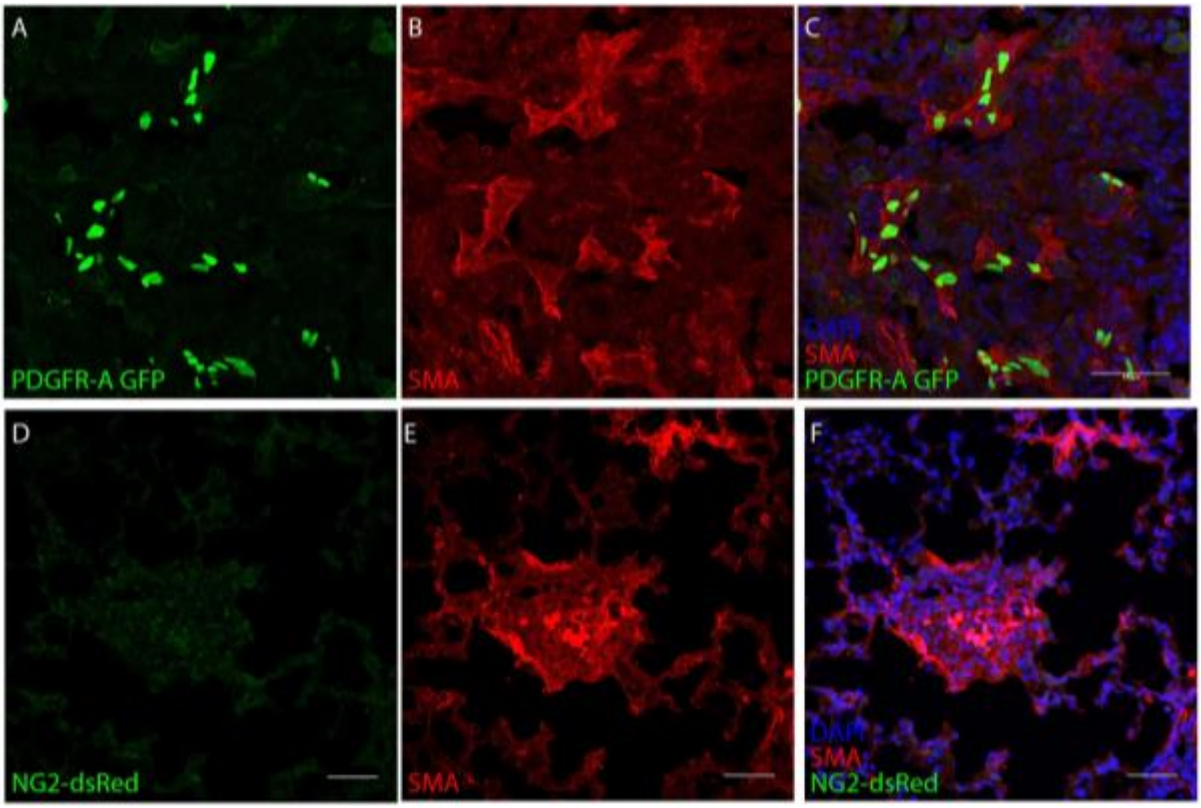

Figure 1. PDGFR-A Cells Engraft and Express a-SMA after Bleomycin Injury

A-C) B6 mice 14 days post-bleomycin injury and 7 days post-pdgfr-a transplant showed succesful engraftment of PDGFR-A cells into regions of fibrosis. These PDGFR-A cells colocalized with a marker of myofibroblasts, alpha-smooth muscle actin (SMA). D-F) B6 mice 14 days post-bleomycin injury and 7 days post-NG2 cell transplant showed no lesions with succesful engraftment. Scale bar =50uM

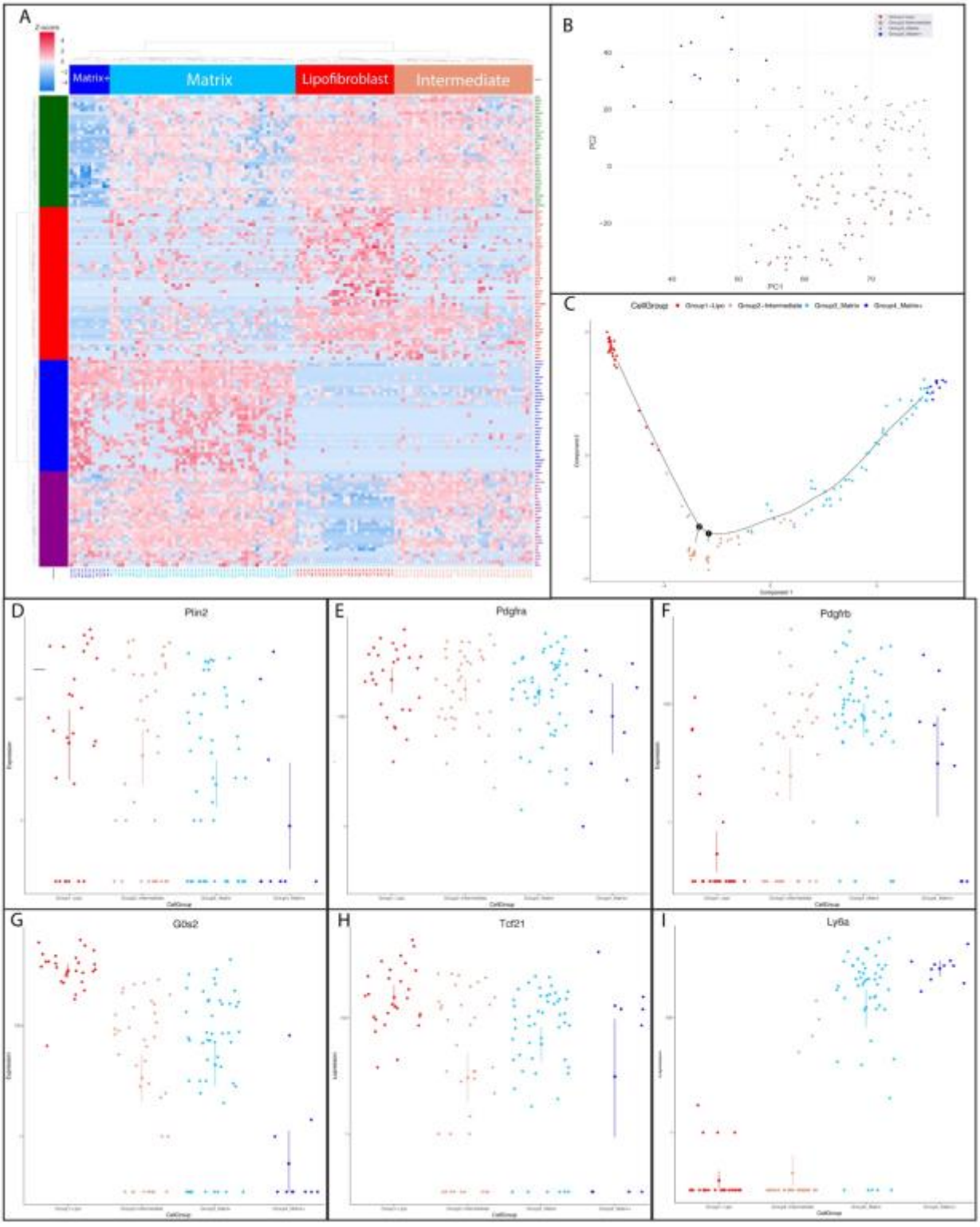
A
Matrix
Lipofibroblast
Intermediate
B
C
D
Plin2
E
Pdgfra
F
Pdgfrb
G
G0s2
H
Tcf21
I
Ly6a

Figure 2. Single-Cell Sequencing Analysis of PDGFRA+ Fibroblasts

A) A heatmap of all cells with genes selected by variance shows distinct differences among healthy lung fibroblasts. Colors of cells are assigned by hierarchical clustering and the coloring of genes by significance testing among the cell groups. Cells labeled with 'all' were sorted by Pdgfra-GFP expression. Cells labeled with 'low' were sorted based upon being low Pdgfra-GFP expressing. B) PCA of all the cells shows that the three cell groups separate along PC1 and PC2. The Gene Loading PCA shows the top genes contributing to the PC1 and PC2 dimensions. Ellipses are centered on the mean of position and the boundary represents two standard deviations of the mean. C) Analysis using the monocle software package[33] reveals a "pseudotime" relationship between fibroblasts where the intermediate subpopulation lies between the lipofibroblast and matrix populations D-I) Jitter plots representing relative expression of a specific across all four defined fibroblast subgroups.

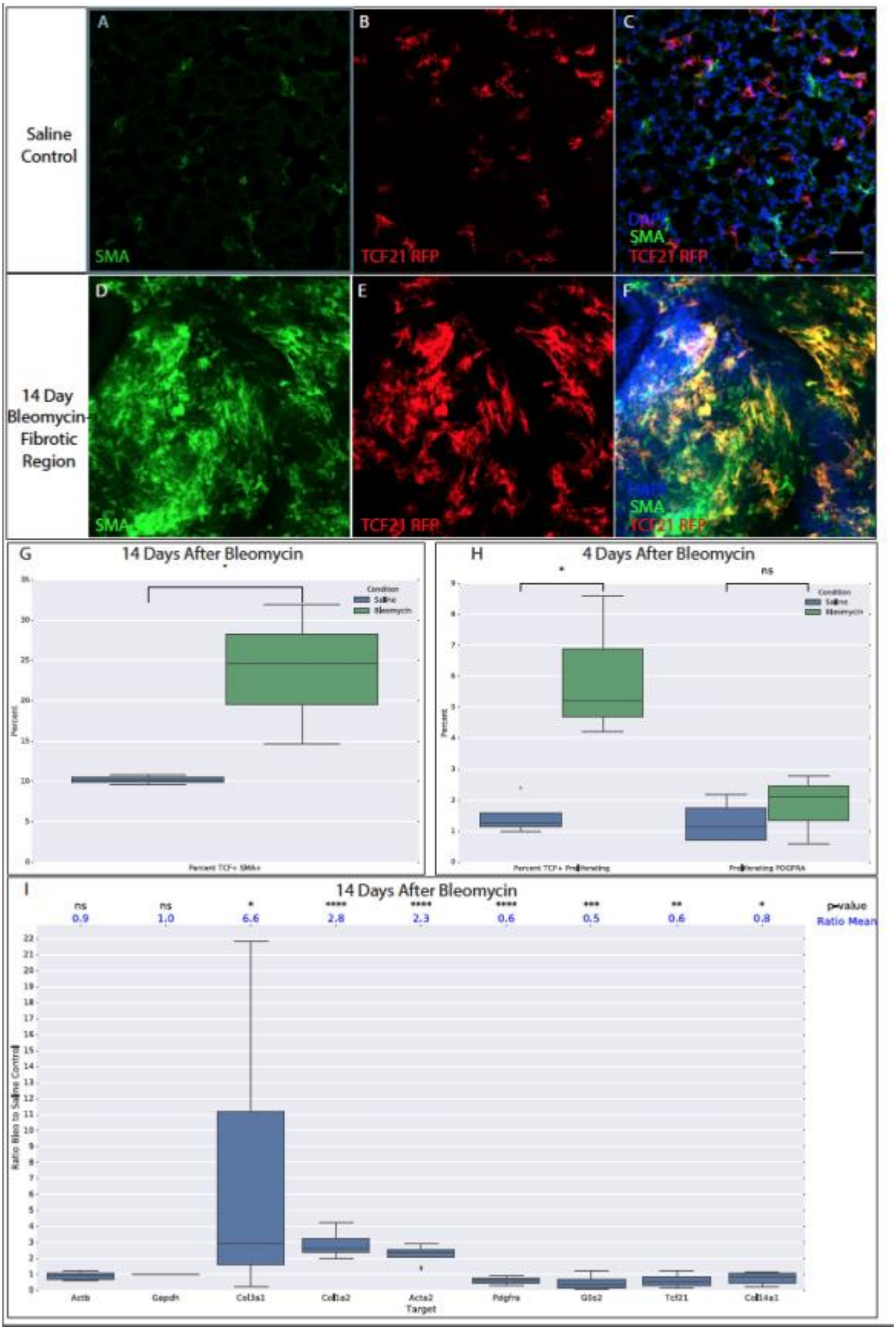
Saline Control
A
SMA
B
TCF21 RFP
C
DAPI
SMA
TCF21 RFP
14 Day Bleomycin-Fibrotic Region
D
SMA
E
TCF21 RFP
F
DAPI
SMA
TCF21 RFP
G
14 Days After Bleomycin
Condition
Saline
Bleomycin
Percent
Percent TCF+ SMA+
H
4 Days After Bleomycin
ns
Condition
Saline
Bleomycin
Percent
Percent TCF+ Proliferating
Proliferating PDGFRA
I
14 Days After Bleomycin
ns ns * **** **** **** *** ** * p-value
0.9 1.0 6.6 2.8 2.3 0.6 0.5 0.6 0.8 Ratio Mean
Ratio Bleo to Saline Control
Actb
Gapdh
Col3a1
Col1a2
Acta2
Pdgfra
Gli2
Tcf21
Col14a1
Target

Figure 3. Tcf21+ Cells Give Rise to aSMA+ cells 14-Days After Bleomycin Injury

A-C) Saline control animals typically have less TCF21 cells present, and none co-express SMA. D-F) 14days post-bleomycin injury, lineage-labeled TCF21 cells can be found expanded in regions of pulmonary fibrosis. These cells co-localize with SMA (arrows). G) 7days post-bleomycin injection, 10% of TCF+ cells are SMA+ in the uninjured lung as compared to ~25% in the injured lungs. H) 7 Days post-bleomycin injury, ~1.2% of TCF21+ cells are proliferative as compared to ~5.2% of TCF21+ cells in the injured lung. There was not a statistically significant difference between the proliferation rate in the TCF21-, Pdgfr-a+ populations. Scale bar =50uM I) Tcf21+ lineage cells were sorted from mice 14 days after Saline or Bleomycin injection and RNA expression was measure with qPCR. Collagens Col3a1 and Col1a2 along with Acta2 were increased and markers of Tcf21+ lipofibroblasts (G0s2 and Pdgfra) were decreased.

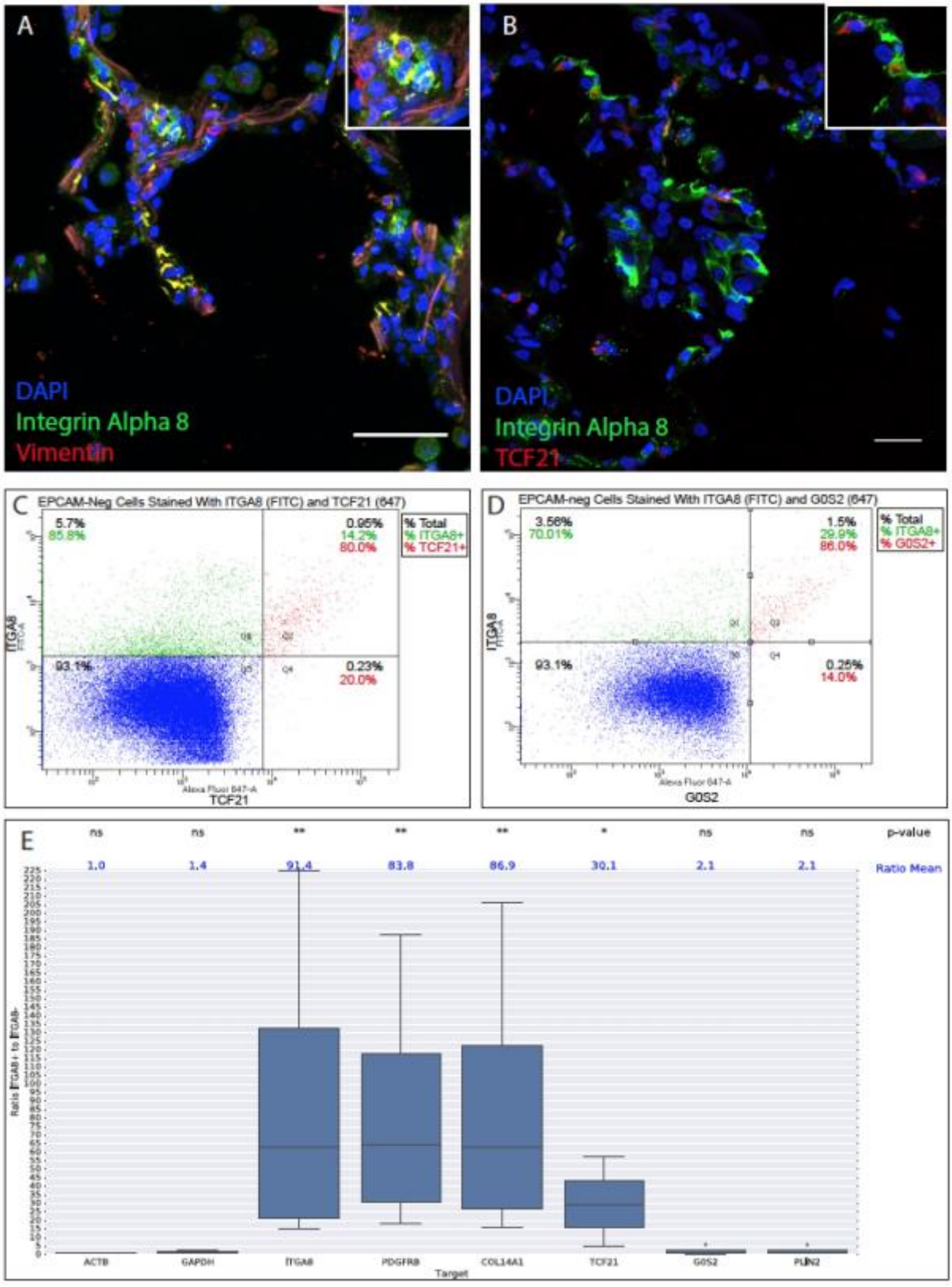
A
DAPI
Integrin Alpha 8
Vimentin
B
DAPI
Integrin Alpha 8
TCF21
C
EPCAM-Neg Cells Stained With ITGA8 (FITC) and TCF21 (647)
5.7%
85.8%
0.95%
14.2%
80.0%
93.1%
0.23%
20.0%
% Total
% ITGA8+
% TCF21+
ITGA8
TCF21
D
EPCAM-neg Cells Stained With ITGA8 (FITC) and G0S2 (647)
3.56%
70.01%
1.5%
29.9%
86.0%
93.1%
0.25%
14.0%
% Total
% ITGA8+
% G0S2+
ITGA8
G0S2
E
ns
ns
**
**
**
*
ns
ns
p-value
1.0
1.4
91.4
83.8
86.9
30.1
2.1
2.1
Ratio Mean
ACTB
GAPDH
ITGA8
PDGFRB
COL14A1
TCF21
G0S2
PLIN2
Target

Figure 4. Anti-Body Staining of Non-Utilized Donor Lung Tissue

A-B) Non-utilized donor lung tissue co-stained positive for the fibroblast marker Vimentin with Integrin Alpha 8, as well as TCF21. C-D) Dissociated human lung tissue was sorted for live EPCAM- CD45- CD31- cells. These cells were then fixed and permeabilized to stain for intracellular proteins TCF21 and G0S2 along with ITGA8. ITGA8+ cells are enriched for both TCF21 and G0S2. E) qPCR analysis comparing integrin alpha 8+ vs alpha 8- populations, reveals that human ITGA8 fibroblasts are enriched for TCF21, but unlike the mice also enrich for PDGFRB.

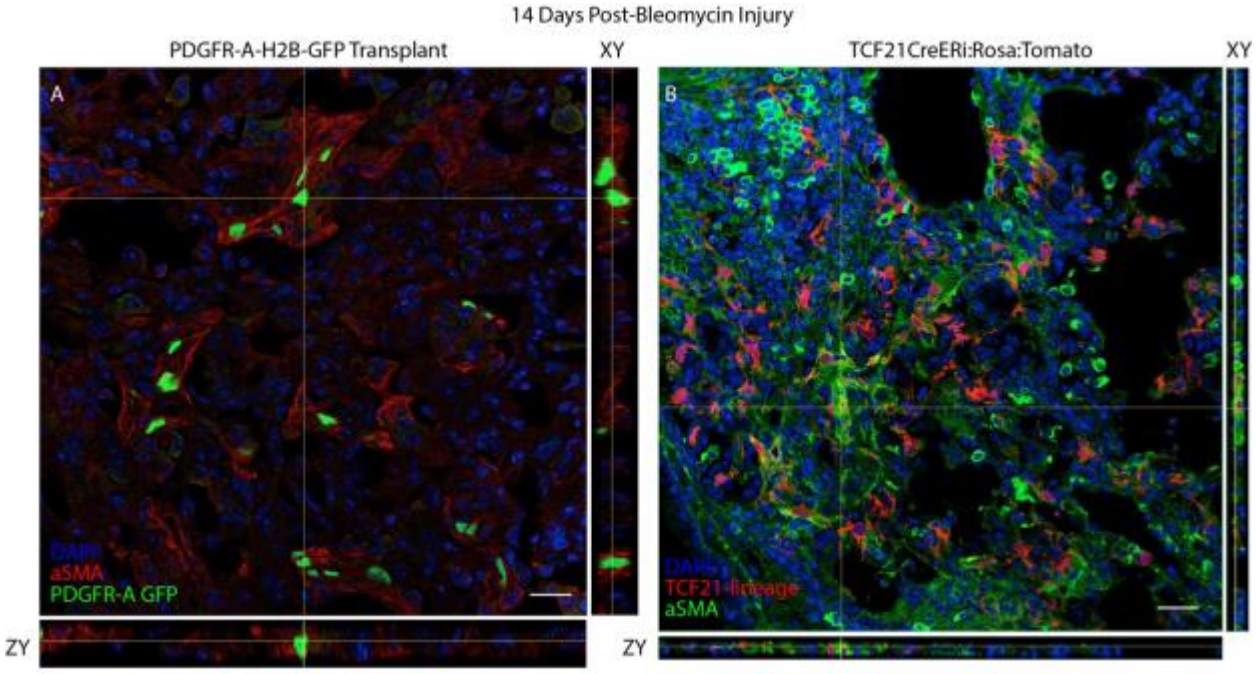
14 Days Post-Bleomycin Injury
PDGFR-A-H2B-GFP Transplant
XY
A
DAPI
aSMA
PDGFR-A GFP
ZY
TCF21CreERi:Rosa:Tomato
XY
B
DAPI
TCF21-lineage
aSMA
ZY

Supplement 1. Orthogonal Views of Transplanted PDGFR-A Cells and Lineage Labeled Tcf21 Cells 14-Days Post-Bleomycin Injury

A) Orthogonal view of a Pdgfr-a transplanted lung showing co-localization of Pdgfr-a GFP and alpha-SMA in a region of fibrosis B) Orthogonal view of a TCF21CreEr;Rosa:Tomato mouse 14days post-injury demonstrating co-staining of the lineage trace marker with alpha-SMA in a region of fibrosis.

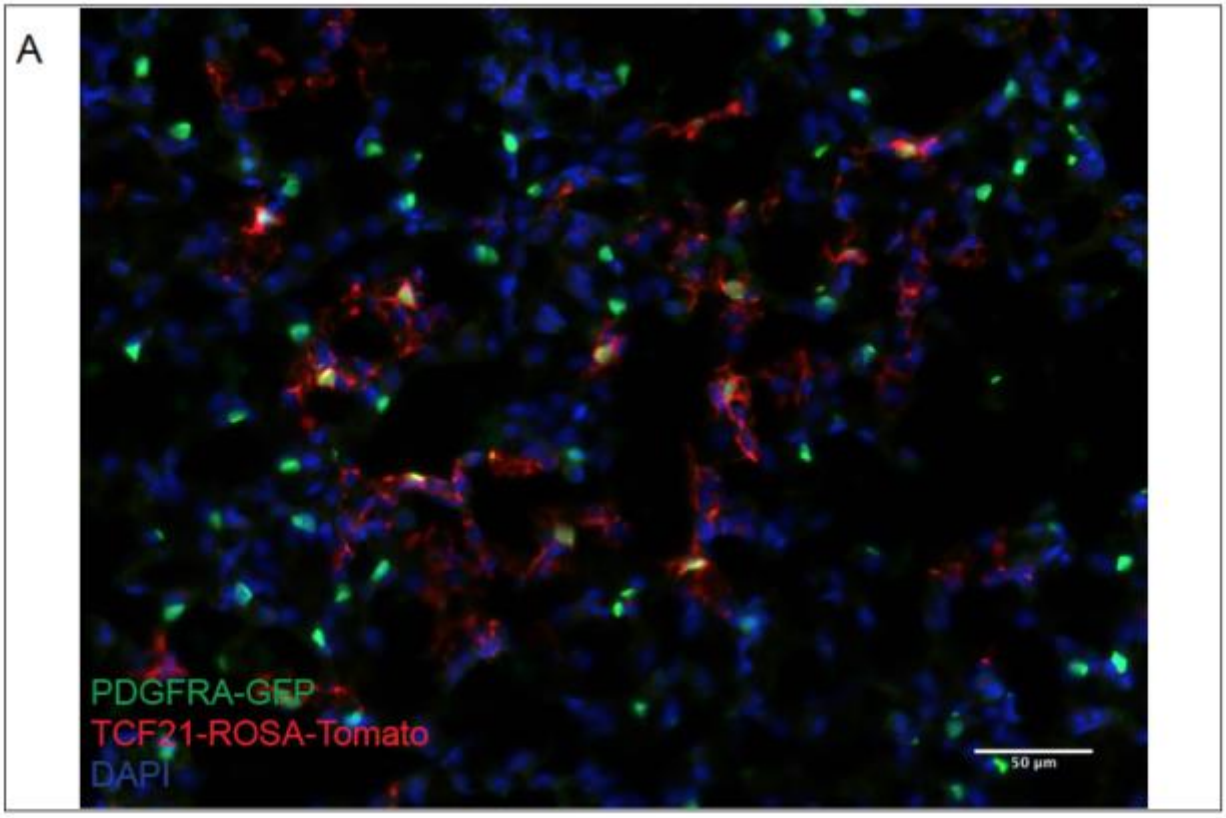
A
PDGFRA-GFP
TCF21-ROSA-Tomato
DAPI
50 µm

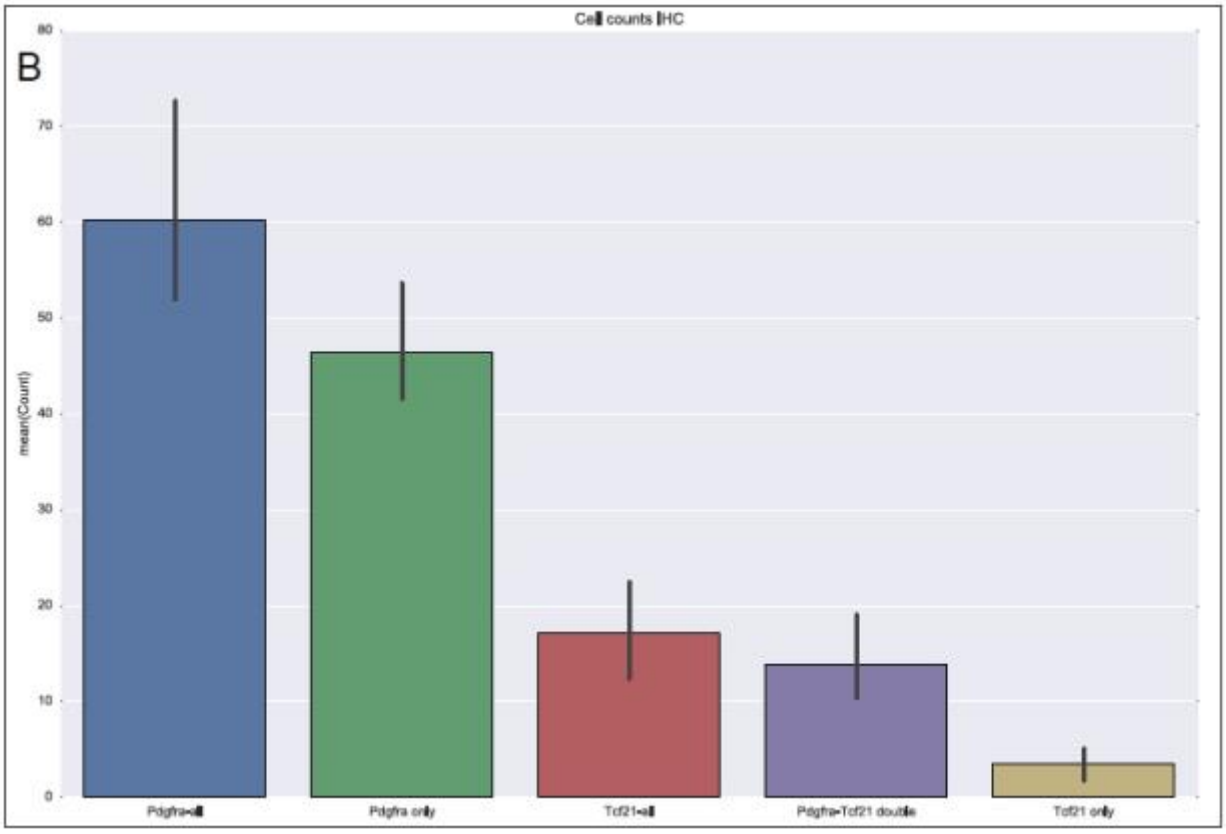
B
Cell counts IHC
mean(Count)
80
70
60
50
40
30
20
10
0
Pdgfra+all
Pdgfra only
Tcf21+all
Pdgfra+Tcf21 double
Tcf21 only

Supplement 2. Analysis of Dual Labeled Tcf21CreER;Rosa:Tomato/PDGFR-A-GFP Mouse

A) A representative image of TCF21-RT and Pdgfra-GFP+ cells from the distal lung. B) Counts from n=6 images from 3 mice reveal that Tcf21-RT cells are mostly a subset of Pdgfra-GFP+ cells. ~22% of all Pdgfra-GFP cells are also Tcf21-RT+ and ~25% of Tcf21-RT+ cells have no or very little Pdgfra-GFP.

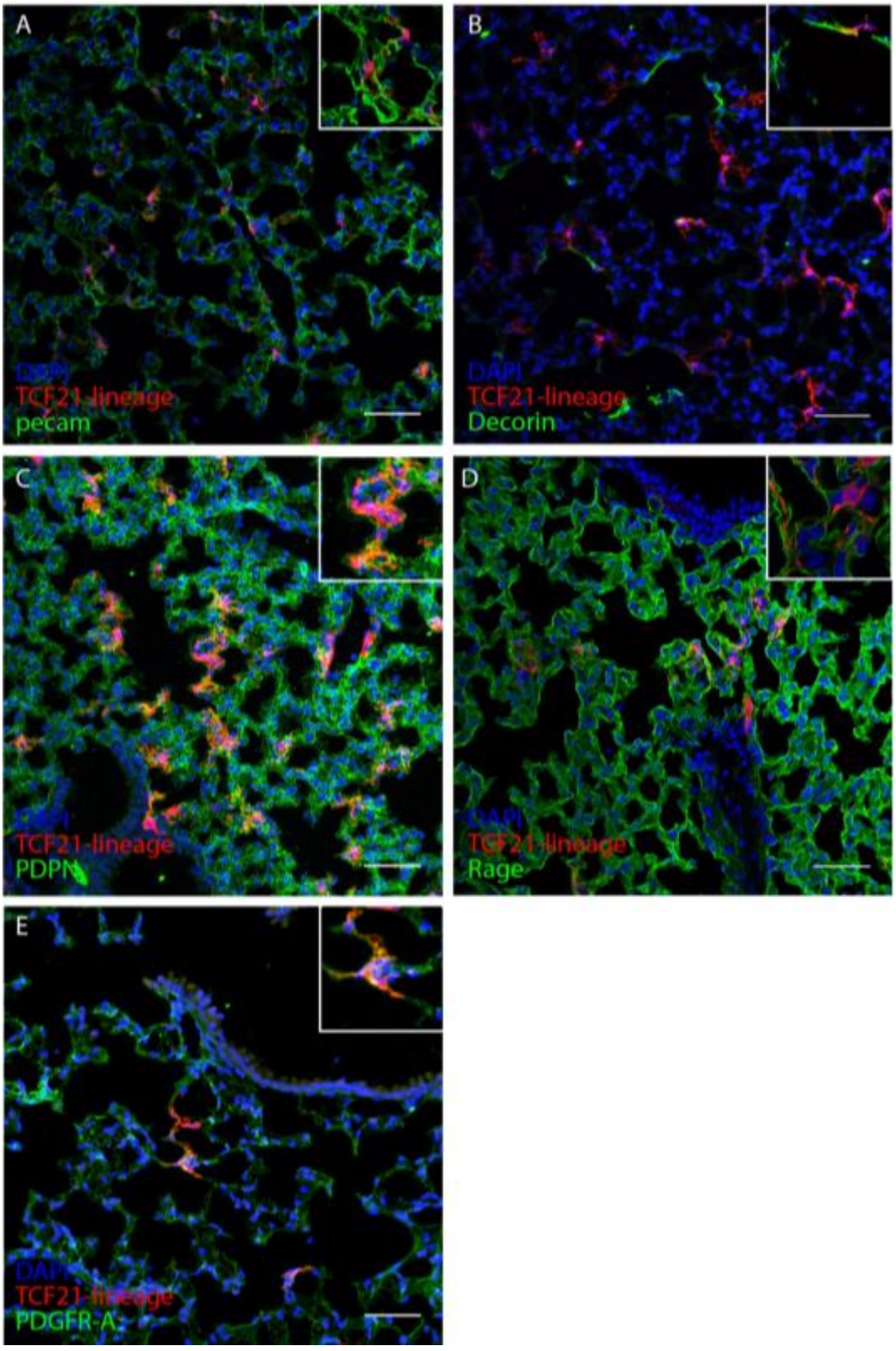
A
DAPI
TCF21-lineage
pecam
B
DAPI
TCF21-lineage
Decorin
C
DAPI
TCF21-lineage
PDPN
D
DAPI
TCF21-lineage
Rage
E
DAPI
TCF21-lineage
PDGFR-A

Supplement 3. IHC Analysis of Tcf21-CreER:Rosa:Tomato Mouse to corroborate several of the genes highlighted by single cell sequencing

A) Tcf21-RT cells sit next to, but do not express PECAM. B) Dcn is expressed mostly in Tcf21- fibroblasts. C) Pdpn staining shows the Pdpn can be found both in the AEC1 cell and in Tcf21-RT fibroblasts. D) Rage staining highlights that AEC1 overlay Tcf21-RT fibroblast, but do not overlap. E) Tcf21-RT cells are also Pdgfra+.

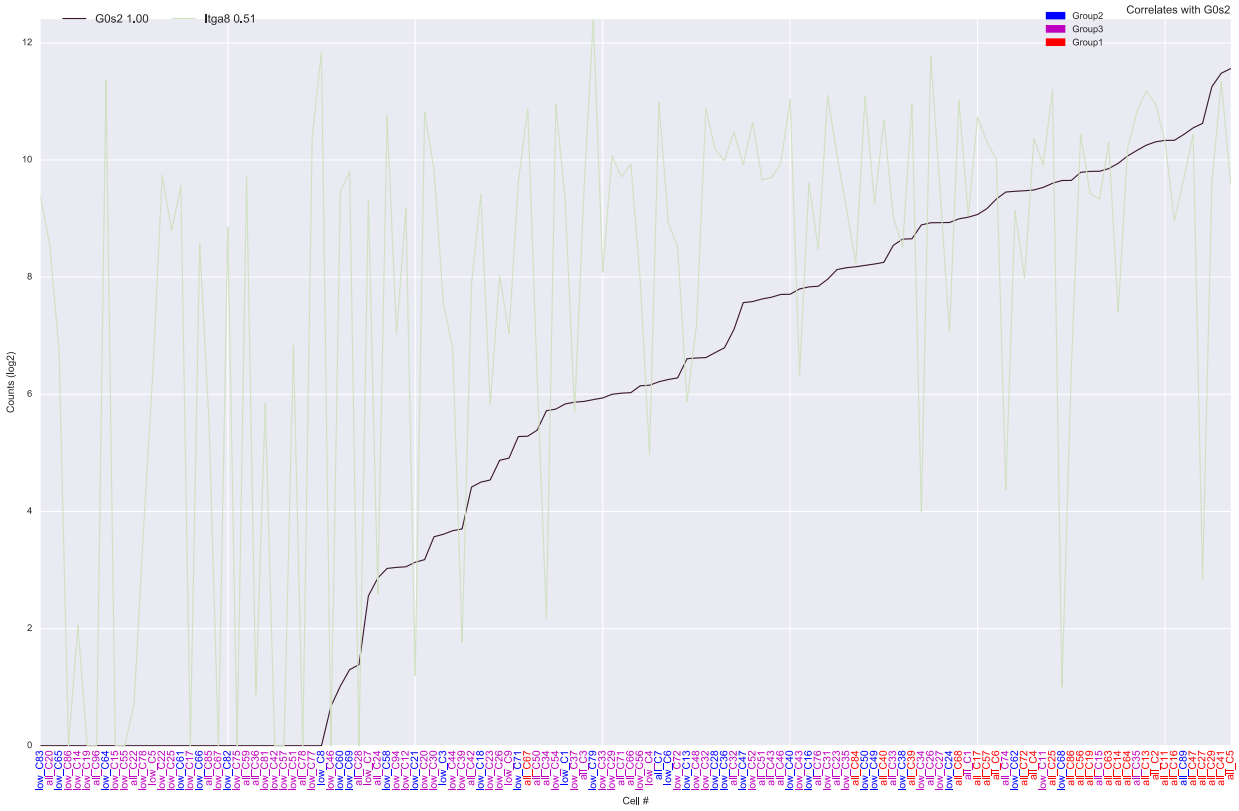
G0s2 1.00
Itga8 0.51
Correlates with G0s2
Group2
Group3
Group1
Counts (log2)
Cell #

Supplement 4. Top correlating genes with G0s2 reveals Itga8 as the only gene that correlates above 0.5

A search of top correlating genes with G0s2 reveals Itga8 as the only gene that correlates above 0.5 (pearson correlation with a minimum period of 3). Levels of expression of both genes are plotted and the cells are ordered by expression of G0s2.

Matrix Components						
Gene	adjusted_p_values	mean_Group1	mean_Group3	mean_all	pvalues	ratio Group1 to Group3
Colq	1.37E-08	5.05E+00	5.93E-01	1.64E+00	2.46E-11	3.80
Col13a1	9.74E-04	4.86E+00	1.97E+00	3.41E+00	1.08E-05	1.98
Col1a1	4.86E-02	8.74E+00	9.84E+00	9.39E+00	1.77E-03	0.90
Col3a1	1.19E-05	9.90E+00	1.16E+01	1.10E+01	5.89E-08	0.86
Col1a2	1.31E-12	1.02E+01	1.19E+01	1.12E+01	1.07E-15	0.86
Col5a2	3.02E-03	5.42E+00	8.10E+00	7.44E+00	4.32E-05	0.71
Col5a1	1.65E-02	2.63E+00	5.30E+00	4.31E+00	4.12E-04	0.58
Col15a1	1.34E-03	2.47E-01	2.99E+00	1.64E+00	1.60E-05	0.31
Col14a1	9.06E-26	1.28E+00	9.18E+00	5.99E+00	1.35E-29	0.22
Lama2	2.95E-02	6.38E+00	8.50E+00	7.62E+00	9.14E-04	0.78
Lamc3	4.48E-02	4.01E-01	2.77E+00	1.68E+00	1.60E-03	0.37
Has1	3.02E-03	7.02E-01	4.44E+00	2.68E+00	4.32E-05	0.31
Matrix remodeling						
Gene	adjusted_p_values	mean_Group1	mean_Group3	mean_all	pvalues	ratio Group1 to Group3
Mmp2	1.18E-03	6.88E+00	9.53E+00	8.46E+00	1.39E-05	0.75
Mmp14	2.09E-03	2.02E+00	5.32E+00	4.03E+00	2.71E-05	0.48
Mmp23	2.97E-02	1.81E-01	2.28E+00	1.21E+00	9.35E-04	0.36
Timp3	2.02E-06	1.13E+01	1.30E+01	1.25E+01	7.40E-09	0.88
Timp2	4.15E-04	9.18E+00	1.05E+01	9.84E+00	3.93E-06	0.88
Timp1	4.40E-04	7.57E-01	4.66E+00	3.35E+00	4.30E-06	0.31
Adamts2	1.96E-07	3.75E+00	8.08E+00	6.49E+00	5.27E-10	0.52
Adam23	5.63E-05	4.55E-01	4.44E+00	2.41E+00	3.53E-07	0.27
Adamtsl1	6.82E-05	2.36E-01	3.96E+00	2.02E+00	4.59E-07	0.25
Adamts5	2.61E-02	2.17E+00	5.21E+00	3.66E+00	7.81E-04	0.51
Immune Signaling						
Gene	adjusted_p_values	mean_Group1	mean_Group3	mean_all	pvalues	ratio Group1 to Group3
Il6	5.36E-05	2.29E+00	7.67E+00	5.44E+00	3.28E-07	0.38
Il33	3.53E-04	0.00E+00	4.08E+00	1.88E+00	3.22E-06	0.20
Il6st	2.11E-03	3.08E+00	6.49E+00	5.19E+00	2.75E-05	0.54
Il11ra1	9.44E-03	3.28E+00	6.11E+00	4.81E+00	1.92E-04	0.60
Cxcl1	1.84E-06	2.81E+00	8.82E+00	7.13E+00	6.60E-09	0.39
Cxcl12	6.31E-06	1.54E+00	6.27E+00	4.68E+00	2.78E-08	0.35
Cxcl14	1.06E-02	6.47E+00	4.26E+00	5.26E+00	2.30E-04	1.42
Cell Matrix Adhesion						
Gene	adjusted_p_values	mean_Group1	mean_Group3	mean_all	pvalues	ratio Group1 to Group3
Arhgap6	3.31E-02	4.31E+00	1.85E+00	2.58E+00	1.09E-03	1.86
Ctgf	4.70E-03	6.80E+00	3.60E+00	4.52E+00	8.03E-05	1.70
Npnt	5.46E-05	1.10E+01	6.83E+00	8.96E+00	3.38E-07	1.54
Itga8	4.64E-03	9.68E+00	6.34E+00	8.01E+00	7.86E-05	1.46
Lims1	7.04E-03	8.87E+00	5.84E+00	6.59E+00	1.32E-04	1.44
Fn1	4.01E-03	1.06E+01	7.99E+00	8.41E+00	6.52E-05	1.29
Macf1	2.06E-02	1.34E+01	1.16E+01	1.26E+01	5.51E-04	1.14

Table 1. Significant genes that are differentially expressed between Group 1 and Group 3.

Four categories of genes are highlighted. Genes up-regulated in Group 1 are in red and genes up in Group 3 are in blue.

Conclusions

Understanding adult lung stem cell biology and regenerative medicine is very much in its infancy, with new progenitor cell populations still being defined[1,2,3] through the modern use of classical techniques[4,5,6,7,8,9,10,11]. In the above work, we utilized the pneumonectomy model system to further define adult stem cells in the lung, as well as necessary signaling pathways involved in compensatory lung growth. A caloric restriction model further supported the role of AECIIs as a progenitor cell population. Lastly, single-cell sequencing allowed us to demonstrate progenitor cell heterogeneity in lipofibroblasts.

In the first study, we utilized lineage tracing analysis, in vitro "alveoloshpere" assays, and targeted deletion of RBPJ to define both AECII behavior post-PNX as well as the role for the Notch signaling pathway during neoalveolarization in the lung. Through collaboration with UC Davis, we also worked with adult rhesus macaques to better understand whether a similar event occurs in non-human primates. Initially, we noted a significant increase in AECII proliferation 7-days post-PNX as compared to the sham operated animals. Furthermore, when animals were allowed to recover to 21-days post-PNX, we found a statistically significant increase in PDPN+ lineage-labeled cells. These data support previous findings [1] that AECIIs are a progenitor cell population in the adult lung. We next sought to determine potential molecular pathways involved with the process of adult alveologenesis through performing qPCR analysis on both lineage-labeled AECIIs as well as a PDGFRA+ lipofibroblast population 4-days post-PNX or sham operation. qPCR analysis showed evidence of up-regulation of various upstream and downstream genes involved in the Notch signaling pathway. Following up on these data, we demonstrated in vivo that inhibition of gamma secretase reduces colony forming efficiency of alveolospheres.

Furthermore, targeted deletion of RBPJ in AECIIs demonstrated a reduction in colony forming efficiency. We then tested the targeted loss of RBPJ in AECIIs in vivo using transgenic mice. Introduction of tamoxifen to both lineage label and KO RBPJ in AECIIs resulted in a significant decrease in both AECII proliferation and differentiation 7 and 21-days post-PNX, respectively. Collectively, our data suggests a necessary role for the Notch signaling pathway in adult AECII proliferation and differentiation during compensatory lung growth. Lastly, we demonstrated for the first time that, similar to mouse, AECIIs in non-human primates are a proliferative population post-PNX.

The second study again uses the pneumonectomy model system, however we looked to determine if the Wnt Signaling Pathway is also involved and necessary for AECII proliferation and differentiation post-PNX. Initially we quantified the number of proliferating, lineage labeled AECIIs 7-days post-pnx in both SPC-CreEr;Ctnnb1$^{flx/flx}$;Rosa:Tomato ("Wnt KO") mice and SPC-CreEr;Ctnnb1$^{flx/+}$;Rosa:Tomato ("Wnt Het"). The Wnt Het mice had a statistically significant increase in AECII proliferation as compared to Wnt KO mice. When these mice were then taken out to 21-days to determine the percent of PDPN+ lineage-labeled cells, again the Wnt Het animals had a significantly greater number than the Wnt KO. Finally we performed dry weight measurements on the accessory lobe of Wnt Het and Wnt KO mice 14-days post-PNX to determine if loss of Wnt signaling results in a reduction in the compensatory growth. We found that the accessory lobe of the Wnt Het mice had a statistically significant increase in weight as compared to the Wnt KO group. These data support that the Wnt Signaling Pathway is involved with alveolar epithelial expansion during compensatory adult lung growth, similar to Notch.

In our third study, we used a previously described caloric restriction model system to further bolster the theory for AECIIs as the main progenitor cell population which gives rise to

new alveolar epithelium during adult lung regeneration. We first determined that there is a significant reduction in lung weight after mice underwent a caloric restriction diet for 15-days, as compared to control animals who were allowed to eat at will. In a follow up study to look at alveolar regeneration after caloric restriction and then *ad libitum* feeding we demonstrated, through lineage-labeling and confocal microscopy, that differentiation of AECIIs into AECIs occurs quickly within just three days of re-feeding. Lastly, when RBPJ Het versus RBPJ KO animals were compared after a similar course of caloric restriction then *ad libitum* feeding, the RBPJ Het animals had a statistically significant increase in AECII into AECI differentiation.

In our fourth study, we utilized new single cell sequencing techniques to better define and demonstrate stem cell heterogeneity in a population of adult lipofibroblast cells found in the lung. Initially, we dosed animals with bleomycin to induce pulmonary fibrosis. 7-days after injury, we transplanted this lipofibroblast population into lungs of injured animals. These pdgfra+ lipofibroblasts engrafted and expressed a myofibroblast marker alpha-smooth muscle actin within fibrotic lesions found in the airspace. We then performed single-cell sequencing of the steady-state lipofibroblast population to better define various sub-populations within this progenitor cell population. One gene which stood out in particular was Tcf21. We used lineage tracing analysis to define the behavior of Tcf21+ cells in the context of pulmonary fibrosis after bleomycin injury. We found that Tcf21+ cells gave rise to myofibroblasts in the fibrotic lesions of the lung. Lastly, we looked to see if other genes found within our sequencing data could also be found within the adult human lung. Non-utilized donor tissue was processed for histological or FACS analysis, and specifically stained for antibodies against ITGA8, Tcf21, and G0s2. We found that the ITGA8 cells represented a cell subpopulation that marked positive for Tcf21 and

G0s2. These data drew positive correlations with our single-cell sequencing mouse data, and bring to light the complexity of this progenitor cell population.

Collectively, the above studies positively contribute to advancing the field of lung stem cell biology and regenerative medicine. From these data, a continued, more granular approach to defining cell types and cell behaviors in the context of compensatory lung growth and lung repair can be undertaken. Future studies to better define the stem cell niche would be ideal to create better targeted drug therapies for patients suffering from such diseases as COPD or IPF. It is quite possible that drug therapies for various forms of lung disease and cancer will come about through further work using such techniques as mentioned above, and through the specific focus on these cell types and cellular pathways.

References

1. Barkauskas, C. E. *et al.* Type 2 alveolar cells are stem cells in adult lung. *J. Clin. Invest.* **123,** 3025–3036 (2013).
2. Frank, D. B. *et al.* Emergence of a Wave of Wnt Signaling that Regulates Lung Alveologenesis by Controlling Epithelial Self-Renewal and Differentiation. *Cell Rep.* **17,** 2312–2325 (2016).
3. Ray, S. *et al.* Rare SOX2+ Airway Progenitor Cells Generate KRT5+ Cells that Repopulate Damaged Alveolar Parenchyma following Influenza Virus Infection. *Stem Cell Reports* **7,** 817–825 (2016).
4. Rock, J. R. *et al.* Multiple stromal populations contribute to pulmonary fibrosis without evidence for epithelial to mesenchymal transition. *Proc. Natl. Acad. Sci. U. S. A.* **108,** E1475–83 (2011).
5. Cao, Z. *et al.* Targeting of the pulmonary capillary vascular niche promotes lung alveolar repair and ameliorates fibrosis. *Nat. Med.* **22,** 154–162 (2016).
6. Buhain, W. J. & Brody, J. S. Compensatory growth of the lung following pneumonectomy. *J. Appl. Physiol.* **35,** 898–902 (1973).
7. Alejandre-Alcazar, M. A. *et al.* Hyperoxia modulates TGF-beta/BMP signaling in a mouse model of bronchopulmonary dysplasia. *AJP: Lung Cellular and Molecular Physiology* **292,** L537–L549 (2006).
8. Stevenson, C. S. & Birrell, M. A. Moving towards a new generation of animal models for asthma and COPD with improved clinical relevance. *Pharmacol. Ther.* **130,** 93–105 (2011).
9. Dhaliwal, K. *et al.* Monocytes control second-phase neutrophil emigration in established lipopolysaccharide-induced murine lung injury. *Am. J. Respir. Crit. Care Med.* **186,** 514–

524 (2012).

10. van Haaften, T. *et al.* Airway delivery of mesenchymal stem cells prevents arrested alveolar growth in neonatal lung injury in rats. *Am. J. Respir. Crit. Care Med.* **180,** 1131–1142 (2009).
11. Almeida, C. *et al.* The role of alveolar epithelium in radiation-induced lung injury. *PLoS One* **8,** e53628 (2013).

Publishing Agreement

It is the policy of the University to encourage the distribution of all theses, dissertations, and manuscripts. Copies of all UCSF theses, dissertations, and manuscripts will be routed to the library via the Graduate Division. The library will make all theses, dissertations, and manuscripts accessible to the public and will preserve these to the best of their abilities, in perpetuity.

Please sign the following statement:

I hereby grant permission to the Graduate Division of the University of California, San Francisco to release copies of my thesis, dissertation, or manuscript to the Campus Library to provide access and preservation, in whole or in part, in perpetuity.

Matthew Donne

Author Signature

12/29/16

Date